Carbon fixation in eukaryotic marine algae: Evolution of photosynthetic machinery and isotopic footprints

Ana Magali Carrera Heureux

Worcester College Oxford and Department of Earth Sciences

University of Oxford

Dissertation submitted for the degree of

Doctor of Philosophy

June 2015

Abstract

Photosynthesis in the world's oceans by marine algae is responsible for approximately 50% of CO_2 fixed into organic carbon. Aquatic primary producers are intricately linked to the climate system due to their reliance on CO_2 as a substrate for photosynthesis and role in the removal and export of carbon from the surface ocean to marine sediments. The evolutionary history of marine algae was shaped by changes in the climate system. As a result, fossilized marine algae and modern representatives of ancient groups have the potential to unlock information about the Earth's climatic past. To use this information and fully understand the role of marine algae in the carbon cycle, however, it is essential to develop an in-depth understanding of CO_2 fixation in these organisms. In this thesis I look at carbon fixation in biomineralizing marine algae from a geological and a biological perspective. First I apply a carbon isotope proxy for CO_2 to organic material preserved in marine diatom frustules from an extremely transformative period in geological history, the Eocene-Oligocene boundary. Subsequently, this thesis aims to address gaps in our understanding of carbon fixation in eukaryotic marine algae. I present a novel dataset of kinetics of the carbon fixing enzyme, Rubisco, in eukaryotic algae, investigate the role of a pyrenoid-based carbon concentrating mechanism, and identify plastic changes in carbon fixing machinery in response to changing CO_2. The findings from this thesis refine our understanding of primary production in the oceans and how we apply algae-based CO_2 proxies to understand ancient climates.

Extended abstract

Unprecedented rates of atmospheric CO_2 and temperature rise over the past five decades have highlighted the necessity for a fuller understanding of the climate system, feedbacks and environmental impacts. The Earth's climate is extraordinarily complex and multifaceted so building this understanding is not straightforward. Scientists have recognized the value in the reconstruction of climatic changes in Earth's history as an analogue for modern change. One source of ancient climatic information comes from fossilized algae in marine sediments. Due to their direct requirement for CO_2 as a substrate for photosynthesis, marine primary producers living in the surface ocean are intricately linked to the climate system.

Photosynthesis is an important regulator of the atmospheric composition of CO_2 and O_2 on geological time scales as it acts as a sink of CO_2 and a source of O_2. The advent of oxygenic photosynthesis approximately 2.7 Ga transformed the atmosphere from one of extremely high CO_2 and negligible O_2 to one with abundant O_2, more similar to today. Modern atmospheric CO_2 is estimated to be 450 p.p.m. higher if drawdown by marine photosynthesis was removed (Siegenthaler & Sarmiento, 1993).

While the photosynthesis reaction is a major control on atmospheric conditions on Earth, the Earth's atmosphere simultaneously regulates the efficiency of photosynthesis. The ability of the carbon fixing enzyme, Rubisco, to use O_2 as well as CO_2 as a substrate makes the ratio of the two gasses in the atmosphere extremely important for determining the throughput of carbon fixation versus the energy wasting photorespiration reaction with oxygen (Laing et al., 1974). Other environmental controls on photosynthesis include the atmospheric impacts on weathering, altering

nutrient availability for algal growth (Harrison et al., 1999), ocean pH, and the role of CO_2 as a greenhouse gas, regulating global temperature. Changes in the climate system have determined the radiation and success of different groups of marine algae throughout geological history. For example, more complex eukaryotic algae did not become abundant in the world's oceans until after the Permian/Triassic extinction event when a decrease in species diversity, lower sea level, and increase nutrients opened up new niches for their success. Since then, eukaryotic primary producers have thrived in the ocean, but the dominance of individual groups is closely linked to the climate system and the habitats in which they live (Ridgwell and Zeebe, 2005; Walker et al., 2002).

Our studies of diverse marine algae, specifically marine haptophytes and diatoms that form biomineral shells, build an understanding of the role of the environment in the evolution of carbon fixing machinery. One way we probe this relationship is by looking at the preservation of ancient lifestyles in modern species. Ancient haptophytes and diatoms are thought to have evolved in shallow, coastal and eutrophic environments (DeVargas et al., 2007). We employ the modern day group of coastal haptophytes, the Pavlovales, as preserved representatives of ancient lineages. This group is estimated to be the earliest branching marine haptophyte and seems to have maintained many characteristics of early haptophyte ancestors (Baldauf, 2003; Peterson and Butterfield, 2005). In contrast, it is believed that later branching haptophyte lineages moved out to the open ocean. These species simultaneously began to live a dominantly autotrophic lifestyle and form a shell of calcium carbonate around their cell (DeVargas et al., 2007). In this study we investigate how these two different groups handle and fix carbon differently as a result of evolutionary pressures to evolve in new environments.

By investigating the diversity of carbon fixing machinery in these organisms we can begin to understand how evolutionary pressure and diverse environments have shaped the function of these cells today. While extremely important in the marine ecosystem and for primary productivity on Earth, the mechanisms by which these organisms fix carbon are relatively poorly understood. Photosynthetic machinery has been extensively studied in terrestrial primary producers due to their large contribution to human livelihood and concerns related to food security in a world with a drastically growing population. It is often assumed that the photosynthetic enzymes in marine eukaryotes function in the same way as other well-studied primary producers. This thesis, however, highlights the extreme diversity in carbon fixing strategies for marine algae and the resulting impacts on enzyme kinetics and carbon isotopes. This information refines our understanding of primary production in the ocean and how we interpret ancient signals of photosynthesis in the geological record.

We begin our work from a paleo-climatic perspective and experiment with the application of an as yet untapped reservoir of ancient biochemical information that has the potential to tell us about one of the most transformative periods in Earth's history, the Eocene-Oligocene boundary. The Eocene-Oligocene boundary is characterized by extreme global cooling, the onset of semi-permanent glaciation in the Southern Hemisphere and a drop in atmospheric CO_2 of over 800 p.p.m.v (Pearson et al., 2009). Understanding the controls and feedbacks on this type of extreme climate change has the potential to shed light on how we might expect the environment to respond to future climatic changes, expected to be rapid and drastic. In this study we use extremely well-preserved, size separated diatom-bound organic carbon isotopes to estimate the magnitude of CO_2 change at this time. We observe interesting trends in our records

that correspond with other current proxy estimates of CO_2 at this climatic transition. However, in this study we simultaneously point out some of the limitations of the application of this proxy.

The second chapter in this thesis addresses these limitations by building a large dataset of information on the carbon fixing machinery across eukaryotic marine algae. We elucidate trends between the function of Rubisco and strategies for overcoming the limitations put forward by the inefficient enzyme. This study leads us to a more in-depth investigation of the function of the pyrenoid, a compartment involved in the photosynthesis reaction, as a carbon concentrating mechanism (CCM) and the role it plays in carbon fixation across four species of marine phytoplankton. These studies build a great understanding of the role of a carbon concentrating mechanism in eukaryotic algae and how it may act to effectively streamline photosynthesis and nutrient-use for cells evolved to live in the open ocean.

The final chapter in this thesis brings the work full circle with an investigation of plastic physiological responses of eukaryotic algae to changing CO_2 in the laboratory. This further confirms our hypothesis that a CCM is a more efficient means of carbon fixation and helps the cell reduce the nutrients required to effectively fix a sufficient amount of carbon to support life. Through the investigation of both ancient algal fossils as well as modern day cultures we build a multifaceted and holistic understanding of the complex systems used to achieve efficient carbon fixation in these single celled organisms. The present work is a culmination of many approaches to understanding photosynthesis in these phylogenetically ancient and globally important organisms. The outputs of this thesis should refine our inputs for carbon fixation in models of the carbon cycle, atmospheric climate change, and marine algae-based paleo-proxies.

Declaration

This thesis is wholly a product of my own work. Work done in collaboration with others has been cited specifically for each chapter. No part of this thesis has been accepted or is currently being submitted for any degree, diploma or certificate or other qualification in this University or elsewhere. This work does not exceed the page limit set out by the Degree committee.

Acknowledgements

I would like to first thank my supervisor, Professor Ros Rickaby, for being so encouraging when I first emailed her about pursuing a PhD at Oxford and helping me to source funding as an international student. Ros's enthusiasm in general has been reassuring from the moment we met, to meetings we have now where she gets excited about new data or possible avenues for the future. I would also especially like to thank Dr. Renee Lee, my postdoctoral supervisor, for showing me so many new techniques in the lab, always being there to work through problems together and for being so unbelievably helpful during the writing process. Thank you to everyone in the Oceanbug lab group, especially Harry McClelland, Michael Hermoso, Maeve Eason-Hubbard, Benjamin Rae, Ian Chan, and Rich Holtham for everything from a hand in the lab to moral support on a particularly tough day.

Thank you to the Oxford Department of Earth Sciences for providing such amazing facilities and staff including Steve Wyatt, Owen Green, Norman Charnley, and Jane Barling. Thank you all for helping me when I came up against a new chemical or machine in the lab that was a complete mystery to me. To the Oxford Department of Plant Sciences for letting me take over their radiation lab space and just generally being so welcoming. Thank you to Maxim Karpralov and Alan Wainman for help with lab techniques in Oxford. I cannot thank Spencer Whitney enough and the rest of the group at the Research School of Biological Sciences at the Australian National University for spending a month with Jodi Young and I measuring Rubisco kinetics and just generally welcoming us to Canberra.

I would like to thank the rest of the PhD students in our 2011 (PG11) cohort for always being there to commiserate with in the hallways and teaching me about everything that falls under the umbrella of "Earth Sciences." A special thanks to Harry McClelland for having faith in me when I was ready to give up. To the beautiful Worcester college and the members that I got to know during my time here. And of course thanks to Laura and Chris for being such great housemates during the final and most stressful stages of this PhD.

Finally, I would like to thank so many of the amazing people I have met along the way on this journey so far. Thanks to all my Brown University friends, especially the sunshine house, for always keeping life full of fun and laughter. Thank you to my best friend who has become a sister over the years, Julianna Tatelbaum, for being my sounding board for ideas and always being up for an adventure. To Allie Wainer and Arielle Waldman for being such steadfast friends that I can always count on and always will. To all my family and lifelong friends in Arizona and Michigan and to my godparents Janet Freedman and Andy Peppard, I can always feel your love and support no matter where I am in the world. To my Mom and Dad, you have instilled in me the mentality that I can achieve anything and without that I would never have taken the chances that I have in my life. Thank you for making no hurdle seem insurmountable. And finally to my brother, Arin, thanks for toughening me up as a kid, and supporting me unconditionally as an adult. I love you all!

Nomenclature

$\delta\ ^{13}C$	fractionation of ^{13}C to ^{12}C
ε_p	isotopic fractionation associated with carbon fixation
μ	growth rate
Ω	Rubisco specificity
‰	parts per million
ATP	Adenosine Triphosphate
ADP	Adenosine Diphosphate
Bicine	N,N-Bis(2-hydroxyethyl)glycine
BSA	bovine serum albumin
CA	carbonic anhydrase
CCD	carbonate compensation depth
CCM	Carbon concentrating mechanism
C_i	internal carbon pool
CO_3^{2-}	carbonate ion
$[CO_{2(aq)}]$	concentration of dissolved CO_2
Da	dalton
DNA	deoxyribose nucleic acid
$DIC_{(aq)}$	concentration of dissolved inorganic carbon
DTT	Dithiothreitol
EDTA	Ethylenediaminetetraacetic acid
EOT	Eocene-Oligocene transition
EPPS	4-(2-Hydroxyethyl)-1-piperazinepropanesulfonic acid
fmol	femtomoles (10^{-15})
G3P	glyceraldehyde-3-phosphate
Ga	billion years
Gt	gigatons
$[HCO_3^-{}_{(aq)}]$	dissolved concentration of bicarbonate ion
K_c	half saturation coefficient for CO_2
K_{cat}	rate of catalysis of reaction
kDa	kilodalton
K_o	half saturation coefficient for O_2
kyr	thousand years
LSU	Large Subunit
Ma	million years
mM	milimolar (10^{-3})
µM	micromolar (10^{-6})
NADPH/NADP+	Nicotinamide adenine dinucleotide phosphate, oxidised/reduced form
nM	nanomolar (10^{-9})
Oi-1	Oligocene isotope event 1
PAL	Present Atmospheric Level
PBS	phosphate buffered saline

PEI	polyethylenimine
PFA	paraformaldehyde
Pg	petagrams, 1 Pg = 10^{15} g
ppm	parts per million
pmol	picomoles (10^{-12})
PSI	Photosystem I
PSII	Photosystem II
rbcL	gene encoding large Rubisco subunit
rbcS	gene encoding small Rubisco subunit
rpm	rotations per minute
RT	room temperature
Rubisco	Ribulose 1, 5-bisphosphate carboxylase/oxygenase
RuBP	Ribulose 1,5- bisphosphate
SA	surface area
SEM	scanning electron microscopy
SSU	Small Subunit
TEM	transition electron microscopy
Tris	2-Amino-2-hydroxymethyl-propane-1,4-diol
V	volume
yr	years

Contents:

Chapter 1: Introduction

This thesis addresses the multifaceted and interdisciplinary nature of the interactions between eukaryotic marine algae and Earth's climate system in the geological record and in the modern day. Marine sediments provide an archive of ancient climatic signals beyond the extent of ice core records of temperature and CO_2 (~800,000 years) (Lambert et al., 2007; Petit et al., 1999). Chemical signals from ocean sediments, however, are primarily of biological origin, adding a dimension to their interpretation for the application to paleo-climate proxies. Throughout this thesis we employ various approaches to bridge the gaps between geology, chemistry and biology and build a holistic understanding of the relationship between ocean primary productivity and climate.

1.1 Primary production in the world's oceans

Primary production by oxygenic photosynthesis is responsible for the majority of the transfer of carbon from the atmosphere and hydrosphere to the biosphere. The photosynthesis reaction converts light energy to chemical energy stored in the form of sugar compounds (Eqn 1-1).

$$6CO_2 + 6H_2O \xrightarrow{light} C_6H_{12}O_6 + 6O_2 \quad (1\text{-}1)$$

Estimates of carbon fixation into organic biomass from CO_2 show that the terrestrial and marine biospheres contribute equally at a rate of about 111 – 117 Pg C yr^{-1} (Behrenfeld et al., 2001). Despite the similar rate of organic matter production, the marine biosphere has a relatively small standing reservoir of carbon, approximately 1 Pg compared to 1900 Pg in the terrestrial biosphere, and a rapid turnover of about one week, compared to around

two decades on land (Barker et al., 2003; Raven et al., 2005). This ability to fix large amounts of carbon with relatively little biomass makes aquatic primary producers key players in carbon cycling and other biologically important elemental cycles in the environment. Unicellular primary producers carry out the majority of oxygenic photosynthesis in the world's oceans. Broadly, they can be separated into prokaryotic organisms, or cyanobacteria, and eukaryotic organisms, or algae. These two groups are thought to contribute roughly equal amounts to aquatic primary production (Falkowski & Raven, 2007).

Marine primary producers form the base of the marine food chain and, specifically biomineralizing algae, play a central role in the cycling of nutrients in the environment. The formation of calcium carbonate ($CaCO_3$) and biogenic silica (SiO_3) make biomineralizing algae key players in the cycling of carbon and silica in the ocean. Their biomineral shells additionally increase sinking and ballasting from the surface ocean to marine sediments making them extremely important for the export of material to marine sediments (Karl & Steinberg, 2001; Raven et al., 2005). The fixing of CO_2 and export from the surface ocean by aquatic primary producers is known as the marine biological pump (Longhurst & Harrison, 1989). This pumping of carbon from the surface to the deep ocean acts as a sink of CO_2 from the atmosphere. The modern ocean is a net sink of atmospheric CO_2, sequestering and removing it at a rate of approximately 1.5-2.0 Pg C yr^{-1} (Takahashi et al., 2009). Over long time scales, marine primary producers control the interplay between atmospheric CO_2 concentrations and export/sequestration of carbon in ocean sediments.

1.2 Ocean chemistry

Life in aquatic environments introduces unique challenges for primary producers. In the ocean, carbon exists in three dissolved inorganic forms: CO_2, HCO_3^-, and CO_3^{2-}. These three forms are individually stable but can be converted from one to the other with changes in pH following Eqn. 1-2.

$$CO_2 + H_2O \Longleftrightarrow H_2CO_3 \Longleftrightarrow H^+ + HCO_3^- \Longleftrightarrow 2H^+ + CO_3^{2-} \quad (1\text{-}2)$$

At equilibrium in the ocean, with pH approximately 8.2 ± 0.3, the relative amount of each carbon form is 91% HCO_3^-, 8% CO_3^{2-} and only 1% CO_2 (Zeebe & Wolf-Gladrow, 2001). This speciation of carbon in the ocean means that marine photosynthesizers have access to only a small concentration of CO_2 when compared to their terrestrial counterparts. The concentration of CO_2 in the surface ocean is around 10-30 μmol kg^{-1}, but the requirement for CO_2 substrate to reach half maximum saturation for photosynthesis in modern eukaryotic algae ranges from 20-90 μmol kg^{-1} (Badger et al., 1998). This suggests that marine primary producers may be limited by CO_2 in the modern ocean and therefore experience evolutionary pressure to concentrate carbon in the cell to carry out the photosynthesis reaction (Iglesias-Rodriguez et al., 2008; Rost & Riebesell, 2004). It is important to note, however, that many other factors may also be limiting for oceanic primary producers including nitrogen, phosphorus and iron.

1.3 Biomineralizing eukaryotic marine algae

The majority of eukaryotic biomineralizers are in the groups Haptophyta or Heterokontophyta. Based on the similarity of their plastids, the haptophytes, heterokonts and cryptophytes were originally classified as a "super-cluster" called the chromalveolates by Cavalier-Smith (1999). It was proposed that the super-cluster descended from one secondary endosymbiotic event with the uptake of a red alga by a biciliate anterokont host (Figure 1-1), however more recent data challenges the monophyly of this lineage (Harper et al., 2005). While all three subgroups posses a red algal plastid, only the haptophytes and heterokonts (diatoms) are known to biomineralize and therefore are preserved in the geological record. Certain haptophyte algae form calcium carbonate scales or liths excreted from the cell interior, while diatoms form a biogenic silica frustule at the perimeter of the cell in a compartment termed the silica deposition vesicle (Brownlee et al., 2002). As a result of their role in photosynthesis as well as biomineralization, these algae are dually important in environmental nutrient cycling and can also be studied both in the modern and in the geological record.

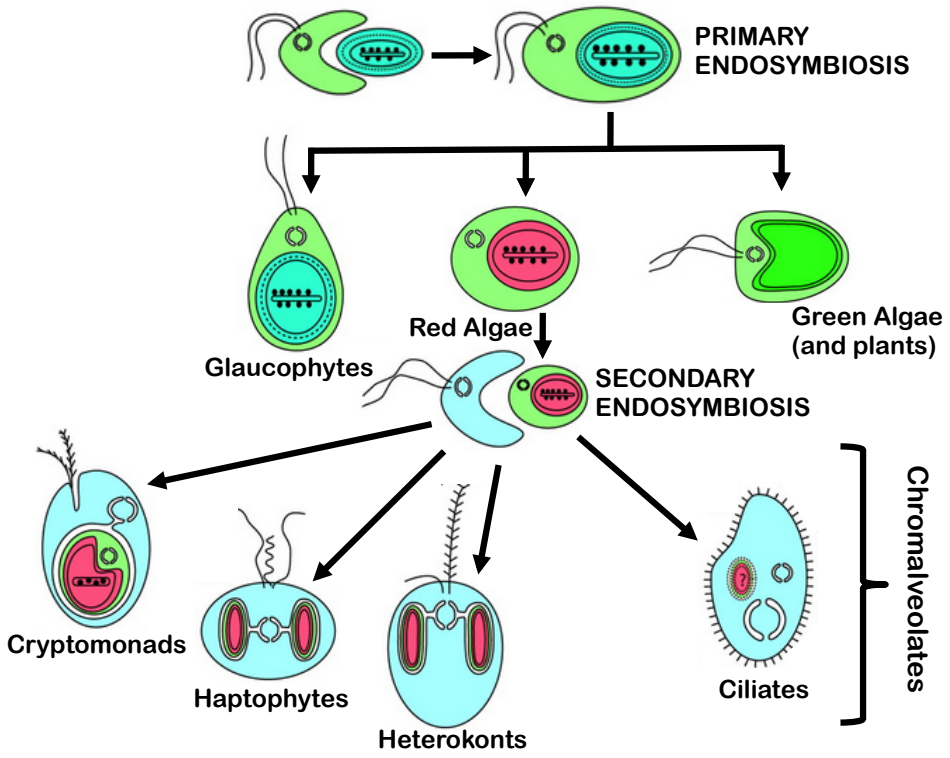

Figure 1-1: Overview of endosymbiosis events leading to the chromalveolate subgroup (shown in blue). Primary endosymbiosis shows the uptake of an unknown cyanobacterium by the eukaryotic ancestor of the plant supergroup. The descendants of this event are the three primary algal lineages: glaucophytes, red algae, and green algae. Plastids are color-coded with the three primary plastid lineages: cyanobacteria (blue-green), red algae (red), and green algae (green). Higher plants are eventually derived from the green algae. Secondary endosymbiosis of a red alga by an ancestor of the chromalveolates produces the cryptomonads, haptophytes, heterokonts, and alveolates represented here by the ciliates (modified from Keeling, 2004).

1.3.1 Haptophyta

The haptophyte lineage is one of the deepest branching groups in the eukaryotic phylogeny dating back to the Early Proterozoic ~1,900 Ma according to maximum likelihood analyses (Baldauf, 2003; Peterson and Butterfield, 2005). The group Haptophyta are uniquely identified by the presence of the organelle termed *haptonema*, a flagellum-like appendage used for prey attachment and capture (De Vargas et al., 2007; Billard & Inouye, 2004). The presence of this distinguishing feature suggests that phagotrophy was an important means for acquisition of food/energy in this group. The

original haptophyte ancestors are thought to have been primarily heterotrophic prior to the acquisition of a red plastid ~1050-1100 Ma and lived in coastal eutrophic habitats (De Vargas et al., 2007; Saez et al., 2004; Yoon et al., 2004). Most non-calcifying or lightly calcified haptophyes from early diverging lineages (Pavlovales, Prymnesiales and Phaeocystales) still demonstrate mixotrophic behavior (Billard and Inouye, 2004; Pinter and Pravasoli 1968) while the later diverging, heavily calcifying lineages (Coccolithophorids) favor autotrophy (De Vargas et al., 2007; see Figure 1-2 for phylogenetic origins of haptophyte groups).

Another characteristic that varies between the early diverging, non-calcifying lineages and the later heavily calcifying lineages is their habitat. While non-calcifying Pavlovales, Prymnesiales and Phaeocystales lived mainly in coastal or neritic habitats, the later diverging Coccolithophores moved out toward the open ocean (Bown, 1987; Farrimond et al., 1986; Yoon et al., 2004). It is believed that this migration away from the coasts did not begin until after the Permian/Triassic extinction event (~250 Ma) when certain prymesiophytes evolved the ability to biomineralize and secrete calcium carbonate.

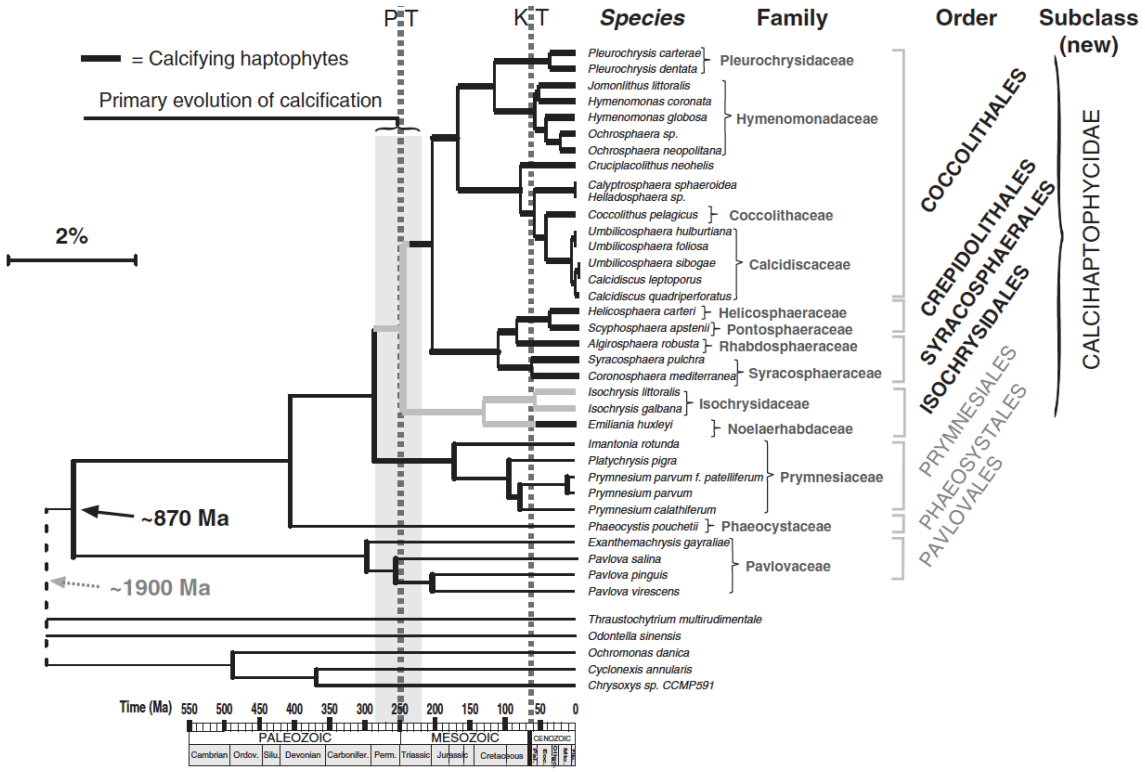

Figure 1-2: The origin and evolution of haptophytes from DeVargas et al. (2007). rDNA trees include 34 haptophyte taxa and representatives of the 7 extant orders within the Haptophyta. Unambiguously aligned sites were used for maximum likelihood analysis enforcing a molecular clock. Maximum time constraints were based on strato-phenetic events. The origin of calcification is thought to take place between the molecular origin of the group and the first apparent coccolith in the fossil record at ~220 Ma. Calcifying haptophyte lineages are highlighted in bold. (taken from DeVargas et al., 2007 and citations within).

These changes are believed to be a result of the combination of the low sea level, decreased shelf area and high Mg:Ca ratios at this time in addition to the decrease in "anti-calcifying" Paleozoic conditions including ocean anoxia and high concentrations of Fe and Mn cations (Ridgwell and Zeebe, 2005; Walker et al., 2002). It is evident from the coincident appearance of various unrelated calicifiers in the Late Triassic including coccolithophores, calcareous dinoflagellates and scleractinian corals that environmental forcings played a role in marine calcification (DeVargas et al., 2007). While much of our understanding of the forcings and origins of these characteristics are hypothetical or inferred from proxies, the modern relatives of these ancient organisms hold information that may further elucidate their evolution. Many earlier diverging haptophytes remain in coastal habitats

today while the later lineages remain in their more recent pelagic niches (Liu, 2010). In this work we will investigate differences in carbon fixing strategies between these lineages to shed light on their evolutionary history.

1.3.2 Diatoms

The origin of the diatoms, members of the Heterokont lineage, is estimated at the earliest to be around 240 Ma, close to when the haptophytes are hypothesized to have moved into the open ocean. However, an average of molecular clock data from four unique genes puts the first appearance much later at 135 Ma (Kooistra & Medlin, 1996; Medlin et al., 1997a). Although there is no consensus, existing hypotheses mainly suggest that diatom ancestors originated in a shallow marine, freshwater or even terrestrial environments (Sims et al., 2006). Modern representatives still occupy some of these habitats, but diatoms now play a large role in the pelagic ecosystem with a particular ability to dominate in areas with high nutrients and silica concentrations (i.e. coastal upwelling zones) (Capone & Hutchins, 2013).

Several groups within the Heterokont lineage in addition to the diatoms produce silica structures (Graham & Wilcox, 2000). The prevalence of silica across the Heterokonts suggests that silicification may be primitive to the lineage; however, a perplexing caveat is that the closest relatives of the diatoms, the Bolidophyceae, are non-silicifying (Sims et al., 2006). The heavily silicified wall, characteristic of the diatoms, suggests resistance to external stresses in their evolutionary past, potentially in an environment highly influenced by the terrestrial ecosystem. Raven (1983) calculated that the production of a

silica cell wall is less energy expensive for the cell than one made of carbohydrate, suggesting silicification as a strategy for energy conservation and maintenance of cell shape.

Marine diatoms play a major role in the ocean carbon cycle as they dominate export production in regions where they prosper. Hypotheses as to why diatoms play such a large role include fast growth rates under low light, high uptake rate of nutrients, effective storage in nutrient vacuoles and the small energy investment in the silica cell wall freeing up nutrients for cell growth (Smetacek, 1999). Diatom silica can be well-preserved in marine sediments due to their high productivity and the undersaturation of silica in the ocean. As a result, diatom silica acts as useful record in marine sediments from regions of high nutrients and silica concentrations.

1.4 Evolution of marine algae and adaptation to a changing CO_2 world

The link between marine primary production and the Earth's atmosphere is evident throughout the geological record. It is estimated that life on earth began as early as 3.7 Ga (Schidlowski, 1988) at which point CO_2 was higher than it has been since, estimated up to 3,000 times Present Atmospheric Levels (PAL) and O_2 was virtually absent from the atmosphere (Anbar et al., 2007; Holland, 2006). Oxygen in the atmosphere remained minimal until approximately 2.4 Ga, a period termed the Great Oxidation Event (Canfield, 2005) when the advent of oxygenic photosynthesis, presumably by cyanobacteria, transformed the atmosphere toward the more modern day conditions of low atmospheric CO_2 and high O_2, an environment equipped to support complex life on earth (Figure 1-3).

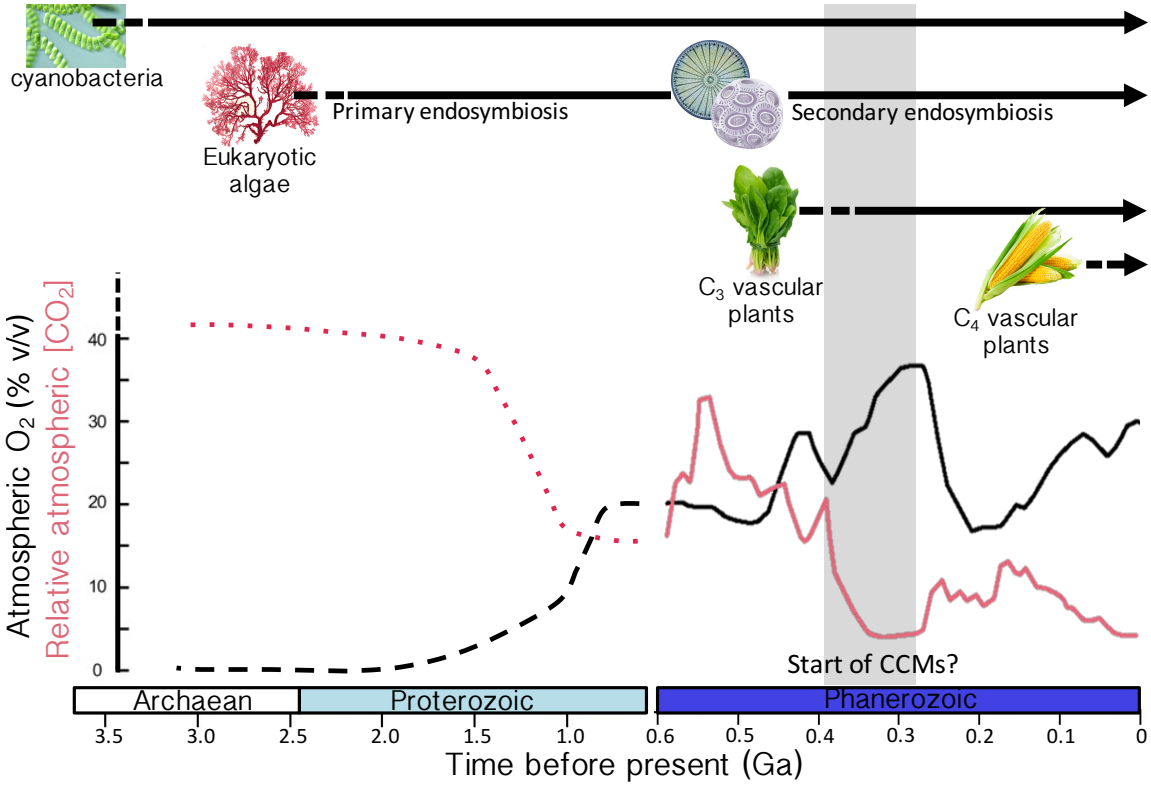

Figure 1-3: The ratio of past versus present concentrations of atmospheric [CO_2] (pink) and percent atmospheric O_2 (% v/v) (black) through geological history plotted against the estimated appearance of key primary producers (modified from Whitney et al., 2011, data from Berner and Canfield, 1989). The grey shaded area suggests the potential rise of carbon concentrating mechanisms (CCMs) in algae (Badger et al., 2002; Raven, 1997b). Arrows represent origin of labelled organisms starting with tentative estimates represented by broken lines.

Due to the dependence of marine algae on CO_2 as a substrate, the make-up of Earth's atmosphere has played a large role in determining the radiation of marine phytoplankton. The appearance of the first eukaryotic photoautotrophs came after the Great Oxidation Event with the endosymbiosis of an autotrophic cyanobacterium by a heterotrophic eukaryote (Yoon et al., 2004) (Figure 1-3). For a long period after their first appearance, however, eukaryotic photosynthesizers were not abundant in the oceans presumably due to relatively low atmospheric oxygen and euxinic conditions beneath the oxygen minimum zone (Brocks et al., 2005). These conditions would likely limit the availability

of nutrients in the surface ocean, a major requirement for productivity in eukaryotic primary producers (Fenner al., 2005).

Atmospheric oxygen did not reach near modern day levels until much later around 0.7 Ga, or the Second Great Oxidation Event (Canfield, 2005). At this time, nutrients were increasingly supplied to the surface oceans, more complex organisms rose to dominance and organic carbon burial peaked (Halverson et al., 2007; Knoll, 2006; Walter et al., 2000). Primary productivity in the oceans remained dominated by cyanobacteria and green algae until the Permian-Triassic mass extinction event (250 Ma), which wiped out around 96% of all marine species (Stanley & Yang, 1994). At this point, red plastid containing marine phytoplankton (diatoms, coccolithophores and dinoflagellates) began their rise to dominance in the marine environment (Falkowski, 2004).

The dominance of red plastid containing marine phytoplankton was temporarily halted by the Cretaceous-Tertiary extinction event where again around 80% of marine species went extinct (Newell, 1963; 1973). This event had the largest impact on marine calcifiers, but following the event eukaryotic phytoplankton rose in abundance again and have remained dominant through to the modern day. In the modern ocean, marine diatoms alone account for around 40% of marine primary productivity and are estimated to produce more than half of the organic carbon that is subsequently exported from the surface ocean (Falkowski and Raven, 2007; Field et al., 1998).

Due to the strong coupling of environmental variability and the abundance and community structure of marine primary producers, these organisms provide a prime target for

understanding Earth's ancient climate. Direct estimates of paleo-atmospheric conditions are limited by the extent of ice cores dating back up to 800 ka (Lambert et al., 2007; Petit et al., 1999). Beyond this, we rely on proxy measurements to illuminate how the Earth's atmospheric make-up has changed throughout geological history. Marine organisms provide a well-preserved, ancient record of interactions with the environment, making understanding the coupling between algal primary production and the environment of utmost importance.

1.5 The crux of it all: the Rubisco enzyme

Rubisco, the most abundant enzyme in the natural world, is the foundation of the photosynthesis reaction. The enzyme catalyzes carbon fixation or the incorporation of CO_2 and ribulose 1,5-bisphosphate (RuBP) to produce two molecules of 3-phosphoglycerate (3-PGA), a metabolic intermediate in the Calvin-Benson cycle, and eventually yields carbohydrates (Andrews et al., 1987; Cleland et al., 1998). Although vital for primary production, Rubisco is incongruously the rate-limiting step in this reaction due to its difficulty differentiating between its intended substrate CO_2 and the energy-wasting substrate O_2. This difficulty stems from the ancient origin of the enzyme. Rubisco evolved with the advent of oxygenic photosynthesis in the Achaean world of high CO_2 and relatively low O_2 (Kasting, 1993). At that time, the enzyme's inability to distinguish between the two compounds as a substrate for photosynthesis did not pose a problem for Rubisco's efficiency. As Earth's atmosphere evolved as shown in Figure 1-3, the enzyme has had to cope with a higher ratio of $[CO_2]$:$[O_2]$ in the atmosphere.

The energy wasting oxygenation reaction reaction can reduce the efficiency of the photosynthetic reaction by up to 60% (Zelitch 1975). Modern primary producers are pressed to find strategies to overcome the poor engineering of Rubisco in a low CO_2 high O_2 world. The notoriously inefficient enzyme has long been a target for improvement with the aim of increasing crop yield to meet the ever-growing demand for food (Morel et al., 1992; Tabita 1999; Uemura et al., 1997). Research of this nature is focused primarily on land plants, a resource more directly utilized by humans. As a result, a wealth of information exists on the function and diversity of Rubisco enzymes in terrestrial plants, but there is a relative paucity of information on aquatic primary producers. Not only does new information about Rubisco in aquatic organisms hold potential for the improvement of crop plants, but knowledge of the photosynthetic machinery in these organisms is key for understanding its evolution and adaptation to modern habitats and functional efficiency in the marine realm.

1.6 Algal strategies to overcome the limitations of the Rubisco enzyme

While the carbon-fixing Rubisco enzyme undoubtedly hinders primary producers, oxygenic photosynthesis remains the dominant form of autotrophic carbon fixation on Earth. Likely due to the need to preserve the only enzyme capable of carrying out this reaction, the enzyme is highly conserved and no other enzyme has proved capable of taking its place. Instead, oxygenic primary producers have been forced to come up with innovative strategies to cope with the enzyme's requirement for CO_2 and inhibition by O_2 in a world with one of the lowest $[CO_2]$:$[O_2]$ ratios in Earth's history. Some of the strategies that primary producers have developed include altering the kinetics of Rubisco

(Sage et al., 2002; Savir et al., 2010; Sharkey, 1988; Tcherkez et al., 2006), increasing the amount of Rubisco produced by the cell (Long et al., 1999) and manipulating the subcellular environment around Rubisco i.e. concentrating carbon at the site of Rubisco (Badger et al., 1998; Reinfelder et al., 2010). We will outline these strategies below, discuss them in detail in the following chapters and assess their impact on carbon fixation in the cell.

1.6.1 Kinetic changes in the Rubisco enzyme

There is evidence that Rubisco has responded to selective pressure and undergone improvements in its evolutionary history (Jordan et al., 1981; Young et al., 2012). To further investigate this hypothesis, Tcherkez et al. (2006) analyzed kinetic and isotopic data from the literature to assess how diverse Rubiscos have adapted to their relative [CO_2], [O_2] and thermal conditions (for original plots see appendix Figure S-1 and Table S-1). They hypothesize that the organisms have evolved a more "product-like" transition state of CO_2, facilitating the discrimination between CO_2 and O_2 but hampering the catalytic throughput of the enzyme. The trade-off between the benefits and restrictions of this change are dependent on the [CO_2]:[O_2] ratio in the environment around the enzyme, and allow only incomplete optimization of the enzyme (Tcherkez et al., 2006).

There is great diversity in the kinetic parameters of the Rubisco enzyme. Form I Rubisco, with 8 large and 8 small subunits (together ~560 kDa), is responsible for the majority of carbon fixation on Earth. The specificity of Rubisco for CO_2 versus O_2 ($S_{c/o}$) in Form I enzymes ranges from 40 in cyanobacteria to 80-100 in land plants. In the search for a

"better" Rubisco enzyme, a strong signal is obscured by the fact that different Rubiscos exhibit trade-offs in their kinetic parameters complicating the interpretation of the overall impact of kinetic variation on an organism *in vivo* (Jordan et al., 1981; Read et al., 1994; Uemura et al., 1997). Studies have found great variation between Rubisco's $S_{c/o}$ and affinity for CO_2 (K_c) across Form 1 Rubisco, suggesting kinetics may be optimized for different substrate conditions (Figure 1-4) (Jordan et al., 1981). K_c shown in Figure 1-4 represents the amount of substrate required to meet half the maximum velocity of the reaction, therefore a high K_c represents a low affinity for CO_2 as a substrate.

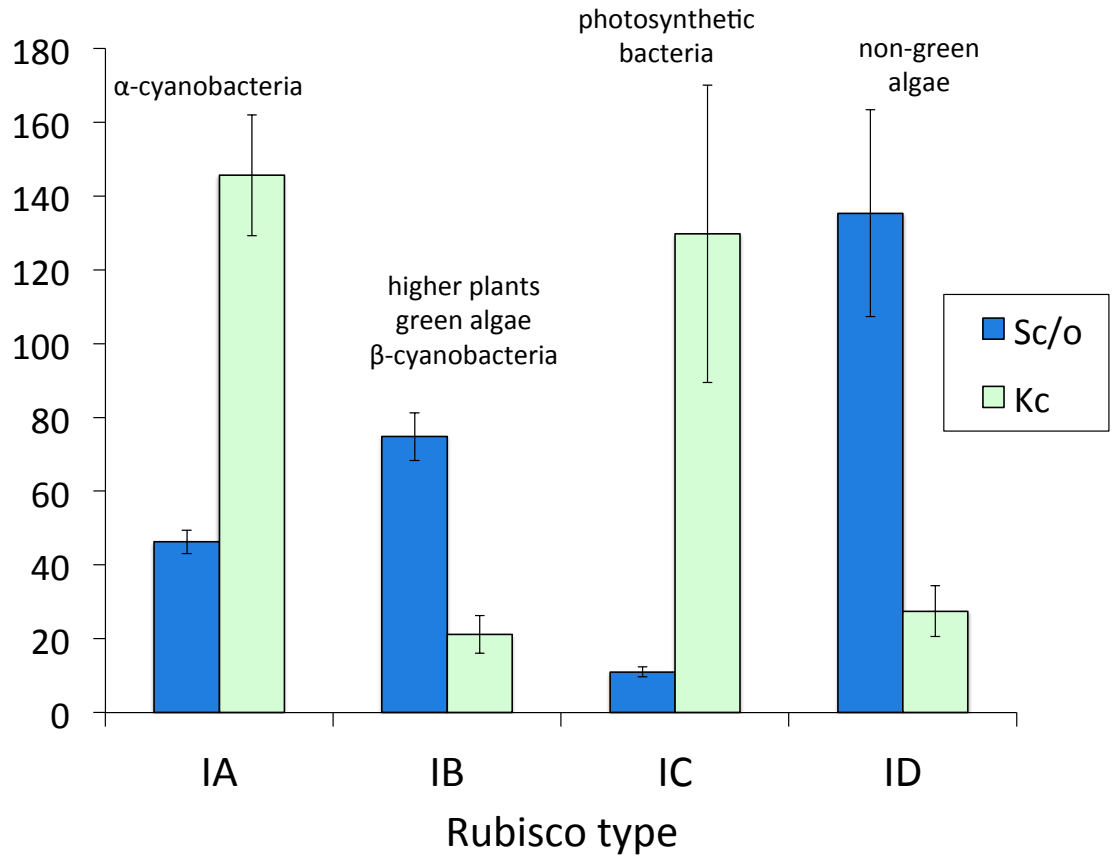

Figure 1-4: Compilation of known specificity factors (Sc/o) shown in blue and affinities for CO_2 (K_c in μM CO_2) shown in light green across all type I Rubisco enzymes. Type IA Rubisco is found in α-cyanobacteria, type IB includes β-cyanobacteria, higher plants and green algae, type IC is typically found in photosynthetic bacteria and type ID encompasses all non-green algae (e.g. eukaryotic red and Chrysophya algae), the focus of this study (data compiled in Badger et al. (1998), Tcherkez et al. (2006) and this study).

1.6.2 Rubisco Quantity

Increasing the amount of Rubisco enzyme a cell produces has the potential to increase the overall amount of carbon fixed by that cell. Increasing Rubisco quantity has been shown in C_3 higher plants that lack the ability to concentrate carbon around the enzyme (Ku et al., 1979; Long et al., 1999; Sage et al., 2002). This strategy for increased carbon fixation is straightforward, but can be problematic because of the high nitrogen demand for the production of such a large enzyme. In some higher plants, up to 50% of nitrogen is taken up by the Rubisco enzyme alone (Parry et al., 2003). Due to this high demand for nutrients as well as energy for the synthesis of proteins, this is only a viable solution for cells not limited by nutrients. We presume that cells living in nutrient limited environments or aiming to conserve energy will opt for different solutions to satisfy the cell's carbon fixing demand.

1.6.3 Location of Rubisco and the pyrenoid

The location of the Calvin cycle is constrained by its requirement for energy in the form of ATP and NADPH. These molecules carry chemical energy produced from light energy in what is termed the light-dependent reactions of photosynthesis. The light reactions are catalyzed by membrane protein complexes present in the thylakoid membranes including Photosystem I (PSI), Photosystem II (PSII), cytochrome b^6f complex, and ATP synthase (Arnon, 1971; Hillier & Babcock, 2001). The initial absorption of light energy occurs in pigments, primarily chlorophylls, starting a chain of redox reactions through the protein complexes where the final electron acceptor is an energy-carrying molecule, e.g. ATP and

NADPH (Eqn. 1-3) (Falkowski and Raven, 2007). Both the thylakoid membranes and the chlorophyll pigments are located inside the chloroplast. As a result, Rubisco is also generally located within the chloroplast where it can easily access the energy products of the light reactions (Hartman & Harpel, 1994).

$$2H_2O + 2NADP^+ + 3ADP + 3P_i \longrightarrow O_2 + 2NADPH + 2H^+ + 3ATP \quad (1\text{-}3)$$

Although Rubisco needs the energy-carrying products of this reaction, oxygen is also a product of the light-dependent reactions supplying fuel for the energy-wasting oxygenation reaction in the place of carbon fixation. This is one reason to assume that Rubisco might benefit from separating itself from this reaction, while being kept close enough to access the energy produced.

A structure, termed the pyrenoid, located within the chloroplast membrane in some species of marine algae has the potential to provide this separation as well as aggregation of the Rubisco enzyme. The pyrenoid was first described in 1803 by Vaucher (1803) and has since been found across all divisions of algae except the Cyanophyta (Brown, 1967). The pyrenoid in microalgae is described as a region within the chloroplast characterized by a denser, more homogeneous matrix material (now understood to be packed Rubisco) (Gibbs, 1962) and in some cases has been observed to have a hexagonally packed crystal structure (Griffiths, 1970; Holdsworth et al., 1968).

This definition is quite broad and the pyrenoid structures identified both across and within classes of algae are extremely variable (Bedoshvili et al., 2009; Bendif et al., 2011). In

addition to the varied nature and location of the pyrenoid in different cells, the function of the pyrenoid is not fully understood. Studies show that in algae with pyrenoid structures, 50-99% of Rubisco is localized within the pyrenoid (Gibbs et al., 1962), suggesting a role in photosynthesis. Other work suggests that localization of Rubisco in the pyrenoid provides an environment of concentrated CO_2 allowing for increased activation of Rubisco as well as favoring the carboxylation reaction over oxygenation (Moroney et a., 1999). Some studies describe 'crystalline' packing of Rubisco complexes in algal pyrenoids (Holdsworth, 1968; Kowallik, 1969) and in the bacterial carboxysome (Iancu et al., 2007). A model of estimated CO_2 and HCO_3^- and relative concentrations (represented by font size) in different cell compartments of eukaryotic microalgae, modified from Moroney et al. (1999) is shown in Figure 1-5.

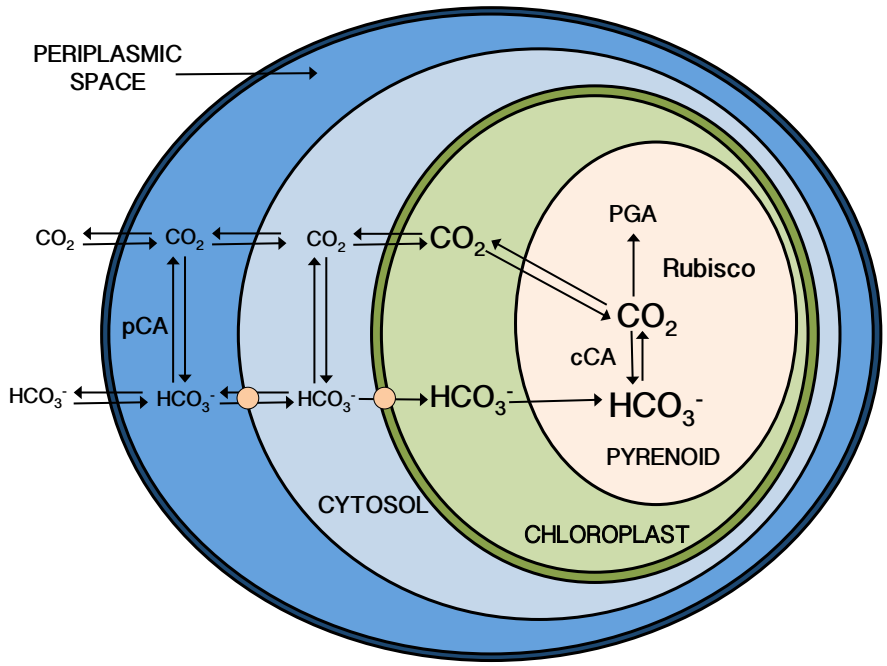

Figure 1-5: Diagram of carbon species transport in a eukaryotic microalgal cell and relative concentration of CO_2 and HCO_3^- indicated by font size (modified from Moroney et al., 1999). Concentration of both CO_2 and HCO_3^- is highest in the pyrenoid assuming active transport of HCO_3^- by bicarbonate transporters (orange circles) and catalyzed conversion between the species by carbonic anhydrase (CA). The figure shows periplasmic carbonic anhydrase (pCA) and chloroplast CAs (cCA) aiding in the transition between the Ci species.

Many questions remain around the exact function of the pyrenoid, but it is recognized that it plays a role in the reactions carried out by Rubisco. An analogy can be drawn between the assumed function of the pyrenoid and known function of the bundle sheath cells in C_4 higher plants. C_4 plants use an inner ring of bundle sheath cells to separate the Calvin Cycle from other photosynthetic reactions (Sage et al., 2004). As algae are unicellular, we might assume that the pyrenoid is acting as this separation but within one cell unit, more similar to the carboxysome structure in Cyanobacteria (Rae et al., 2014). Building our understanding of differences in Rubisco characteristics (i.e. kinetics) compared against structural differences in the pyrenoid may tell us about the role the pyrenoid plays in altering Rubisco's immediate environment and ultimately determining its efficiency and function.

1.6.4 Carbon concentrating mechanisms (CCMs)

In order to cope with limited CO_2 concentrations in the ocean, most marine phytoplankton concentrate carbon at the site of Rubisco using a carbon concentrating mechanism (Badger et al., 1998; Giordano et al., 2005; Reinfelder, 2010). The relative effectiveness of CCMs and the timing of their emergence in eukaryotic marine algae are still poorly understood (Reinfelder, 2010). Some of these mechanisms include the ability to use bicarbonate (HCO_3^-) as a substrate for photosynthesis (Rost et al., 2003), HCO_3^- and CO_2 transporters (Trimborn et al., 2007), carbonic anhydrase (CA) facilitating the interconversion between HCO_3^- and CO_2 (Tachibana et al., 2011), and macromolecular structures (Engle et al., 2015; Rae et al., 2014), such as the pyrenoid outlined above (Table 1-1).

CCM strategy	Description
Pyrenoid	Specialized compartment to provide elevated $[CO_2]$:$[O_2]$ environment for Rubisco and localize the enzyme
Carbonic anhydrase (CA)	Catalyzes the interconversion between HCO_3^- and CO_2 both internally and externally to the cell.
HCO_3^- and CO_2 transporters	Catalyzation of substrate transport (i.e. by aquaporins)
Use of HCO_3^- as a substrate	Allows the use of HCO_3^- as a substrate for photosynthesis, a carbon species much more available in aquatic environments.

Table 1-1: Descriptions of carbon concentrating mechanisms employed by marine eukaryotic algae.

Carbon concentrating mechanisms in cyanobacteria and higher plants have been extensively studied. In cyanobacteria, the carboxysome has been shown to concentrate carbon up to 1000 fold compared to external CO_2 (Price et al., 2008; Rae et al., 2014). These mechanisms may provide a streamlined and effective way to provide an environment for Rubisco more closely resembling that in which it was originally optimized, allowing the enzyme to function as it was intended.

Eukaryotic marine phytoplankton are ideally suited for the adoption of carbon concentrating mechanisms due to their generally larger and more complex cell structure and genome. A large diversity in evolutionary solutions for overcoming the shortcomings of the Rubisco enzyme has already been observed in these organisms (Badger et al., 1998; Reinfelder, 2010). In the freshwater model algal species, *Chlamydomonas reinhardtii*, studies have found evidence for the active uptake of inorganic carbon and elevated internal carbon pools (Giordano et al., 2005). Some work has also revealed that both marine

diatoms and coccolithophores can utilize HCO_3^- (Rost et al., 2003; Trimborn et al., 2007). However, other algae seem to lack carbon concentrating abilities altogether (Badger et al., 1998, this study) supporting the hypothesis that there is large diversity in strategies for eukaryotic phytoplankton to survive in a low CO_2 world.

1.7 Carbon isotopic footprints in the geological record

Interest in the Earth's changing climate and feedbacks in the climate system are growing as a result of unprecedented rates of atmospheric CO_2 rise over the last 50 years due to anthropogenic inputs (Tans, 2011). On geological timescales, it has been recognized that chemical signals in marine algae, including carbon and boron isotopes, record variability in atmospheric CO_2. The empirical relationship between organic carbon isotope fractionation ($\delta^{13}C$) and aqueous carbon dioxide concentration ($[CO_2]$) has been established in marine algae grown in culture, observed in the environment, and measured in the geological record (Francois et al., 1993; Freeman et al., 1992; Hayes et al., 1987,1999; Pagani et al., 2005,2011; Popp et al., 1989; Rosenthal et al., 2000; Zhang et al., 2013). The interpretation of isotope fractionation associated with carbon fixation (ε_p) in marine algae was originally based on a model from C_3 plants (Farquhar et al., 1982; 1989). The model describes fractionation as a series of fluxes including carbon into the cell, "leakage" out of the cell, and the flux of inorganic carbon fixed as organic carbon biomolecules (Bidigare et al., 1987; Pagani, 2014).

Many studies use alkenones, well-preserved organic long-chain ketones, to measure compound-specific carbon isotopes in marine sediment. Alkenones are produced in one

modern taxon of marine haptophyte, the Nöelaerhabdaceae. Alkenone-based paleo-proxies are limited to low latitudes, where these organisms live, and calibrations are limited for the application to ancient sediments by the fact that the species used to calibrate the proxy, e.g. *Emiliania huxleyi*, have only been present for the past 270 thousand years (Muller et al., 1997; Plancq et al., 2011). The relationship between organic carbon fractionation from photosynthesis (ε_p) and growth rate (μ)/CO_2 modulated by cell geometry has also been tested in over 9 species of marine diatom and calibrated in the field in diatom suspended particulate organic and core top material (Rosenthal et al., 2000; Popp et al., 1998). The calibration and calculation of CO_2^{atm} from ε_p measured in diatom material is outlined in detail in Chapter 2.

The calibration of ancient organic biomarkers has been improved since the relationship was established to incorporate the growing understanding of group or species-specific, habitat-specific, and environment-specific differences in carbon handling and fractionation. The first chapter of this thesis is work published in the journal *Earth and Planetary Science Letters* on the application of two calibrations of $\delta^{13}C$ measured in organic material from well-preserved diatom-bound organic material. From preserved ancient diatoms, we can measure both the carbon isotopic composition of the organic material and the size/morphology of the frustule, an important parameter for applying the modelled relationship between carbon fractionation and CO_2. By using a multi-proxy approach, we increase the confidence in estimates of ancient climatic conditions at this time.

Although the findings of this study are encouraging for the application of a diatom organic matter-based paleo-proxy, significant uncertainty remains in the biological mechanisms controlling the signal measured in ancient compounds. The remainder of this thesis address some of the gaps in our understanding of the physiological and biological responses of marine phytoplankton to changing CO_2. For $\delta^{13}C$ proxies, our insufficient understanding of the machinery and mechanisms carrying out carbon fixation limits our ability to interpret small differences observed across different sizes or species of algae. Although it is understood that Rubisco from marine algae is phylogenetically distinct from terrestrial plants, it is generally assumed that enzymatic isotopic discrimination is similar (Boller et al., 2015). Recent work, however, has shown that the isotopic discrimination (ε_f) from Rubisco of higher plants (22-29 permil) is much higher than that observed in the diatom *Skeletonema costatum* (18.5 permil) and the coccolithophore *Emiliania huxleyi* (11 per mil) (Boller et al., 2011; 2015). In order to use $\delta^{13}C$ as a measure of the isotopic effects of CO_2, growth rate, etc., we need to understand the controls on the baseline of Rubisco kinetic isotopic fractionation values (ε_f) as well as physiological isotope fractionation (ε_p) and how they differ between groups and species of primary producers.

The differing baselines of isotopic fractionation elucidated by Boller et al. (2015) have the potential to greatly shift the current estimates of CO_2 and other parameters using algal $\delta^{13}C$ as a paleoproxy. In addition, the relationship observed in Tcherkez et al. (2006) between the kinetic specificity ($S_{c/o}$) of Rubisco and the isotopic fractionation again emphasize the importance of minute differences in Rubisco on isotopic information. This data, suggesting increased fractionation with increased Rubisco specificity, further highlights the importance of understanding Rubisco kinetics and cell physiology for better

interpretation of the chemical data so widely used in paleoclimate reconstructions. Understanding the variability in photosynthetic potential across geologically relevant algal species could refine our application of algae-based paleo-proxies as well as help us to constrain how primary production in the oceans might respond to future climate changes.

1.8 A holistic view of photosynthetic diversity in eukaryotic algae and implications for the environment

We begin our work from a paleoclimatic perspective and experiment with the application of an as yet untapped reservoir of ancient biochemical information that has the potential to tell us about one of the most transformative periods in Earth's recent geological history, the Eocene-Oligocene boundary. We were able to observe interesting trends in our records of diatom-bound organic carbon isotopes that corresponded with other current proxy estimates of CO_2 at this time. However, in this study we simultaneously point out some of the limitations of the application of this proxy.

In the remainder of this thesis we investigate diversity of primary production in marine phytoplankton from a biological perspective. In this work we dig deeper into the physiological controls on carbon fixation in these organisms, how they vary and what the implications are for the lifestyle and productivity of the organisms. With an understanding of the evolutionary histories and habitats of different groups, preserved to some extent in their modern ecologies, we consider how their lifestyles have selected for the diversity in carbon fixing strategies. We find a strong relationship between ecological origins and the

photosynthetic mechanisms employed by the different species. We investigate in great detail the diversity in Rubisco kinetics and how this variation relates to physiological and macromolecular differences between species of haptophyte and diatoms. Finally, we look at short-term plastic adaptations in the physiology of these species to changes in CO_2. Throughout this thesis we will highlight the importance of our findings on the application to algal based paleo-CO_2 records and the impact on understanding primary production in the world's oceans.

Chapter 2: Refining our estimate of atmospheric CO_2 across the Eocene-Oligocene climatic transition

---

Contributions: This work was published as Heureux A. M. C. and Rickaby, R. E. M. (2015) in *Earth and Planetary Science Letters* 409, 329-338.

Abstract

The Eocene-Oligocene transition (EOT) followed by Oligocene isotope event 1 (Oi-1) is a dramatic global switch in climate characterized by deep-sea cooling and the first formation of permanent Antarctic ice. Models and proxy evidence suggest that declining partial pressure of atmospheric carbon dioxide (CO_2^{atm}) below a threshold may explain the onset of global cooling and associated ice formation at Oi-1. However, significant uncertainty remains in the estimated values and salient features of reconstructed CO_2^{atm} across this interval. In this study, we present novel carbon isotope records from size separated diatom associated organic matter ($\delta^{13}C_{diatom}$) preserved in silica frustules. Physical preservation of this material allows concurrent investigation of isotopic and cell size information, providing two input parameters for biogeochemical models and the reconstruction of CO_2^{atm}. We estimate CO_2^{atm} in two ways; firstly we use size and reaction-diffusion kinetics of a cell to calculate a CO_2^{atm} threshold. Secondly we use the calibrated relationship between $\varepsilon_{p(diatom)}$ and carbon dioxide from culture and field studies to create a record of CO_2^{atm} prior to and across the transition. Our study, from site 1090 in the Atlantic sector of the Southern Ocean, shows CO_2^{atm} values fluctuating between 900 and 1,700 ± 100 p.p.m.v. across the EOT followed by a drop to values in the order of 700 to 800 ± 100 p.p.m.v. just prior to the onset of Oi-1. Our values and magnitude of CO_2^{atm} change differ from previous estimates, but confirm the overall trends inferred from boron isotopes and alkenones, including a marked rebound following Oi-1. Due to the intricate nature of the climate system and complexities in constraining paleo-proxies, this work emphasises the importance of a multi-proxy approach to estimating of CO_2^{atm} in order to elucidate its role in the emplacement of Antarctic ice-sheets at the EOT.

2.1 Introduction

Earth system changes at the Eocene-Oligocene boundary (~33.7 Ma) include major global cooling, the formation of a permanent ice-sheet on Antarctica and a shift toward modern climate and biota on Earth. In addition to direct evidence from glaciomarine sediments and the fossil record, the positive anomaly in benthic $\delta^{18}O$ across the EOT is the largest in the Cenozoic. Benthic $\delta^{18}O$ and Mg/Ca records estimate 2-3°C cooling in the Southern Ocean and ice volume growth to 60-130% modern day (Bohaty et al., 2012; Coxall et al., 2005; Diester-Haass and Zahn, 1996; Ehrmann & Mackensen, 1992; Pusz et al., 2009; Salamy & Zachos, 1999; Zachos et al., 1994). A multitude of suggested drivers of glaciation across the transition include the reorganization of ocean gateways and the effects on the biological pump (Egan et al., 2013; Rabosky and Sorhannus, 2009; Scher and Martin, 2006), thermal isolation of Antarctica (Kennett, 1977) and continental uplift (Torres et al., 2014).

DeConto et al. (2008) identified a link between the onset of glaciation and carbon dioxide concentration in the atmosphere. Coupled global climate model simulations predict that a drop in CO_2^{atm} below a threshold of approximately 750 p.p.m.v. induces ice formation in the Southern Hemisphere. The proposed relationship between glaciation and CO_2^{atm} could account for both the magnitude and timing of glaciation leading into Oi-1 at ~33.4 Ma (DeConto et al., 2008; Zachos & Kump, 2005). To verify this hypothesis and to achieve a more robust understanding of the trigger for Antarctic glaciation at Oi-1, quantitative and precise estimates of CO_2^{atm} through the EOT are crucial.

Current estimates of CO_2^{atm} from this interval come from boron isotopes, the CO_2 and temperature dependent precipitation of nahcolite and the $\delta^{13}C$ of reticulofenestrid biomarkers (Lowenstein and Demicco, 2006; Pagani et al., 2011; Pearson et al., 2009; Zhang et al., 2013). Boron isotope estimates infer CO_2^{atm} using the relationship between pH and the boron isotope fractionation between $B(OH)_3$ and $B(OH)_4^-$ dissolved in seawater recorded via substitution of the $B(OH)_4^-$ in precipitated carbonate minerals. The largest uncertainties in this measurement come from the need to assume an additional carbonate system parameter in order to infer CO_2 from pH. Additionally, our understanding of the boron isotope ratio in paleo-seawater is limited due to the 20 Ma residence time of boron in the ocean (Pearson et al., 2009). Another method employed to estimate Cenozoic CO_2^{atm} is the equilibrium assemblage of precipitated sodium carbonate minerals. The formation of certain minerals, e.g. nahcolite, occurs under specific CO_2 and temperature conditions. Documenting the occurrence of nahcolite sheds light on the paleo-environment at the time of formation (Lowenstein and Demicco, 2006).

Alternatively, the empirical relationship between organic carbon isotopes ($\delta^{13}C_{org}$) and the carbon system can be used to unlock information about paleo-CO_2^{atm}. Isotopic fractionation associated with carbon fixation (ε_p) is determined from the isotopic difference between atmospheric CO_2 estimated from inorganic carbon ($\delta^{13}C_{carb}$) in marine calcifiers, and the organic material produced during photosynthesis (Eqn. 2-1).

$$\varepsilon_p = \left[\frac{\delta_a+1000}{\delta_o+1000} - 1\right] \cdot 10^3 \approx \delta_a - \delta_o \qquad (2\text{-}1)$$

where δ_a is the carbon isotopic composition of CO_2^{atm} and δ_o is the isotopic composition of the primary organic material. The theoretical effects of diffusion and carbon fixation on ε_p are estimated with the equation:

$$\varepsilon_p = A + (B - A)\, C_i \div C_e \quad (2\text{-}2)$$

where C_i and C_e represent internal and external concentrations of CO_2, respectively, and A and B are discrimination factors for diffusion of CO_2 into the cell and fixation within the cell, respectively. Here we assume growth rate (μ) to be proportional to net CO_2 transport into a cell, transport of CO_2 into a cell is proportional to the concentration of external CO_2 or C_e and transport out is proportional to internal CO_2 or C_i using the equation:

$$\mu = K_1 C_e - K_2 C_i \quad (2\text{-}3)$$

assuming K_1 and K_2 are constants, we can substitute $(K_1 C_e - \mu)/ K_2$ for C_i in Eqn. 2-2 to calculate:

$$\varepsilon_p = A + (B - A) \cdot \frac{K_1 - \mu/C_e}{K_2} \quad (2\text{-}4)$$

Eqn. 2-4 describes a linear relationship between ε_p and μ/C_e. This relationship is exploited to reconstruct external or environmental concentrations of CO_2 (C_e) from organic material preserved in the geological record (Francois et al., 1993; Laws et al., 1995, 1997; Popp et al., 1998; Rau et al., 1996).

Recent studies use alkenones, well-preserved organic long-chain ketones, to measure compound-specific carbon isotopes in marine sediment. Alkenones are produced in only one modern taxon of marine algae, the haptophytes, specifically the Nöelaerhabdaceae. Questions exist on the transferability of calibrations achieved from modern species, e.g. *Emiliania huxleyi,* for ancient sediments. Studies of nannofossil assemblages from the Late Oligocene to Early Miocene suggest that alkenone producing coccolithophores from the genus *Cyclicargolithus* (~10 μm) explain ~40% of alkenones observed in their samples, but are not used to calibrate alkenone estimates of CO_2^{atm} (Müller et al., 1997; Plancq et al., 2011).

The relationship between ε_p and μ/C_e has been tested in over 9 species of marine diatom, including taxa abundant at the EOT. Popp et al. (1998) find a significant inverse linear relationship between ε_p and (μ/CO_2) x (volume/surface area) at CO_2^{atm} concentrations higher than 9 μmol/kg when plotting 3 eukaryotic species, including a centric and pennate diatom, with a robust linear correlation ($r^2 = 0.70$). Other studies show that although [CO_2] is a main driver of changes in ε_p, the effects of growth rate and cell size are not easily decoupled (Bidigare et al., 1997; Burkhardt et al., 1999; Laws et al., 1995,1997). The relationship between ε_p in diatom-bound organic material and μ/CO_2 has additionally been calibrated in the field in suspended particulate organic and core top material (Rosenthal et al., 2000). The work to date supports the relationship in diatom material, however, emphasizes the importance of species or group specific biomarkers for paleo-reconstructions to reduce uncertainty (Francois et al., 1993; Freeman et al., 1992; Hayes

et al., 1987,1999; Pagani et al., 2005,2011; Popp et al., 1989; Rosenthal et al., 2000; Zhang et al., 2013).

Under this premise, this study employs size separated $\delta^{13}C_{org}$ from marine diatoms to exploit for information about ancient carbon systems as explored in Berg et al. (2012), Crosta & Shemesh (2002) and Singer & Shemesh (1995). Diatom-bound organic matter, from the *Bacillariophyceae* family of algae, consists of polycationic proteins and long-chain polyamines used in the nucleation of biominerals and formation of silica frustules or shells (Frigeri et al., 2006; Kröger et al., 1997b; Poulsen & Kröger, 2004). Due to the physical protection of these compounds provided by the surrounding silica frustule, relatively labile compounds normally susceptible to diagenesis are preserved in ancient sediments.

Evidence for the preservation of Cretaceous/Eocene age diatom-bound organic material is shown in Bridoux and Ingalls (2013). They compare organic compounds released from Cretaceous age samples to HF soluble compounds from modern diatom sediments (Bridoux & Ingalls, 2010; Bridoux et al., 2011) and culture material (Kroger et al., 2000) and conclude that the compounds are identical when identified using ion trap, triple quadrupole, and time-of-flight mass spectrometry as well as MS/MS fragmentation. Short-chain polyamines are easily remineralized by bacteria (Hofle, 1984), thus the presence of intact compounds in Cretaceous age samples is explained by physical protection of the compounds by the silica frustule. Preservation of organic compounds inside the frustule allows us to simultaneously constrain the carbon isotopic composition

of the organic material and the size/morphology of the frustule, an important parameter for modelling the relationship between CO_2 and ε_p.

2.2 Materials and methods

2.2.1 Study site and age model

Sediment was obtained from the Integrated Ocean Drilling Program at the Bremen Core Repository in Bremen, Germany. Samples were analyzed from core ODP Leg 177, Site 1090B, a site in the central Subantarctic Zone on the Agulhas Ridge paleo-location 42°54.82'S, 8°53.984'E. Paleowater depth at 34 Ma is estimated between 3000-3300 m, at or below the CCD at the time. The age model for our record comes from magnetostatigraphy correlated to the geomagnetic polarity time scale by Channell et al. (2003) on the CK95 GPTS (Cande and Kent, 1995) (Table 2-1).

Core	Section	Depth (mbsf)	Depth (mcd)	Age (Ma)	$\delta^{13}C_{inorg}$	$\delta^{13}C_{diatom}$	ε_p	Lithology
21X	2	186.2	194.25	32.39	1.78	-26.87	15.17	Muddy diatom ooze
22X	5	200.4	208.01	32.72	1.82	-27.28	15.65	Muddy diatom ooze
23X	5	209	217.4	32.95	1.98	-28.88	17.49	Mud and radiolarian-bearing diatom ooze
24X	2	215.3	226.26	33.16	2.31	-28.43	17.36	Diatom nannofossil ooze
24X	5	219.8	230.76	33.27	2.26	-27.76	16.62	Diatom nannofossil ooze
25X	2	225	235.71	33.39	2.45	-27.92	16.70	Nannofossil diatom ooze
25X	3	226.5	237.21	33.42	2.68	-27.79	16.50	Nannofossil diatom ooze
25X	5	229.5	240.21	33.49	2.35	-26.24	14.74	Nannofossil diatom ooze
25X	6	231	241.71	33.53	2.22	-26.20	14.66	Nannofossil diatom ooze
26X	3	236.2	248.19	33.68	2.14	-28.49	17.24	Mud-bearing nannofossil diatom ooze
26X	5	239.2	251.19	33.76	1.96	-29.03	17.76	Mud-bearing nannofossil diatom ooze
27X	2	244.4	256.39	33.88	1.79	-28.26	16.57	Radiolarian-bearing mud diatom ooze
28X	3	255.6	267.59	34.15	1.82	-27.73	16.27	Mud diatom ooze
28X	5	258.6	270.59	34.22	1.82	-28.85	17.48	Mud diatom ooze
29X	4	266.8	278.79	34.42	2.12	-27.42	16.42	Radiolarian-bearing mud diatom ooze
29X	6	269.8	281.79	34.49	2.11	-28.27	17.34	Radiolarian-bearing mud diatom ooze
30X	2	273.5	285.49	34.58	1.97	-28.51	17.50	Mud and radiolarian-bearing diatom nannofossil ooze
30X	5	278	289.99	34.68	1.90	-28.84	17.80	Radiolarian and mud-bearing nannofossil ooze

Table 2-1: Table of core information, depth in meters below sea floor (mbsf) and meters composit depth (mcd), age, $\delta^{13}C_{inorg}$, $\delta^{13}C_{diatom}$, ε_p (this study) and lithology for core ODP 177-1090B paleo-location 42°54.82'S, 8°53.984'E compiled from the core log.

Site 1090 in the Atlantic sector of the Southern Ocean lies north of the modern Sub-Antarctic Front and just south of the modern Sub-tropical Front. North of the modern upwelling zone in the Polar Front, site 1090 experiences indirect effects of upwelling as this water is moved northward via Ekman transport (Ito et al., 2005). As a result, the site resides in a belt of high diatom productivity providing a reservoir of well-preserved diatom material (Egan et al., 2013; this study). It is known that the site stayed close to its modern location through the Cenozoic and evidence from silica isotopes suggests a stabilization in upwelling and utilization at this site prior to 35 Ma (Egan et al., 2013). The

coupled model developed by the University of Victoria (UVic) provides estimates of the state of air-sea CO_2 disequilibrium during the Eocene. This model estimates reduced Southern Ocean upwelling relative to present-day. At the Eocene, site 1090 in the Southern Ocean is approximately at air-sea CO_2 equilibrium according to the model with a disequilibrium value of -84.7 p.p.m.v. compared to a range of -49.6 to -238.8 p.p.m.v. across the other 9 sites shown in Pagani et al. (2011). High diatom productivity and relatively low air-sea disequilibrium at site 1090 makes it a suitable candidate for reconstruction of atmospheric CO_2 using diatom material (Figure 2-1).

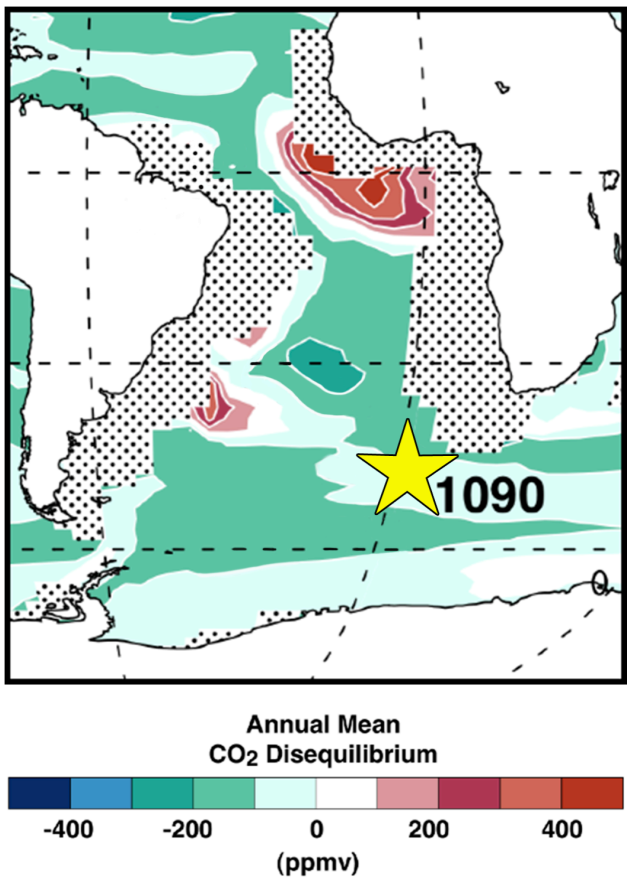

Figure 2-1: Location of site 1090 in the Atlantic sector of the Southern Ocean (paleo-location 42°54.82'S, 8°53.984'E) plotted on a map of modelled late Eocene air-sea CO_2 disequilibrium estimated using the University of Victoria (UVic) coupled climate model. Stippling signifies Eocene paleo-positions of continents and continents outlined in black represent the modern. Site 1090 (yellow star) is -84.7 p.p.m.v. away from equilibrium according to this model. For comparison, sites 929, 925, 516, 511 and 513, used in *Pagani et al.* [2011], are -123.2, -125.3, -67.5, -136.3, and -104.0 p.p.m.v., respectively away from equilibrium according to this model. Figure modified from Pagani et al. (2011).

2.2.2 Physical and chemical cleaning

Samples were treated with a series of physical and chemical cleaning steps in order to target only organic material entrapped within the diatom frustules. Our protocol incorporates cleaning steps from a number of established methodologies and is optimised for our samples.

Eighteen samples were dried in an oven at 35°C and weighed. Biogenic silica was physically separated from the carbonate and clay sediment fractions using heavy liquid (sodium polytungstate) flotation (Hendry & Rickaby, 2008; Morley et al., 2004; Sigman et al., 1999). An aliquot of the non-silica fraction (predominately coccolithophore carbonate) was taken and measured for inorganic carbon isotopes ($\delta^{13}C_{inorg}$ or $\delta^{13}C_{carb}$).

The remaining silica fraction was chemically cleaned following an adapted protocol from Robinson (2004) and Brunelle et al. (2007). Briefly, we applied 20% HCl overnight to remove any remaining $CaCO_3$, boiled in 30% H_2O_2 to oxidize organic material exposed to supernatant, and finally oxidized in 60% $HClO_4$ on a hotplate for 2 hours. Samples were filtered or rinsed with DI water at least 3 times between each step. During cleaning tests, both total organic carbon and $\delta^{13}C_{org}$ ($\delta^{13}C_{diatom}$) reached a plateau with increasing oxidation intensity. We chose the strongest oxidation to ensure samples were clean and analysed them under a scanning electron microscope (SEM) and light microscope to control for dissolution or breakage during the cleaning process.

2.2.3 Size separation

Using a light microscope, we made preliminary measurements and morphology characterizations of the diatom fossils present to our samples. Cleaned frustules were separated into 6 different size fractions using microfiltration modified from Minoletti et al. (2009). We chose the size fractions <8 μm, 8-12 μm, 12-20 μm, 20-41 μm, 41-100 μm and >100 μm to target dominant diatom species. The gentle sonication used in the microfiltration step was optimised for diatom samples, simultaneously providing a second physical cleaning step as shown by Egan et al. (2012).

Through light microscopy and SEM, we have concluded that the smallest two size fractions (8-12 and <8 μm) are primarily mixed fragments (Figure 2-2). These records are thus excluded in the discussion to follow.

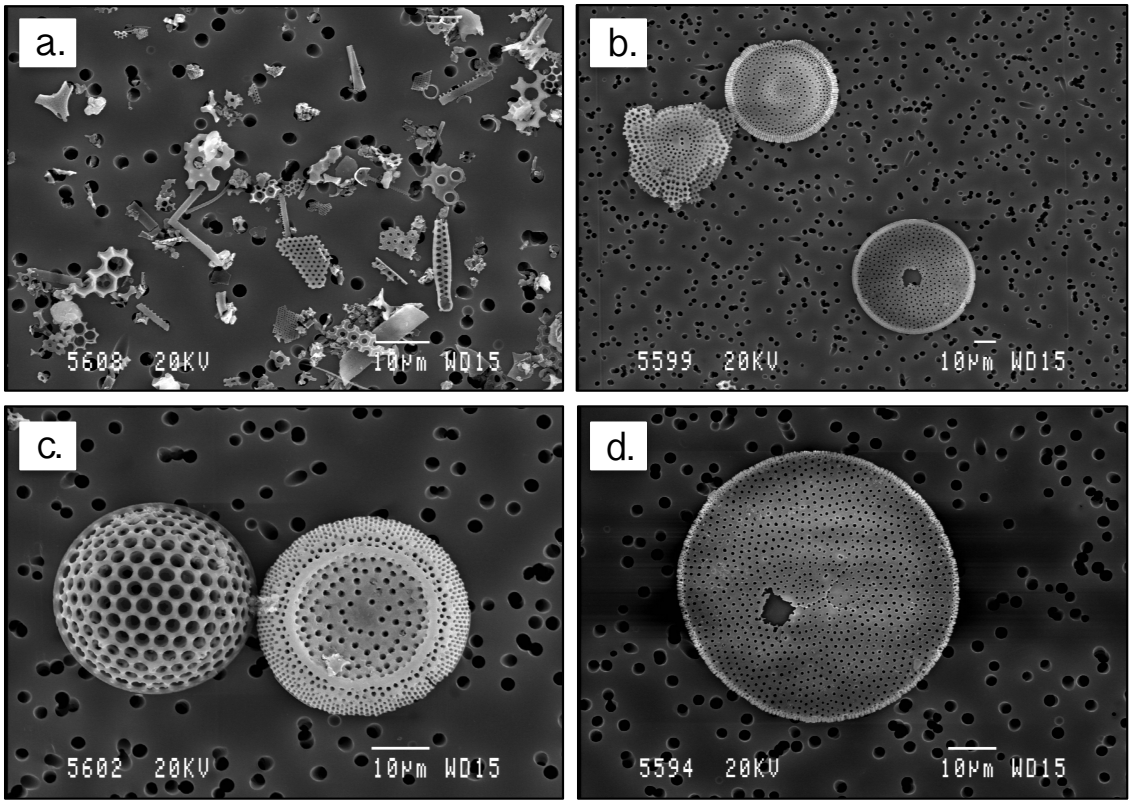

Figure 2-2: SEM images showing size-separated sediments (a.) >80% fragments in the less than 8 µm size fraction, (b.,c.) well-preserved centric diatoms in the 12-41 µm size group and (d.) a large centric diatom in the 41-100 µm fraction.

2.2.4 Analytical methods: $\delta^{13}C_{org}$ and $\delta^{13}C_{inorg}$

Cleaned diatom-bound material was weighed into tin capsules and the organic carbon isotopes ($\delta^{13}C_{org}$ or $\delta^{13}C_{diatom}$) measured in duplicate or triplicate on an automated carbon and nitrogen elemental analyser (Carlo Erba EA1108) at the Research Laboratory for Archaeology and the History of Art in Oxford. Internal reproducibility is 0.16‰ at 1 σ. The $\delta^{13}C_{diatom}$ values fall in the range expected of organic material.

Isotopic composition of inorganic carbon, from coccolithophore calcite, $\delta^{13}C_{carb}$, in our samples was measured in duplicate on the VG Isogas Prism II mass spectrometer in the Department of Earth Sciences at the University of Oxford. Calibration to the V-PBD standard via NBS-19 was made daily using the Oxford in-house Carrara marble standard; reproducibility was approximately 0.1‰.

2.2.5 Calculating ε_p

ε_p was calculated using the equilibrium relationships between carbon species described in Eqn. 1 with $\delta_{a,}$ or $\delta^{13}C$ of CO_2^{atm} estimated using the temperature dependent fractionation factors relating $\delta^{13}C$ of calcite to gaseous CO_2 ($CO_{2(g)}$), and aqueous CO_2 ($CO_{2(aq)}$) to $CO_{2(g)}$ (Eqns. 2-5 and 2-6):

$$\varepsilon_{calcite} - CO_{2(g)} = 11.98 - 0.12 \cdot T(℃) \quad (2\text{-}5)$$

$$\varepsilon_{CO_{2(aq)}} - CO_{2(g)} = \frac{-373}{T°K} + 0.19 \quad (2\text{-}6)$$

determined by Mook et al. (1974) and Romanek et al. (1992).

$\delta^{13}C$ of inorganic calcium carbonate ($\delta^{13}C_{carb}$ or $\delta^{13}C_{inorg}$) measurements from coccolith calcite in our samples and benthic foraminifera calcite from Pusz et al. (2011) were used to estimate $\delta^{13}C$ of CO_2^{atm}. The values of ε_p in this study use $\delta^{13}C_{carb}$ from coccolith calcite allowing us to estimate planktonic δ_a values from the same samples used to measure $\delta^{13}C_{diatom}$. At high CO_2 concentrations, Rickaby et al. (2010) show that smaller

coccolithophores species largely rely on a diffusive CO_2 supply, therefore we assume coccolith calcite forms in equilibrium with the environment. $\delta^{13}C_{carb}$ and temperature estimates from U_K'37 are shown in Table 2-2.

1090 Age	$\delta^{13}C_{carb}$	Temp (U_K'37)
32.39	1.78	21.426
32.72	1.82	21.555
32.95	1.98	21.643
33.16	2.31	21.726
33.27	2.26	21.826
33.39	2.45	19.588
33.42	2.68	17.174
33.49	2.35	18.679
33.53	2.22	19.413
33.68	2.14	21.583
33.76	1.96	22.625
33.88	1.79	21.026
34.15	1.82	22.789
34.22	1.82	23.138
34.42	2.12	24.092
34.49	2.11	24.441
34.58	1.97	24.871
34.68	1.90	25.125

Table 2-2: Sample age, $\delta^{13}C_{carb}$ measured in coccolith calcite from samples used to measure $\delta^{13}C_{diatom}$, and U_K'37 temperature estimates from (Liu et al., 2009) extrapolated across this interval.

Equation 2-1 employs the term $\delta^{13}C_{org}$ to represent $\delta^{13}C$ of bulk organic material, therefore to input this parameter, we must use a correction factor for our measured $\delta^{13}C_{diatom}$ to estimate $\delta^{13}C_{bulk}$. The offset between $\delta^{13}C_{diatom}$ and $\delta^{13}C_{bulk}$ depends on environmental conditions and carbon source, and likely differs between localities and through geological time. Studies find that $\delta^{13}C_{diatom}$ is more depleted than $\delta^{13}C_{bulk}$, but the degree of the offset

is variable. Berg et al. (2012) show a systematic depletion between 0.5 and 4.5‰ across Holocene and Last Glacial Maximum sediments while Barker et al. (2013) find up to 6‰. Here we use an average of 3.25‰, but note that this estimate is an oversimplification of the offset.

2.2.6 Calculating CO_2^{atm}

CO_2^{atm} was calculated using two calibrations, one from culture data (Eqn. 2-7) and the other from modern diatom suspended particulate organic carbon (SPOC) samples and core top data from the Southern Ocean (Eqn. 2-8) (Popp et al., 1998; Rosenthal et al., 2000).

$$\varepsilon_p = -182\left[\frac{\mu}{CO_2} \times \frac{V}{SA}\right] + 25.3 \quad (2\text{-}7)$$

$$\varepsilon_p = \frac{-270\mu}{CO_{2(aq)}} + 23 \quad (2\text{-}8)$$

For the SPOC and core top calibration, a correction factor between $\delta^{13}C_{diatom}$ and $\delta^{13}C_{bulk}$ is not required as ε_p is calibrated using $\delta^{13}C_{diatom}$. In addition, SA/V is not incorporated into the field data calibration.

Maximum growth rate (μ_{max}) can be estimated for Southern Ocean phytoplankton using the relationship between μ_{max} and temperature, $\log_{10}\ \mu_{max} = 0.0275T°C\text{-}0.070$ (Eppley, 1972). However, due to the reliance of Antarctic phytoplankton on micronutrient availability, studies have found that this relationship makes unreasonably high estimates of growth rate for Antarctic species (Popp et al., 1997; Rosenthal et al., 2000). Considering

this, we employed the relationship between [$Si(OH)_4$]] and growth rate with Eqn. 2-9 from (Martin Jezequael et al., 2000) to estimate μ at $Si(OH)_4$ concentrations of 10, 50 and 100 μmol/kg.

$$\mu = \mu_{max} \times \left(\frac{[Si(OH)_4]}{K\mu}\right) + [Si(OH)_4] \quad (2\text{-}9)$$

Measured natural growth rates of Antarctic diatoms show a range between 0.19 and 0.75 day^{-1} during summer blooms. We use the mean Antarctic growth rate of 0.43 day^{-1} for μ_{max} as shown in Rosenthal et al. (2000) and supported by measured growth rates of large cold water diatoms in culture (Table 2-3). To estimate Kμ, or the $Si(OH)_4$ concentration that limits μ to 0.5 μ_{max}, we use an average of measured values from modern centric and cold diatom species (Table 2-3) (Davis, 1976; Goering et al., 1973; Guillard & Kilham, 1973). Surface area and volume were calculated using centric diatom frustule dimensions proportional to calculations in Popp et al. (1998), but with radii representative of the samples in our size fractions.

Species	μ_{max} (day^{-1})	K_{μ} (µM)
Porosira glacialis	0.40	
Chaetoceros furcellatus	0.42	
Thalassiosira antarctica	0.60	
Thalassiosira nordenskioldii		0.02
		0.09
Thalassiosira pseudonana		0.04
Chaetoceros debilis		0.18
Chaetoceros gracilis		0.47
Average	**0.47**	**0.16**

Table 2-3: Laboratory measured values of μ_{max} (maximum rate of cell division) and Kµ ($Si(OH)_4$ concentration that limits µ to half μ_{max}) from a range of centric cold diatom species. Average is shown in bold. (Conway et al., 1977; Gilstad & Sakshaug, 1990; Olsen & Paasche, 1986; Paasche, 1975; Thomas & Dodson, 1975).

2.3 Results and discussion

2.3.1 Size specific records of diatom-bound ε_p

We find that size-separated $\delta^{13}C$ and ε_p records show similar values across the measured time period (Figure 2-3), but differ in magnitude of change across the transition of interest. All size fractions of diatom $\delta^{13}C$ (Figure 2-3.1a – 2-3.1g) fluctuate between approximately -29 and -28.5 ± 0.3‰ leading up to Oi-1 from ~35 to 33.7 Ma. At this point, the smaller size fractions (12-20 and 20-41µm) experience an increase in $\delta^{13}C$ to ~ -26 ± 0.3‰. In larger fractions, this increase, if present, does not exceed variation in the record prior to the transition. Following the isotopic minimum at approximately 33.4 Ma at the start of Oi-1, all records temporarily rebound to pre-EOT values (~-28.5‰) before increasing

again to values approaching the peak at Oi-1. Similarly ε_p (Figure 2-3.2a – 2-3.2g) values vary between about 17 and 15 ± 0.3 prior to the EOT to about 33.7 Ma where the 20-41 and 12-20μm fractions drop to ~13.5 ± 0.3. In the large fractions, ε_p continues to fluctuate between ~17 and 14 with the exception of a small peak following Oi-1 to around 17.5 ± 0.3. The rebound to pre-EOT values is observed across all fractions following the drop at Oi-1. Finally, there is a more gradual decline in ε_p through to the end of the record to ~15 ± 0.3.

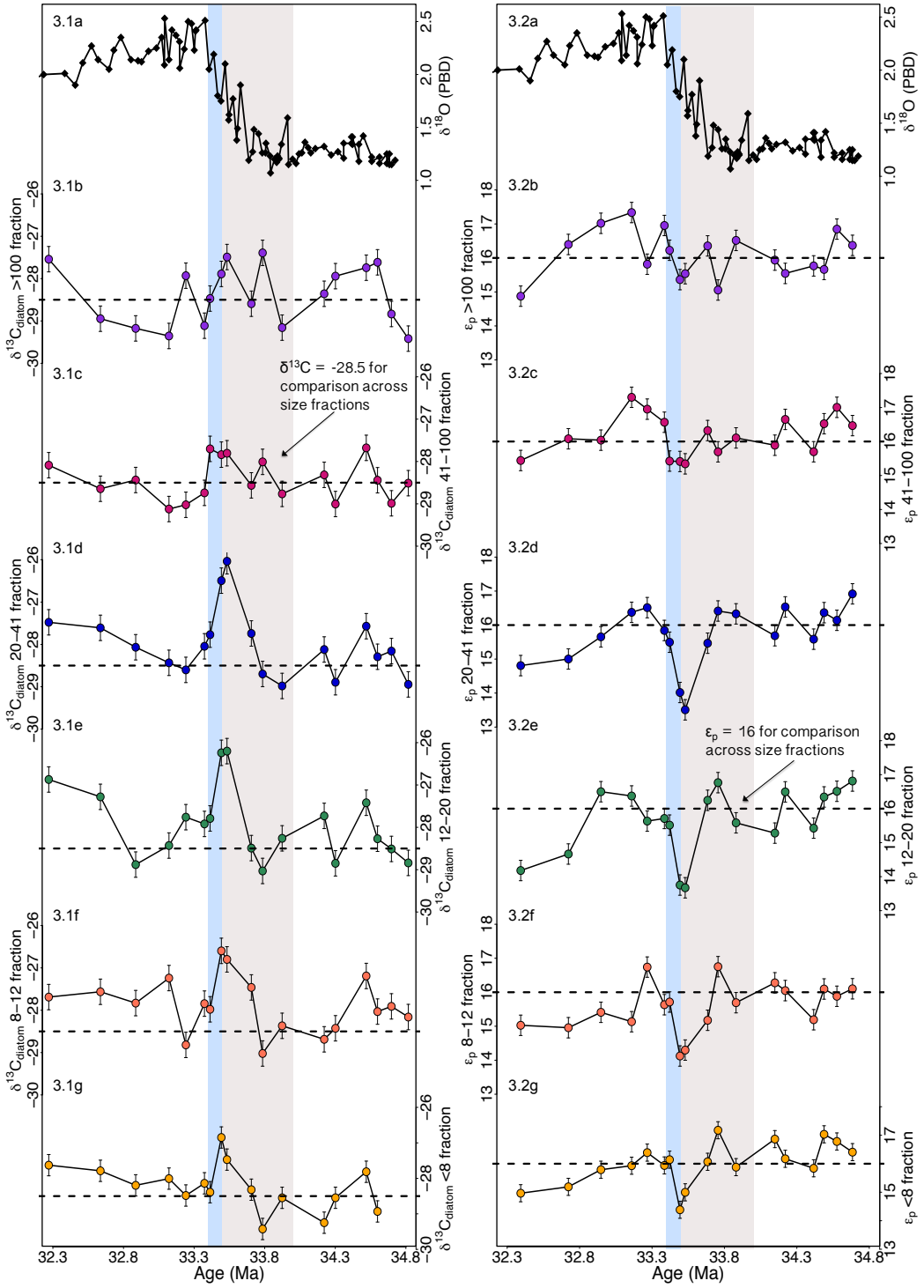

Figure 2-3: Records of (3.1a; 3.2a) high-resolution oxygen isotopes from site ODP 689 in the Southern Ocean (Diester-Haass & Zahn, 1996), (3.1) $\delta^{13}C_{diatom}$ and (3.2) $\varepsilon_{p\ datiom}$ in size fractions (3.1b; 3.2b) >100, (3.1c; 3.2c) 41-100, (3.1d; 3.2d) 20-41, (3.1e; 3.2e) 12-20µm, (3.1f; 3.2f) 8-12µm and (3.1g; 3.2g) <8µm spanning the EOT and Oi-1. The light grey shading represents the EOT and the blue shading represents Oi-1. Error bars denote internal precision at 95% confidence. Dashed lines mark $\delta^{13}C_{diatom}$ at -28.5‰ and ε_p at 16‰ for reference between plots.

2.3.2 Using size and reaction-diffusion kinetics to estimate a threshold of CO_2^{atm}

Diffusion of CO_2 depends on the surface area (SA) of a cell and the requirement for carbon depends on the volume (V). Large cells, with a large V will have a higher requirement for carbon, but a lower SA/V ratio, decreasing the relative diffusion rate of carbon into the cell (Figure 2-4). A simplified view suggests that larger cells will have a higher requirement for CO_2 than smaller cells of the same relative shape (Reinfelder, 2011).

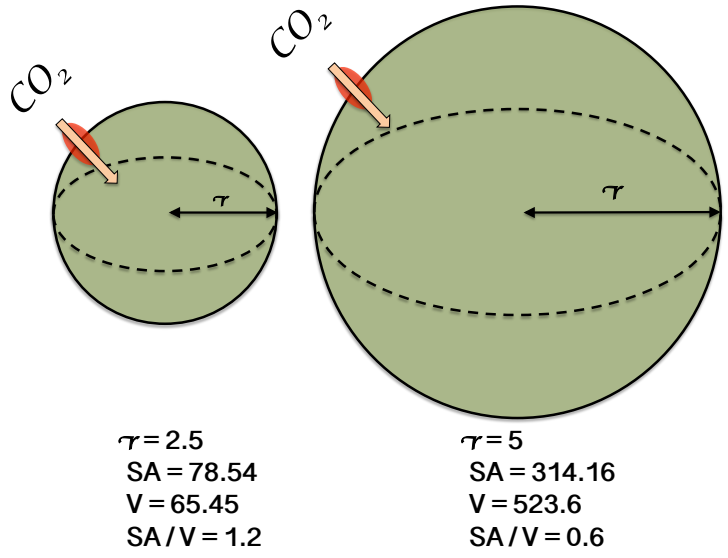

Figure 2-4: Illustration of two hypothetical spherical cells with radii (r) of 2.5 and 5 and calculated surface area (SA), volume (V) and the SA/V ratio. The figure illustrates that larger cells have a larger V, or cell carbon requirement, relative to their SA, or surface through which diffusion of carbon substrate into the cell can occur. A smaller SA/V ratio makes it more difficult for these cells to satisfy their carbon demand.

To probe the differences in our size fractionated ε_p records, we group the fractions into large (> 41μm) and small (12-41μm), representing the two different trends we see in the $\delta^{13}C$ and ε_p records. In the large size group, the magnitude of change in ε_p throughout the record is muted compared to the small size group. When we plot ε_p of the two size groups

(Figure 2-5a) and the difference between them (Figure 2-5b), we can see a distinct divergence in the isotopic signal and a persistent positive offset of small from large beginning at ~33.7 Ma shown by the black dotted line.

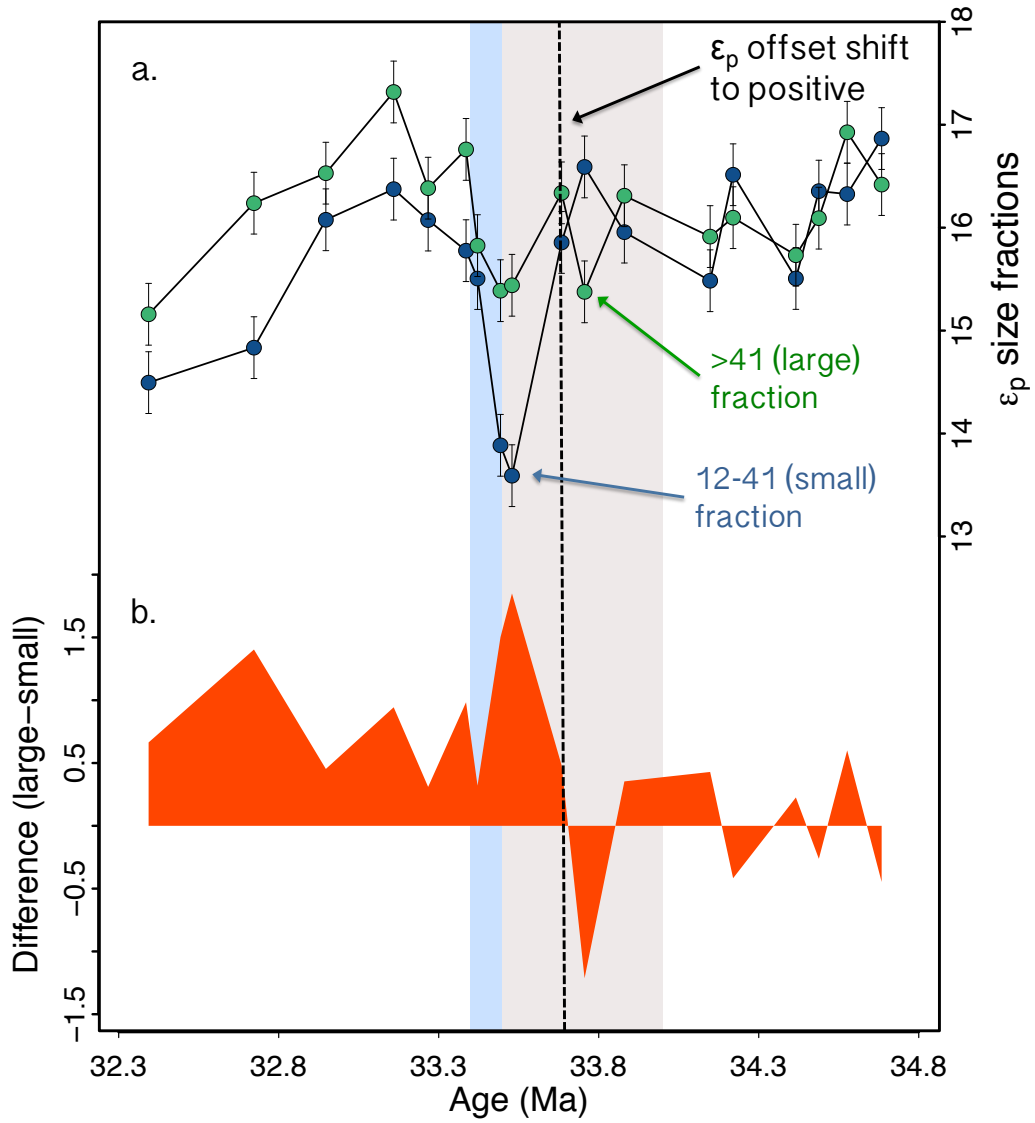

Figure 2-5: Records of ε_p from the small (12-41μm) size group in blue and large (>41) size group in green. In (a.) the two size groups trace each other up to ~33.7 Ma at which point they diverge for the remainder of the record, with the small size fraction consistently lower than the large (b.). Figure 5b. shows the offset of the small from the large size group. The light grey shading represents the EOT and the blue shading represents Oi-1. The black dotted line shows where the offset between the two groups becomes positive for the remainder of the record. Error bars represent 95% confidence in plot 5a. The propagated error when calculating the difference in plot 4b. is 0.4%.

In the modern ocean, most diatom species use carbon concentrating mechanisms (CCMs) to overcome carbon limitation during photosynthesis (Burkhardt et al., 2001; Hopkinson et al., 2011; Medlin et al., 1993; Reinfelder, 2011). However at the EOT, with atmospheric CO_2 estimated to be approximately 4 times that of modern day, it is unknown whether or not cells needed to invest energy into concentrating carbon or could rely on diffusive uptake. We hypothesize that the observed offset between large and small ε_p records may be explained by larger cells, with an insufficient supply of carbon from diffusion, employing or up-regulating a CCM. As a result, larger cells maintain a constant internal carbon pool throughout the transition and exhibit less variation in ε_p. In this scenario, small cells are satisfied by diffusion of CO_2 and are therefore not expressing energy-dependent methods for carbon uptake.

There is evidence for such a difference in carbon isotope fractionation response in culture from Burkhardt et al. (1999) where larger cells demonstrate a critical CO_2 concentration or C_{min} (below which cellular carbon demand was not satisfied by passive diffusion) one order of magnitude higher than the smaller species in their study. The two species identified to have a higher C_{min} also exhibit a reversal in the relationship between ε_p and $[CO_2]$ and minimal trend in ε_p vs. μ/CO_2. This suggests that cells with a high CO_2 requirement may concentrate carbon inside the cell, complicating or possibly eliminating the relationship between growth rate, εp, and $[CO_2]$.

To investigate this hypothesis, we estimate the diffusive requirement of carbon at "steady state," or 2/3 of the maximum diffusion flux of CO_2, for cells at the size boundary between the large and small size groups (41μm). Using the model of reaction-diffusion kinetics of

CO_2 at a cell's boundary layer from Reinfelder (2011), we employ our size groups to estimate the CO_2^{atm} concentration required for cells in the small size group to reach steady state. We use the equation calculating the total reaction-diffusion rate at the surface of the cell (mol $cell^{-1}$ h^{-1}) or Q_T:

$$Q_T = 14.4\pi RD\left[R\left(\frac{k'}{D}\right)^{\frac{1}{2}} + 1\right] \cdot 2/3[CO_2]_{bulk} \quad (2\text{-}10)$$

where R is the cell radius (cm), D is the diffusivity of $CO_{2(aq)}$ in water (cm^2 s^{-1}), k' is the combination of rate constants for hydration of CO_2 by reaction with H_2O and OH^- multiplied by the concentration of OH^-, and $CO_{2(bulk)}$ is the concentration of carbon in the environment. 2/3 of the maximum diffusion flux is assumed when CO_2 at the cell surface is equal to 1/3 of $CO_{2(bulk)}$. In this model, cell carbon is assumed to be 20 fmol C μm^{-3} and CO_2 supply rate is normalized to this value. When we apply the Reinfelder model to cells in the small size group, we calculate a $CO_{2(bulk)}$ concentration of approximately 47 μM or 1,320 ± 100 p.p.m.v. (calculated using Henry's Law) required for cells of that size or smaller to reach steady state using diffusion. From this calculation, we can infer that cells in the large size group (>41 μm) will require CO_2^{atm} higher than 1,320 ± 100 p.p.m.v. to satisfy their diffusive requirement for carbon. If CO_2 was at or below 1,320 ± 100 p.p.m.v. at the excursion, large cells would need to up-regulate the concentration of carbon in the cell. This adds support to our hypothesis and may explain the divergence between the two size groups in Figure 2-5. We therefore infer that just prior to the divergence in ε_p at ~33.7 Ma, CO_2^{atm} must be or drop below ~1,320 ± 100 p.p.m.v. to account for the observed isotopic offset. This model, of course, is theoretical and incorporates a number of

assumptions that add uncertainty to the calculation including difussivity and maximum diffusion flux.

2.3.3 Reconstructing a continuous record of CO_2 from ε_p

To further refine our estimate of CO_2^{atm}, we use $\delta^{13}C_{diatom}$ to create a continuous record across the transition. We use $\delta^{13}C_{diatom}$ from the 12-20 μm size fraction and the regressions between μ/CO_2 and ε_p shown in diatom cultures and diatom field material. We used the 12-20 μm size fraction for reconstruction of CO_2 because 1) the smaller size fractions had a high percentage of broken frustules as well as a greater mix of centric and pennate diatoms as shown in Figure 2-2 and 2) as illustrated above, in the larger size fractions we assume a more complex relationship between ε_p and CO_2^{atm} as a result of active carbon uptake. In addition, the 12-20 μm fraction was the best preserved and contained predominately centric diatoms limited to a radii of 6-10 μm. Egan et al. (2012) also note a larger contribution of radiolarian and sponge material in fractions larger than 20 μm.

As discussed above, ε_p varies in response to $[CO_2]$ as well as growth rate (μ). In this study, we use a constant range of growth rates across the interval. Although this is likely an oversimplification, evidence from diatom and radiolarian silicon isotopes ($\delta^{30}Si$) from Egan et al. (2013) shows a stabilization of $\delta^{30}Si$, representing silica utilization, as well as $\Delta\delta^{30}Si_{1090\ diatom\text{-}689\ sponge}$, a measure of the degree of utilization of supplied silica accounting for ocean-wide shifts in silicon isotope, just prior to the interval observed in this study (~35-32 Ma) (Figure 2-6). This suggests that the change associated with increasing supply and increasing diatom silicic acid utilization of that supply occurs prior to the start of our

record. Across the interval measured in this study, there is no major change in $\delta^{30}Si$ or $\Delta\delta^{30}Si_{1090\ diatom\text{-}689\ sponge}$ coincident with the major event we find in $\delta^{13}C$ (Figure 2-6). We therefore assume that growth rate is not the primary control on ε_p.

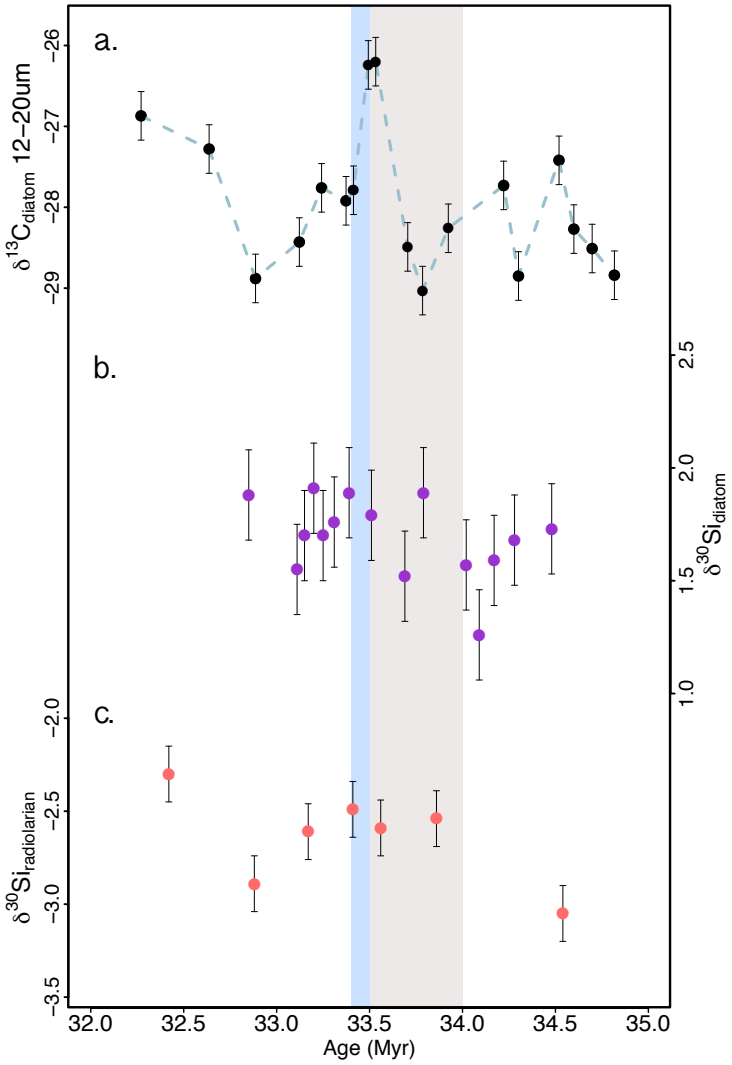

Figure 2-6: Plot of (a.) $\delta^{13}C_{diatom}$ from the 12-20µm size fraction from this study, (b.) silica isotopes from diatom material from site 1090 across this interval and (c.) silica isotopes from sponge and radiolarian material from site 689 (Egan et al., 2013). $\delta^{30}Si_{diatom}$ represents diatom utilization across this interval and sponge/radiolarian $\delta^{30}Si$ represents the silicic acid availability or supply. The difference between these two parameters (plotted in Egan et al., 2013) represents the utilization when normalized to changing concentration and isotopic composition of upwelling waters. Both parameters stay stable within error across the transition studied here and there is no significant change coincident with the peak we observe in $\delta^{13}C_{diatom}$. The light grey shading represents the EOT and the blue represents Oi-1.

A compilation of reconstructed CO_2^{atm} across the EOT from this study, alkenones (Pagani et al., 2011), boron isotopes (Pearson et al., 2009), and nahcolite (Lowenstein and Demacco 2006) is shown in Figure 2-7. The compilation illustrates that a combination of all proxies focuses our estimates of CO_2 at this transformative period in Earth history. Through the late Eocene leading up to Oi-1, estimates of CO_2^{atm} from boron, nahcolite, and this study using the culture calibration from Popp et al. (1998) corroborate that CO_2^{atm} was about 1,000 ± 200 p.p.m.v. Low latitude alkenone estimates predict CO_2^{atm} slightly lower, however, considering the range of possible parameters (i.e. ε_f, proxy vs. modelled temperature, and estimated PO_4^{3-}) applied in Pagani et al. (2011), these estimates encompass the range predicted by the other proxies. High latitude alkenone and values from this study calculated from the field calibration in Rosenthal et al. (2000) estimate higher CO_2^{atm} values prior to Oi-1. Pagani et al. (2011) attributes this offset in alkenone estimates to low mixed-layer nutrient concentrations, difficulty in estimating PO_4^{3-} at high latitude and potential air-sea disequilibrium. In the diatom-bound material, there is uncertainty in growth rate, the absence of SA/V in the field calibration, or other limitations in calibrating the proxy. All proxy estimates have notable uncertainty associated with the various input parameters, however relative agreement in absolute values seems to be emerging from combining the different approaches.

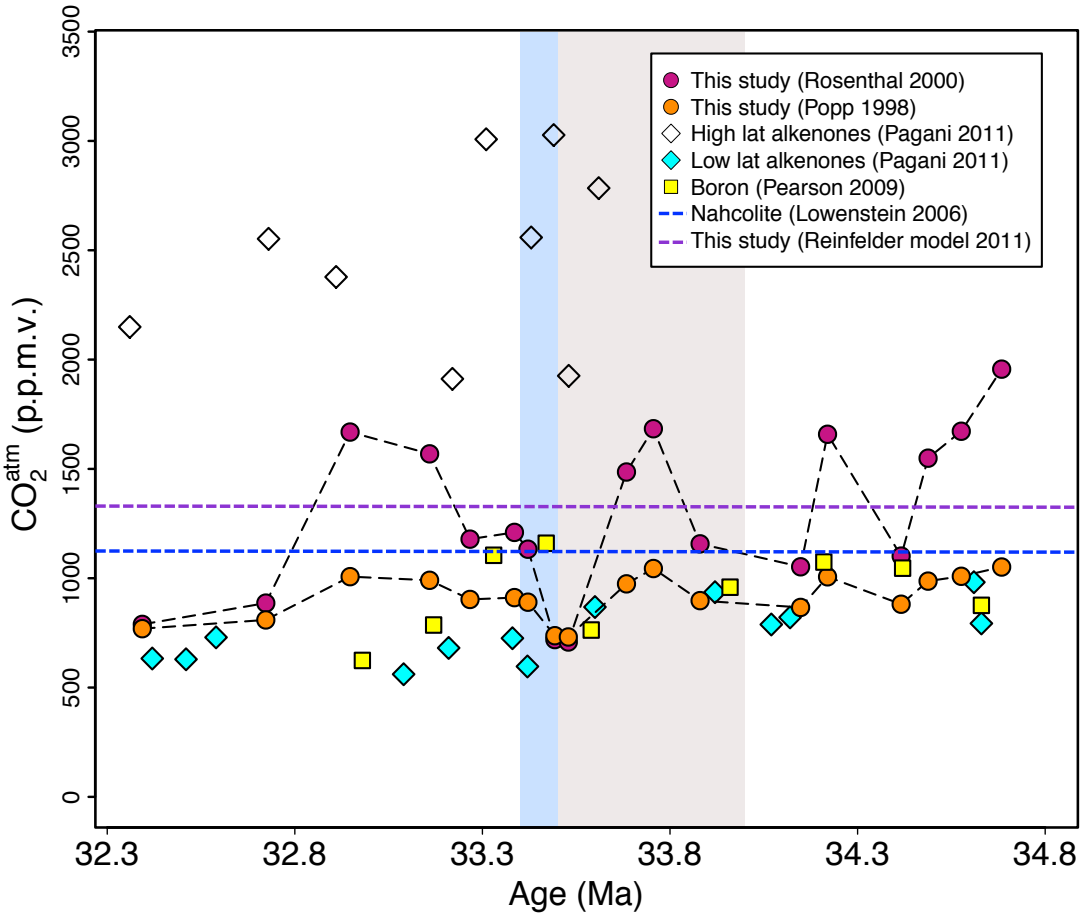

Figure 2-7: Compiled estimates of CO_2^{atm} across the period investigated in this study. Data from this this study culture calibrated (orange), field calibrated (fuchsia), and estimated from the Reinfelder reaction-diffusion model (purple dotted line). Other estimates from high latitude alkenones (open diamond), low latitude alkenones (aqua blue diamond), boron isotopes (yellow square), and nahcolite (navy blue dotted line). We use alkenone data from Pagani et al. (2011) calculated with UK'_{37} temperature estimates and ε_f at 25. The light grey shading represents the EOT and the blue shading represents Oi-1. Records from this study are connected with dotted lines to elucidate trends.

A significant drop in CO_2^{atm} leading into Oi-1 is observed in diatom-bound data in both culture and field calibrations as well as in the record from boron isotopes. Low latitude alkenone estimates support the absolute value of CO_2^{atm} at this time and suggest a gradual decline from pre-EOT CO_2^{atm}. Prior to the EOT, CO_2^{atm} reconstructed from $\delta^{13}C_{diatom}$ fluctuates between 900 and 1,100 ± 200 p.p.m.v. calculated with the culture calibration and between 1,000 and 1,800 ± 200 p.p.m.v. calculated with the field calibration. CO_2^{atm} begins to decline at ~33.7 Ma to between 700 and 800 ± 100 p.p.m.v. in both data sets until the beginning of Oi-1 at ~33.4 Ma. Following this drop, our records experience a two-step rebound to pre-EOT CO_2^{atm} values (up to 1,000 p.p.m.v. calculated with culture data and 1,600 ± 200 p.p.m.v. calculated with field data) until about 32.8 Ma where we see a final gradual decline to the end of our record. Our record terminates at about 32.5 Ma when reconstructed CO_2^{atm} has dropped again to ~800 ± 200 p.p.m.v.

	$[Si(OH)_4]$	μ (day^{-1})	V/SA	Temp (°C)	Salinity	ε_f
High	100	0.55	3.3	25	34	25.3
Low	10	0.39	2.5	17	34	23

Table 2-4: Range of parameters used to calculate high and low brackets for reconstructed CO_2^{atm} plotted in Figure 2-8.

Diatom reconstructed CO_2^{atm} supports the suggestion by Pearson et al. (2009) that CO_2^{atm} experienced a significant decrease just prior to the onset of glaciation in Antarctica (Oi-1) (Figure 2-8). The high and low brackets shown in Figure 2-8 are calculated using the parameters outlined in Table 2-4. The difference between the records may be explained in

part by differences in geographic location, age model, and the sensitivity/calibration of respective proxies. The boron record comes from foraminifera in the equatorial Indian Ocean while our record is of Atlantic Southern Ocean diatoms. However, the main features in the records are consistent, including the decline through the EOT leading into Oi-1. All three records simultaneously reach a minimum at the end of the EOT and just before the onset of Oi-1. The field-calibrated diatom-record, however, estimates a higher range of values prior to and following the event. All records show a recovery following the drop into Oi-1 consistent with original observations in the alkenone records (Pagani et al., 2005). In the boron record, this recovery is rapid compared to the two-step gradual recovery through to 32.8 Ma we see in this study. The recovery in CO_2^{atm} exhibited across all proxies following this major transition suggests strong feedbacks in the climate system, such as silicate weathering and marine carbon burial, causing an overshoot and recovery in CO_2^{atm} as predicted in carbon cycle models (Zachos and Kump, 2005).

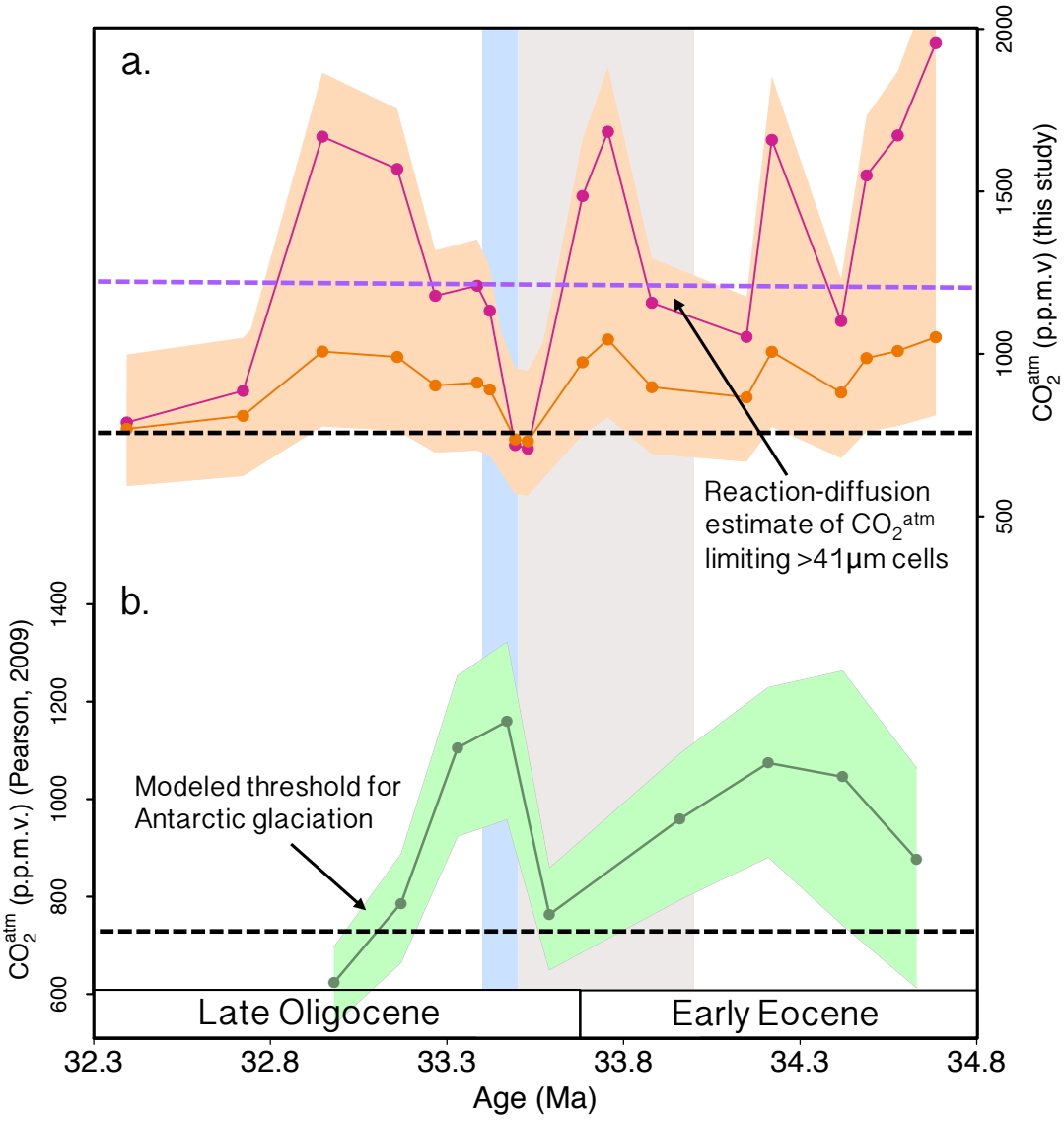

Figure 2-8: Plot (a.) shows diatom-bound reconstructed CO_2^{atm} culture calibrated (orange) and field calibrated (fuchsia) with a bracket of uncertainty in our calculations (shown in light orange) incorporating the effects of silica concentrations on growth rate, increased growth rate across the interval, and V/SA ratios present in 12-20 µm size fraction for culture calibrated data. The bracket also encompasses field calibrated CO_2^{atm} estimates, however this calibration does not incorporate volume or surface area (Rosenthal et al., 2000). Table 2-4 shows calculation parameters for the high and low CO_2^{atm} brackets shown on this plot. Plot (b.) shows boron reconstructed CO_2^{atm} (green) with the published range of uncertainty. The light grey shading represents the EOT and the blue represents Oi-1. The black dotted lines denote DeConto's estimate of the CO_2 threshold for glaciation (750 p.p.m.v.) and the purple dotted line represents the Reinfelder reaction-diffusion estimate of 1,320 p.p.m.v. from this study.

2.3.4 Considerations for future application: constraining the diatom-bound CO_2^{atm} proxy

The agreement of our record with existing CO_2^{atm} data, other paleoproxies, and modelling of CO_2^{atm} using a reaction-diffusion model gives us confidence in proxy compilations for providing quantitative insight into paleo-CO_2. The use of various methods for CO_2^{atm} reconstruction is essential to solidify our understanding of the concentration and trends in CO_2^{atm} and the role of CO_2^{atm} in driving glaciation at the EOT. However, we must address the limitations of this study. This work represents one site in the Southern Ocean, in an area of high diatom productivity where diatom-bound $\delta^{13}C$ can be measured. Samples from this area may be impacted by the turbulent and high nutrient environment required by diatoms, but $\delta^{30}Si$ from diatom material suggests that near-modern day conditions of upwelling and utilization were already established at Site 1090 before this crucial transition (Egan et al., 2013).

Although Popp et al. (1998) demonstrates that upon consideration of SA/V ratio and growth rate, the relationship between ε_p and μ/CO_2 is linear across a range of species, culture studies of many more modern analog species to our samples would be ideal to clarify our inferences. More precise isolation of single species in sediments will also allow us to strengthen the application of a calibration to ancient material; however, the similarity between our size fractions suggests this may be unnecessary. Finally, difficulty in measuring accurate estimates of growth rate, an important parameter in calculating ε_p, adds complexity in this proxy. Although estimates of silica utilization have been made using $\delta^{30}Si$, and can give insight into diatom productivity, the interpretation and resolution

of this data poses challenges. We know that there is a period of significant change at this location in the Southern Ocean prior to the interval we present. As the change seems to stabilize prior to our data (Egan et al., 2013), we are assuming no change in the silica supply or utilization across the period in this work.

Finally, we note that the models of carbon fixation used in this study greatly simplify the diversity in carbon fixing strategies between species of marine algae. A better understanding of the mechanisms controlling carbon fixation and the diversity across organisms used for paleo-climate reconstruction will play an important role in the interpretation of ancient chemical data in the future. Constraining these limitations should strengthen the application $\delta^{13}C$ to understand CO_2^{atm}.

2.4 Summary and Conclusions

A novel and well-preserved source of organic carbon refines our estimate of Southern Ocean CO_2^{atm} at the most transformative climate transition the Earth has seen in the past 65 Ma. Diatom-bound organic carbon isotopes from the Atlantic sector of the Southern Ocean elucidate consistency in the response of diatom organic material and other CO_2^{atm} proxies to changing climatic conditions. Applying the relationship derived from culture and field studies between ε_p and CO_2 in addition to the reaction-diffusion equations for different size cells allows us provide a reconstruction of atmospheric CO_2^{atm} through the transition as well as to pinpoint CO_2^{atm}. Our estimates of CO_2^{atm} support the hypothesis that a significant global decline leading into Oi-1 acted to trigger glaciation and further constrains the timing and absolute values of CO_2^{atm} before and during the event. In

addition, the record confirms salient features seen in the boron isotope-derived CO_2 record including a recovery of CO_2^{atm} to pre-glaciation values due to climatic feedbacks after maximum ice growth. This work adds confidence to our interpretation of CO_2^{atm} across the Eocene-Oligocene climatic transition and recognizes the potential of diatom-bound organic material as an important source of ancient climatic information.

Chapter 3: Trade-offs in the carbon fixing system in marine Haptophyta and Heterokontophyta algae

Contributions: This work is part of a larger project funded by Professor Ros Rickaby's ERC proposal and has been carried out by PhD students Dr. Jodi Young, Dr. Renee Lee, Maeve Eason-Hubbard and myself. Dr. Maxim Karpralov and Dr. Nick Kruger from the Department of Plant Sciences in Oxford aided in protocol optimization. Some of the kinetic measurements in this study were done in collaboration with Dr. Jodi Young, Dr. Spencer Whitney and Dr. Rob Sharwood at the Australian National University. Pyrenoid morphologies used in this study were characterized by Maeve Eason-Hubbard and δ-carbon anhydrase measurements were done by Dr. Renee Lee. Where others have contributed, it is highlighted explicitly throughout the chapter.

Abstract

Marine primary producers, especially those that form biomineral shells, are key drivers of biogeochemical cycles in the ocean and form the base of the marine food chain. Understanding the mechanisms and machinery used in the photosynthesis reactions is essential for elucidating the photosynthetic potential, relative efficiency and geologically relevant isotope fractionation for these organisms. In biogeochemical models and paleoclimate proxies, estimates of photosynthetic parameters and carbon used for marine algae are often extrapolated from other, well-studied photosynthetic organisms. In this study we establish an understanding of the diversity in photosynthetic enzyme kinetics, enzyme production, and morphology of photosynthetic structures specifically across the geologically relevant Haptophyta and Heterokontophya algae. We find a large amount of variation in these parameters across the species studied and conclude that these groups of algae do not show the same linear trade-offs between kinetics observed across more diverse primary producers. We report novel trends in kinetic trade-offs as well as identify trade-offs between whole cell strategies for achieving an efficient carbon fixing system. The present study provides the largest data set of Rubisco kinetics in marine algae to date and gives new insight into the role of carbon concentrating mechanisms (CCMs) and efficiency of photosynthesis in this group.

3.1 Introduction

3.1.1 Evolution of carbon concentrating mechanisms in marine algae in response to changing environmental [CO_2]:[O_2]

The evolution of the carbon fixing enzyme D-Ribulose 1,5-bisphosphate carboxylase/oxygenase in the Achaean world, characterized by high atmospheric carbon dioxide (50-fold higher than modern concentrations) and negligible oxygen (Berner, 2006, 2009; Tabita et al., 2008), has left the enzyme ill suited to function as the atmospheric make-up has shifted over geological time. The inefficiencies of the Rubisco enzyme, i.e. its ability to use O_2 as an alternative substrate, low affinity for CO_2, and low catalytic rate, were easily overcome by early primary producers, as oxygen was not a readily available substrate in the environment 3.5 billion years ago. With the advent of oxygen evolving photosynthesis by cyanobacteria, levels of O_2 in the atmosphere have risen since the early Proterozoic (2.5 Ga), and more dramatically from 1.5 Ga, while CO_2 levels have subsequently declined through to modern day (Canfield et al., 2005) (see Figure 1-1).

The modern atmosphere with inhibitory levels of O_2 and limiting levels of CO_2 for Rubisco has put evolutionary pressure on oxygenic primary producers. This burden is exacerbated for aquatic photosynthesizers due to even lower availability of CO_2 in the oceans as a result of slow diffusion (~10,000 times slower in water than in air), pH controlled partitioning of carbon, as well as physical constraints such as mixing in the surface ocean (Zeebe & Wolf-Gladrow, 2001).

The question remains as to whether or not this environmental pressure since the evolution of Rubisco has resulted in any notable improvements in the kinetic function of the enzyme. While some argue that the use of oxygen as a substrate is an "inherent architectural constraint" that cannot be ameliorated by natural selection (Gould and Lewontin, 1979; Somerville et al., 1984), others suggest that the significant natural variation in the catalytic abilities of photosynthetic organisms points toward directed adaptation of the enzyme (Jordan and Ogren, 1981; Tcherkez et al., 2006).

Assessment of kinetic diversity in Rubiscos from divergent groups of primary producers shows that an optimization in one kinetic parameter generally results in a decline in efficiency of another (Tcherkez et al., 2006; Savir et al., 2010). If selective improvements in enzyme kinetics result in subsequent relaxation elsewhere as proposed by Tcherkez et al. (2006), evolutionary changes in the enzyme may have a limited ability to improve the overall photosynthetic ability of Rubisco. In the terrestrial system, C_4 and CAM plants have circumvented this inherent limitation by making anatomical and biochemical changes in the cell structure to create a subcellular environment for Rubisco more conducive to carboxylation over oxygenation (Sage, 2004; 2014).

This approach has been extremely beneficial to C_4 plants, allowing them to relax their affinity for CO_2 and therefore increase the turnover rate of carboxylation (Bainbridge et al., 1995; Jordan and Ogren, 1984; Long, 1999; Sage et al., 2002; Sharkey, 1988). Ultimately this adaptation has allowed C_4 plants to avoid the energy wasting oxygenation reaction and utilize resources more efficiently. By reducing the amount of enzyme

required, C_4 plants are able to survive in more arid and nutrient limited environments (Lara and Andreo, 2011).

Characterization of the initial steps in carbon assimilation in marine algae has illuminated the possibility of the C_4 pathway in aquatic organisms. The first evidence for an algal C_4 pathway came from marine diatom C_4 carboxylase activities and identification of C_4 acids during photosynthesis (Beardall et al., 1976; Morris et al., 1980). Further work identified C_4 compounds in short-term ^{14}C labelling experiments in the marine diatom *T. weisflogii* (Reinfelder et al., 2000; 2004) and in the pennate diatom *Haslea ostrearia* at growth-saturating light levels (Rech et al., 2008). Genes required for the C_4 pathway, including PEPC, PEPCK, PPDK, ME and MDH, have been identified in the diatoms *T. pseudonana* and *P. tricornutum* (Armbrust et al., 2004; Montsant et al., 2005). In conclusion, while various lines of evidence exist to support the presence of the C_4 pathway in marine primary producers, to date few species have been examined and differences in methodologies complicate the results (Reinfelder, 2011).

A unique structural feature in eukaryotic algae known to be associated with the Rubisco enzyme is termed the pyrenoid. To date, the individual components and exact functional implications of the pyrenoid remain relatively elusive when compared to other components of the CCM. The structure of the pyrenoid in the algal species *Chlamydomonas reinhardtii* is made up of a starch sheath (Engel et al., 2015; Moroney et al., 2011), but significant diversity in pyrenoid perimeter has been observed across divergent species of marine eukaryotes (Badger et al., 1998; Bedoshvili et al., 2009). No shell proteins have been identified to date, but a macromolecular Rubisco complex may

not need a shell structure if the activity of carbonic anhydrase (CA) is sufficient within the pyrenoid (Rae et al., 2014; Reinhold et al., 1987; 1991; Villarejo et al., 1996). From the available data, a pyrenoid-based CCM model is one of the most effective mechanisms in marine eukaryotic algae for increasing the internal carbon pool for Rubisco (Badger et al., 1998).

The structural and genetic diversity in eukaryotic algae is large (Badger et al., 1998), but relatively little is known about their kinetic diversity when compared to higher land plants and prokaryotic marine organisms. Due to their relative complexity, marine eukaryotic organisms are generally more difficult to manipulate and genetically transform. In this study we aim to increase the amount of data on the diversity of photosynthetic machinery in these organisms. Our interest in this information stems not only from the relative paucity of data in these organisms, but also from their importance in the marine environment and use for biomarkers in the geological record.

3.1.2 Rubisco forms and structure

Four distinct forms of the Rubisco enzyme exist in nature. Marine algae, as well as the majority of all carbon fixers, have a Form I Rubisco holoenzyme. The other form of Rubisco used in oxygenic photosynthesis is Form II, a dimer of two large subunits (LSU) found in dinoflagellates and some prokaryotes (Morse et al., 1995). Other forms include Form III, a decamer of five large LSU dimers found in archaeoabacteria (Finn & Tabita, 2003; Maeda et al., 1999). Form IV, also known as a Rubisco-like protein (RLP), does not

carry out the photosynthetic reaction (Hanson & Tabita, 2001; Li et al., 2005). Figure 3-1 shows representative structures of Rubisco forms I-IV (taken from Tabita et al., 2008).

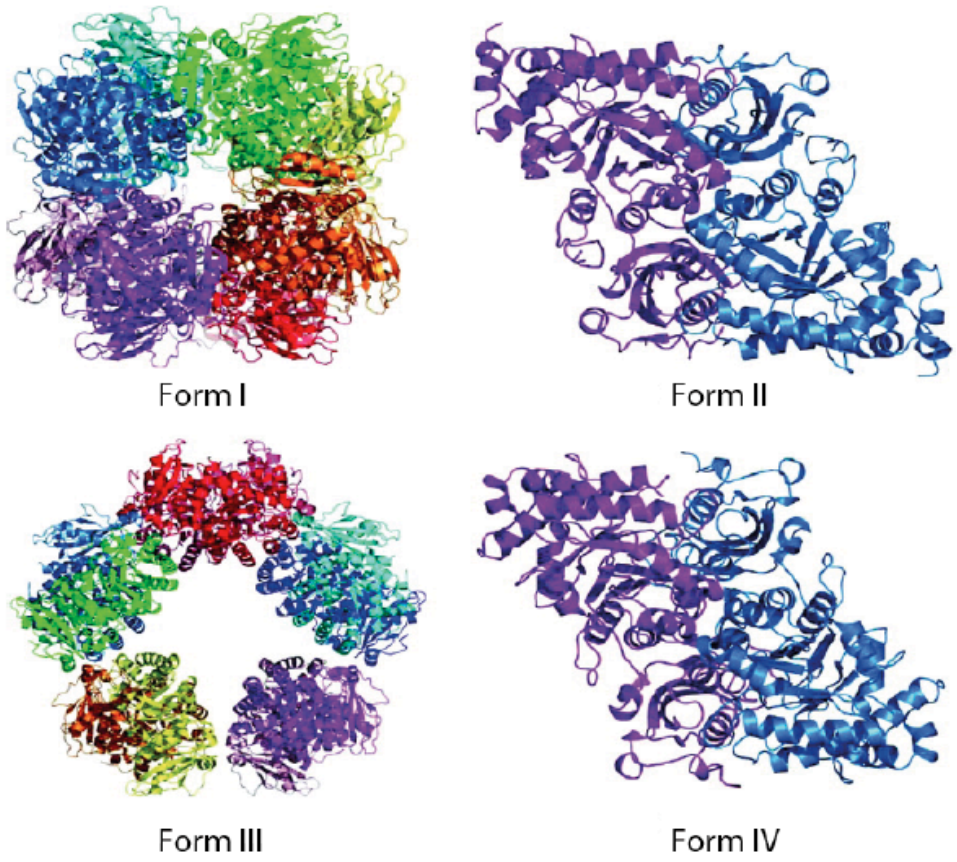

Figure 3-1: Structures and configurations of Rubisco froms I-IV (taken from Tabita et al., 2008).

Form I Rubisco is composed of eight large (51-58 kDa) subunits (LSU) and eight small (12-18 kDa) subunits (SSU), which together form a hexadecameric structure with a molecular mass of ~560 kDa, one of the largest enzyme complexes found in nature (Baker et al., 1975). The functional unit of Form I Rubisco is made up of four pairs of LSU dimers capped on each end by four SSUs. Form I Rubisco, responsible for most primary carbon fixation, can be further classified into Forms IA, IB, IC and ID on the basis of molecular genetic evidence. Form IA is found in α-cyanobacteria (e.g. *Prochlorococcus* spp. and

Synechococcus), Form IB is predominantly found in β-cyanobacteria (e.g. *Synechocystis*), green algae and higher plants, Form IC is typically found in photosynthetic bacteria and Form ID is found in all non-green algae (e.g. eukaryotic red and Chrysophyta alga) (Spreitzer & Salvucci, 2002; Tabita et al., 1999; 2008).

The classic L8S8 hexadecamer configuration has been observed in crystal structure. Figure 3-2 shows the crystal structure of Rubisco enzymes from spinach (a.) and the red algae *Galdiera partita* (b. and c.) (Sugawara et al., 1999). Comparing *G. partita* and spinach Rubisco sequences, the large subunit has approximately 60% sequence identity and the small subunit has approximately 30%, however, as reported in Sugarwara et al. (1999), there is minimal difference in the overall crystal structure between the two complexes. *G. partita* is of particular interest as it has the highest yet reported specificity value (discussion of the significance of kinetic specificity to follow) of 238 (Sugarwara et al., 1999), making the small amount of structural variation from other Rubisco crystal structures perplexing.

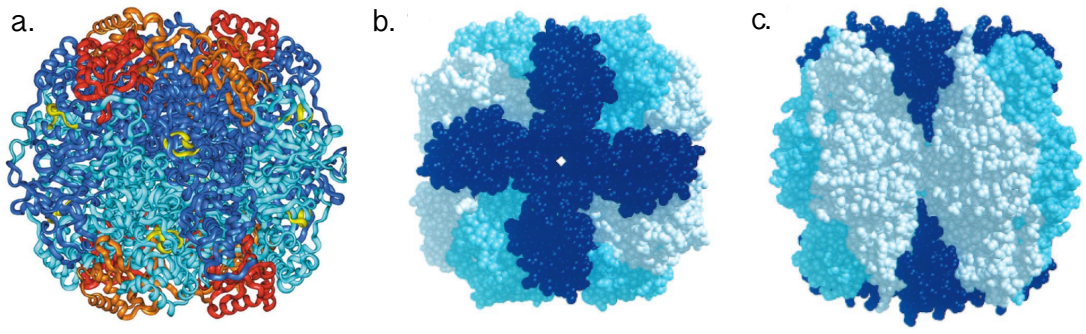

Figure 3-2: Stereo image of (a.) spinach Rubisco X-ray crystal holoenzyme made up of 8 large subunits (dark and light blue) and eight small subunits (red and orange). Yellow denotes the active sites formed between two neighboring large subunits (Andersen 1979). Figures (b.) and (c.) show the crystal structure of activated *G. partita* Rubisco. The large subunit is represented by cyan and light blue/grey and the small subunits are shown in dark blue. 4-fold axes of perpendicular small subunits are displayed in (b.) and (c.) shows large subunits perpendicular to this 4-fold structure displayed as parallel pillars dispersed between each axis of small subunits (Sugarwara et al., 1999).

3.1.3 Rubisco activation and reactions

The activation of the Rubisco enzyme starts with the formation of an enzyme-CO_2 complex and is dependent on the concentration of CO_2 and pH at the active site (Eqns. 3-1 and 3-2). The second rapid and irreversible binding of Mg^{2+} takes the enzyme from a catalytically incompetent to a catalytically competent enzyme priming it for the binding of RuBP (Jensen & Bahr, 1977; Spreitzer & Salvucci, 2002).

$$E_{(inactive)} + CO_2 \overset{slow}{\Longleftrightarrow} E \cdot CO_{2(inactive)} \quad (3\text{-}1)$$

$$E \cdot CO_2 + Mg^{2+} \overset{fast}{\Longleftrightarrow} E \cdot CO_2 \cdot Mg^{2+}_{(active)} \quad (3\text{-}2)$$

Once activated, Rubisco binds RuBP and substrate CO_2 to form the intermediate 2,3-enediol(ate) (Harpel et al., 1996; 1998). The addition of the gaseous substrate CO_2 (or O_2) to the enol-RuBP is the partial reaction that regulates the rate and specificity of the overall carboxylation (or oxygenation) reaction (phase 1 Figure 3-3). The six-carbon transition state is hydrolysed by H_2O and the bond between C-2 and C-3 in RuBP is broken and two molecules of 3-phosphoglycerate (carboxylation) or one molecule of 3-phosphoglycerate and one molecule of 2-phosphoglycolate (oxygenation) are formed (phase 2 Figure 3-3). This irreversible reaction produces 3-phosphoglycerate which is subsequently converted to 1,3-bisphosphoglycerate using ATP as an energy source (Chen et al., 1995; Pierce et al., 1986). Finally, after the release of one Glyceraldehyde-3-phophate (G3P) as a sugar product, the remaining five G3P produced in the reaction are used for the regeneration of RuBP with energy from ATP (phase 3 Figure 3-3).

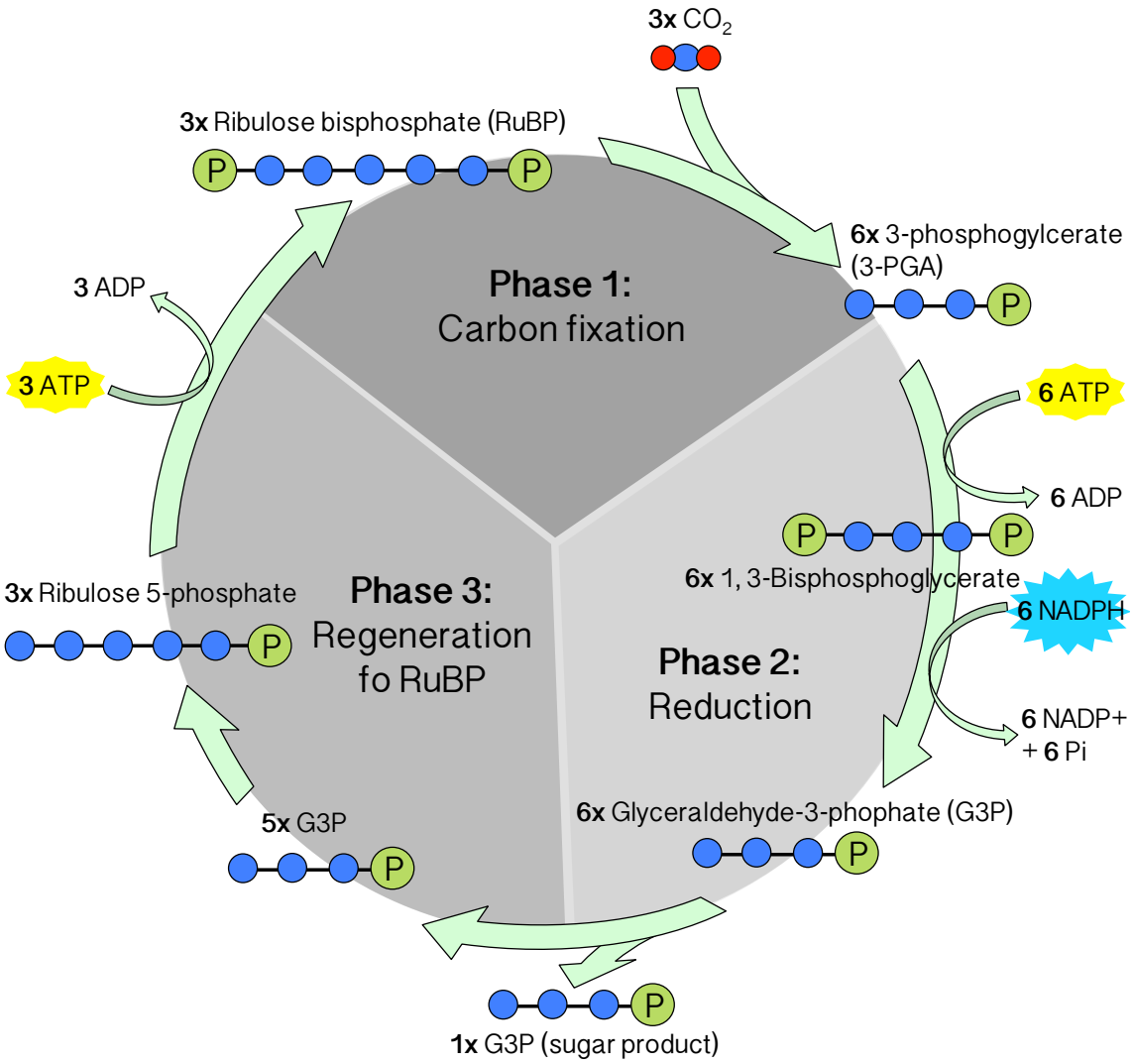

Figure 3-3: Diagram illustrating the processes in the dark reactions of photosynthesis. Phase 1 shows the carboxylation or fixation of CO_2 carried out by the Rubisco enzyme. Phase 2 is the reduction of the six-carbon transition state that is then hydrolysed by H_2O and the bond between C-2 and C-3 in RuBP is broken and two molecules of 3-phosphoglycerate and one G3P is released as the sugar product. Finally phase 3 is the regeneration of the remaining 5 G3P to RuBP to restart the reaction.

3.1.4 Rubisco kinetics

The kinetic parameters measured in this study, Michaelis-Menten half saturation constants for CO_2 (K_c) and O_2 (K_o), turnover rate for carboxylation (K_c^{cat}) and oxygenation (K_o^{cat}) and the specificity for carboxylation over oxygenation ($S_{c/o}$), describe the function and rate of the chemical processes carried out by the Rubisco enzyme. Building an understanding of how all the kinetic parameters differ within individual Rubisco enzymes will provide new insight into the function of the enzymes in different subcellular environments.

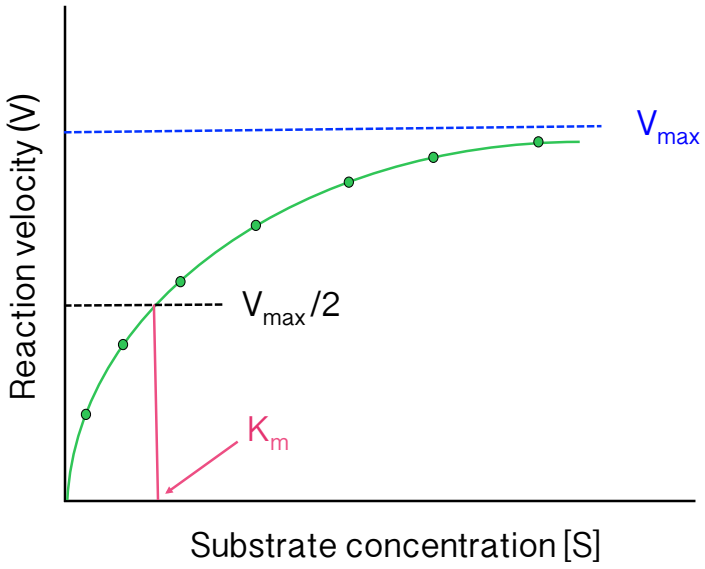

Figure 3-4: Simple Michaelis-Menten curve illustrating the kinetic parameters measured in this study. The plot shows how the reaction velocity (V) of a biochemical reaction involving a single substrate will evolve as the concentration of the substrate increases [S]. The V_{max} parameter shown in blue shows the maximum possible rate the reaction can achieve at saturating substrate concentrations. K_m shown in pink is the concentration of substrate at ½ of V_{max}. These parameters together describe the function and rate of chemical processes.

Michaelis-Menten half saturation constants (K_m) represent the amount of substrate at which the given reaction reaches half its maximum velocity (Figure 3-4). This parameter

represents the relative affinity of the enzyme for a given substrate. A higher affinity (lower K_m) means the enzyme is more efficient at recognizing and binding the substrate. In the case of CO_2, the cell will benefit from a high affinity Rubisco (low K_c) to carry out the carboxylation reaction and vice versa for O_2 and the oxygenation reaction. The turnover rate of a given reaction is calculated using the maximum velocity of the reaction (V_{max}) shown in Figure 3-4, and normalized to the number of Rubisco active sites. For CO_2 fixation, a cell will benefit from a high turnover rate for carboxylation.

Rubisco's specificity factor (Ω or $S_{c/o}$) is expressed as the ratio of the catalytic efficiency of carboxylation (V_c/K_c) to oxygenation (V_o/ K_o) shown in Eqn. 3-3 (Laing et al., 1974; Spreitzer & Salvucci, 2002).

$$S_{c/o} = \frac{V_c K_o}{V_o K_c} = \frac{v_c}{v_o} \times \frac{[O_2]}{[CO_2]} \quad (3\text{-}3)$$

Eqn. 3-3 expresses that $S_{c/o}$ also describes the ratio of the velocity of carboxylation (v_c) to that of oxygenation (v_o) when the concentrations of O_2 and CO_2 are known (Jordan et al., 1981). The specificity factor is a useful kinetic parameter to assess how well an enzyme differentiates between its substrates. However, as it is a ratio, it can be difficult to decouple the individual effects of the different kinetic parameters. Table 3-1 defines the kinetic parameters discussed in this section for reference.

Parameter	Definition
K_c	Michaelis-Menten half saturation constant for CO_2
K_o	Michaelis-Menten half saturation constant for O_2
V_{max}	Maximum velocity (rate) of a biochemical reaction
K_c^{cat}	Turnover rate for carboxylation (V_{max} of carboxylation normalized to Rubisco active sites)
K_o^{cat}	Turnover rate for oxygenation (V_{max} of oxygenation normalized to Rubisco active sites)
Ω or $S_{c/o}$	Ratio of catalytic efficiency of carboxylation (V_c/K_c) to oxygenation (V_o/K_o)
K_c^{cat}/K_c	Carboxylation efficiency
K_o^{cat}/K_o	Oxygenation efficiency

Table 3-1: Reference table of kinetic parameters referred to throughout this chapter.

Studies have found that kinetic differences in Rubiscos from different primary producers generally show a system of trade-offs between optimization and relaxation. The trade-off between K_c and K_c^{cat} is illustrated by Savir et al. (2010) and Tcherkez et al. (2006). Tcherkez et al. (2006) (for original plots see appendix Figures S-1, S-2 and S-3) hypothesize that an increase in affinity for CO_2 is a result of a shift to a more product-like transition state of CO_2, differentiating the chemical structure and allowing Rubisco to identify it more easily. This in turn causes the Rubisco to bind more tightly to the product later on in the reaction slowing down the turnover rate (Tcherkez et al., 2006). Due to the system of trade-offs undergone when acquiring catalytic changes, it has been a challenge for scientists to engineer a kinetically "better" Rubisco enzyme (Whitney et al., 2011).

In this study we present the largest dataset of kinetic information from eukaryotic marine algae, from the groups *Bacillariophyceae*, *Calcihaptophycidae* and *Pavlovophyceae*. The data provides insight into the extent of natural variability in Rubisco kinetics from these

closely related groups. Here we reinvestigate the correlations observed by Tcherkez et al. (2006) in aquatic eukaryotic organisms to see if we find the same trade-offs in the kinetic system. Finally, we look at the kinetic data in relation to other measured photosynthetic machinery in these organisms. This study presents a large amount of new kinetic information, allowing us to make novel hypotheses about carbon fixation for the currently understudied, but environmentally significant biomineralizing eukaryotic marine algae.

3.1.5 Overview of pyrenoid morphologies in marine eukaryotes

The exact structure and function of the pyrenoid remains elusive in many ways, however diversity in algal pyrenoid morphologies is well documented (Bedoshvili et al., 2009; Bendif et al., 2011; Giordano et al., 2005; Griffiths, 1970; Moroney and Somanchi, 1999; Tortell, 2000). From transition electron microscopy (TEM) images, we have identified three main morphologies in the haptophyte and diatom algae of interest in this study, outlined in Figure 3-4 below.

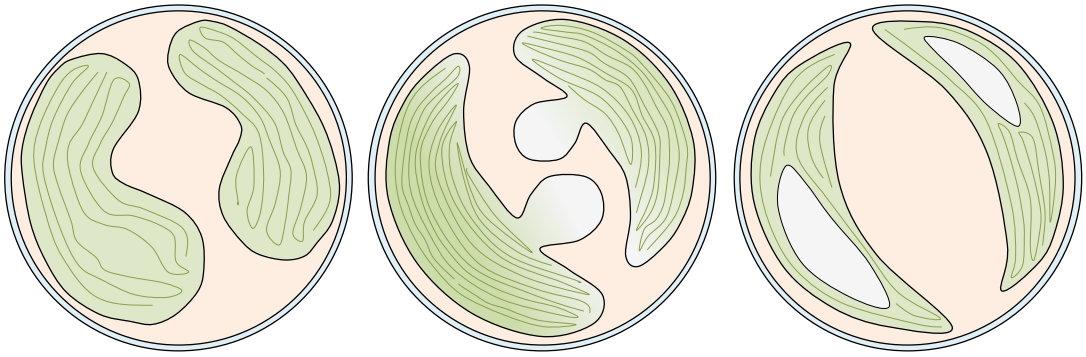

Figure 3-4: Simplified schematic of the pyrenoid morphologies to be discussed in the present study. (a.) shows a cell with two chloroplasts but lacking a pyrenoid. (b.) illustrates a cell with two bulging pyrenoids, importantly they bulge to the interior of the cell. It has also been observed for pyrenoid to bulge towards the cell exterior. (c.) shows two pyrenoids completely immersed within the chloroplast. In all cases the cytoplasm is shown in beige, the chloroplast is green and the pyrenoid is shown in light grey.

Figure 3-4a illustrates a simple schematic of a cell lacking a pyrenoid where the Rubisco resides throughout the chloroplast structure. In cells with a pyrenoid (Fig 3-4b and 3-4c), between 50-90% of the Rubisco is thought to be within the pyrenoid structure (Borkhsenious et al., 1998; Griffiths, 1970), indicated in grey in Figure 3-4. The pyrenoid has been shown to increase internal C_i pools, have increased CA activity as well as contain carbonic anhydrase localized within the Rubisco dense structure (Badger et al., 1998; Tachibana et al., 2011). We presume that the pyrenoid provides a high CO_2, low O_2 environment for the Rubisco enzyme that is largely separated from the O_2 producing light reactions.

This three-part study introduces a large amount of new data on carbon fixation in eukaryotic marine algae. We aim to put the data in the context of kinetics trade-offs and diverse strategies for achieving sufficient carbon fixation. In part one of this study, we look at how the presence of a pyrenoid influences the affinity of Rubisco for CO_2. In part two, we take a closer look at 4 species of marine algae with 3 distinct pyrenoid morphologies to see how the entire suite of kinetic variables varies with pyrenoid morphology. And finally in part three we look more broadly at cell trade-offs and the potential physiological impacts of different carbon fixing machinery.

3.2 Methods

3.2.1 Culturing

Culturing was carried out in the Rickaby microbiology laboratory in the department of Earth Sciences at the University of Oxford and at the Research School for Biological

Sciences and Medicine at the Australian National University. At the University of Oxford, algal strains were obtained from Roscoff Culture Collection (RCC) (http://www.sb-roscoff.fr/Phyto/RCC/) and Plymouth Culture Collection of Marine Microalgae (PLY) (http://www.mba.ac.uk/culture-collection/) and grown in batch or semi-continuous batch cultures. All haptophyte species were grown in natural seawater (NSW) from the Marine Biological Association in Plymouth (MBA) enriched with K/2 nutrients, trace metals, and vitamins (Guillard, 1975). Bacilariophyceae species were grown in K media plus silicon (Si). After addition of nutrients, NSW was filtered through a Millipore Steri-cup 0.22 µm filter, bubbled with air and titrated to pH 8.2 by adding 0.2M NaOH. All cultures were carried out in 2.7 L or 10 L Nalgene® polycarbonate flasks or carboys. Cultures were illuminated by daylight fluorescent bulbs maintaining a light intensity of ~150 µmol photons m^{-2} s^{-1} (approximately photic zone irradiance) at 15°C. A 16:8 light:dark cycle was maintained throughout all experiments. Cell counts were taken throughout the growth period and all cultures were harvested during early to mid-exponential growth phase.

At the Australian National University, algal strains were obtained from the Australian National Algae Culture Collection CSIRO (http://www.csiro.au/Organisation-Structure/National-Facilities/Australian-National-Algae-Culture-Collection.aspx) and grown in batch culture in a constant temperature lab space. Cultures were grown in F/2 media (Jeffrey et al., 1997) filtered and autoclaved sterile. Polycarbonate culture flasks of various sizes were cultured at 20°C and illuminated by daylight fluorescent bulbs on a 16:8 light:dark cycle. Species and culture conditions are outlined in Table 3-2.

Species	Collection number	Media	Temperature
Emiliania huxleyi	RCC1256	K/2	15° C
Pleurochrysis placolithoides	RCC1401	K/2	15° C
Coccolithus braarudii	PLY682G	K/2	15° C
Rebecca salina	PLY465	K/2	15° C
Prymnesium faveolatum	RCC1446	K/2	15° C
Exanthemachrysis gayraliae	RCC	K/2	15° C
Thalassiosira pseudonana	RCC950	K+Si	15° C
Cylindrotheca closterium	RCC1713	K+Si	15° C
Phaeodactylum tricornutum	RCC69	K+Si	15° C
Pavlova lutheri	CS182	F/2	20° C
Pleurochrysis carterae	CS287	GSe	20° C
Isochrysis sp.	CS177	F/2	20° C
Phaeodactylum tricornutum	CS29	F/2	20° C
Chaeotoceros calcitrans	CS178	F/2	20° C
Thalassiosira oceania	CS427	F/2	20° C

Table 3-2: Species name, collection number, standardized medium conditions and temperature of cultures used in this study. Cultures labelled RCC are from the Roscoff culture collection, PLY samples are from the Plymouth Marine Laboratory and CS samples are from the CSIRO culture collection in Australia.

3.2.2 CO_2 affinity (K_c) in algal Rubisco extracts (University of Oxford)

In the Department of Plant Sciences, University of Oxford, we measured half saturation coefficients for CO_2 (K_c) as follows. After harvesting and pelleting cultures via centrifugation, cells were resuspended in an extraction buffer [1 mM EDTA, 20 mM $MgCl_2$, 50 mM Bicine, and 100 mM $NaHCO_3$ at pH 8.0 with 5 mM DTT and one cOmplete EDTA-free protease inhibitor cocktail tablet per 10 ml buffer (Roche) with the addition of protease inhibitor Leupeptin (100 μM Sigma-Aldrich) for diatom extracts].

Cells were ruptured on ice via ultrasonication with a UP200S Sonicator (Hielscher) on 70% amplitude for 8-10 cycles of 0.5 second intervals. After sonication, all non-soluble material (cell debris) was removed via centrifugation at 16,000 x *g* for ~10 minutes at 4°C. Supernatant was transferred into a fresh eppendorf tube and kept on ice until assayed. We used a crude protein extraction due to the amount of material required for this assay and as Rubisco is the only protein capable of carbon fixation, the other proteins should not interact with the assay.

Prior to running the radiocarbon K_c assay, the extract was activated with 20 mM $MgCl_2$ and 20 mM $NaHCO_3$ at room temperature for 30 minutes. Assay buffer [50 mM EPPS, 15 mM $MgCl_2$ pH 8.0] was bubbled overnight with nitrogen to remove any dissolved CO_2 or O_2. 2 ml septum sealed vials were purged with N_2 to run 3 technical replicates and controls. To each 2ml vial we added 500 µl of assay buffer and 10 µl of 20 mM RuBP (Sigma, made with 10 mM HCl). Radiolabeled sodium bicarbonate ($NaH^{14}CO_3$ 1mCi, 37 MBq Perkin Elmer) was added to the reaction mixture at varying concentrations (Table 3-3) and left to incubate for 1 minute at 25°C. To start the reaction, 20 µl of Rubisco extract was added, mixed, and left to incubate at 25°C for exactly 1 minute. The reaction was promptly stopped by the addition of 500 µl 10% v/v formic acid.

Vial No.	$NaH^{14}CO_3$ (µl)	Stock Concentration (mM)	Final concentration (mM)
1	1	100	0.25
2	2	100	0.5
3	5	100	1
4	10	100	2
5	25	100	5
6	10	500	10
7	20	500	20

Table 3-3: Radiolabelled sodium bicarbonate added to each vial across substrate range 0.25 to 20 mM in radiocarbon K_c assays.

After the completion of all bicarbonate concentrations and replicates, samples were left to dry on a heating block at 80-90°C to evaporate all unbound $NaH^{14}CO_3$. The dried material containing all organic bound $NaH^{14}CO_3$ was subsequently resuspended in 500 µl H_2O and 1.5 mL Ultima gold Scintillation Fluid (Perkin Elmer). Scintillation was quantified in disintegrations per minute (dpm) on a Tri-Carb 2810 Liquid Scintillation counter (Perkin Elmer) in the Department of Plant Sciences, University of Oxford.

The rate of the reaction (nmol bicarbonate fixed $minute^{-1}$ µl of $extract^{-1}$) was calculated for each sample assuming a pKa of 6.3 and constant pH of 8.0 using the Equation 3-4.

$$CO_2(\mu M) = \frac{NaHCO_3\ (\mu M)}{10^{(pH-pKa)}+1} \quad (3\text{-}4)$$

The specific activity of the samples (dpm/mol) was determined using the measured specific activity of 1 µl of the stock solutions used during the assay (100 mM and 500 mM

$NaH^{14}CO_3$) assuming 100 nmoles in 1 µl of 100 mM stock when added to 500 µl of 0.1 M NaOH. The alkalinity of NaOH maintains the bicarbonate in the forms $H^{14}CO_3^-$ or $^{14}CO_3^{2-}$ rather than $^{14}CO_2$ that can be lost (Zeebe & Wolf-Gladrow, 2001). With a known stock specific activity, and known dpm measured in the scintillation counter for each sample, the nmol of bicarbonate fixed and reaction rate can be calculated.

Finally, the calculated rate is plotted against the CO_2 concentration added to each vial and a single hyperbola curve is fitted using a least square regression of sigma. K_c and V_c are calculated according to the best fit produced by the regression. As a check on the estimation of K_c and V_c, we use a Lineweaver-Burk plot (or double reciprocal plot) to represent the data linearly. The Lineweaver-Burk plot manipulates the data so that the y-intercept is equivalent to the inverse of V_c and the x-intercept is equivalent to $-1/K_c$. These plots can be difficult to interpret, but are very useful for visual interpretation of data and to check estimates from the least square regression. Two or three experimental replicates were averaged to estimate K_c (examples of raw data in Figure 3-5) unless there was any experimental error skewing the reliability of the data. Standard deviation between replicates for the species *E. huxleyi*, *P. placolithoides*, *R. salina*, *C. braarudii* and *E. gayraliae* are 2.09, 0.64, 25.86, 3.90 and 2.30, respectively.

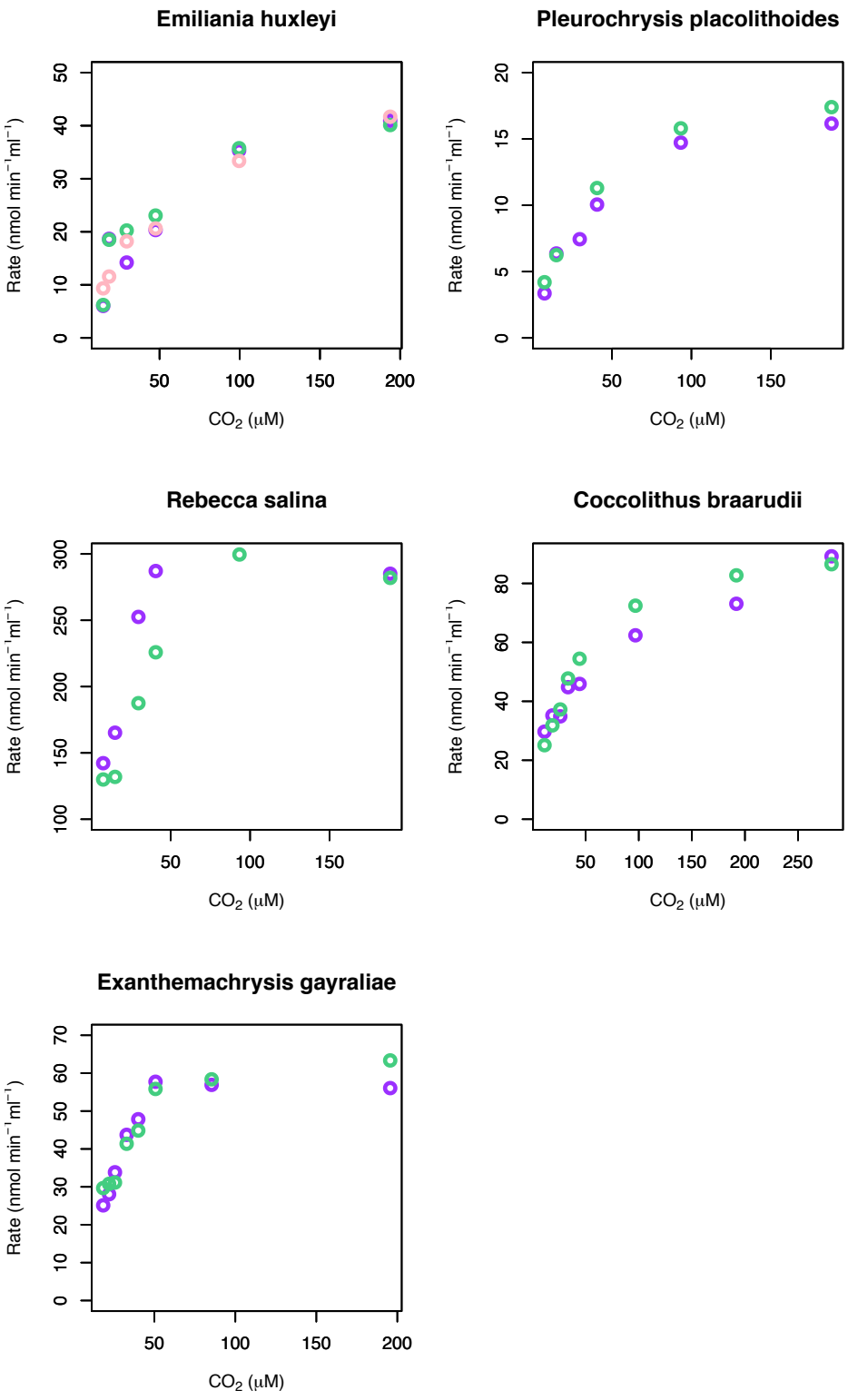

Figure 3-5: Raw data showing rate (nmol min^{-1} ml^{-1}) against concentration of CO_2 (μM) experimental replicates from radioactive K_c assay. Colors indicate technical replicates. Standard deviation between replicates for the species *E. huxleyi*, *P. placolithoides*, *R. salina*, *C. braarudii* and *E. gayraliae* are 2.09, 0.64, 25.86, 3.90 and 2.30 respectively.

3.2.3 Kinetic measurements (Australian National University)

Measurements of a suite of Rubisco kinetics (K_c, K_o, K_c^{cat}, K_o^{cat}) were carried out at the Research School for Biological Sciences and Medicine at ANU in collaboration with Dr. Spencer Whitney, Dr. Robert Sharwood, and Dr. Jodi Young. Algal cells were harvested via centrifugation and pellets were frozen in liquid nitrogen and stored at -80°C until assay. Prior to the assay, pellets were resuspended in extraction buffer [50 mM Hepps-NaOH, pH 8.0, 1 mM EDTA, 2 mM dithiothreitol, 1% (v/v) plant protease inhibitor cocktail (Sigma-Aldrich), and 1% (w/v) polyvinylpolypyrrolidone] and cells were lysed in a french press kept on ice. Extracts were then spun down at 13,000 rpm at 4°C for 5-10 minutes to remove debris. Assays were done in 7-ml septum-capped scintillation vials in reaction buffer [50 mM Hepes-NaOH (pH 7.8), 10 mM $MgCl_2$, 0.5 mM RuBP] with $NaH^{14}CO_3$ for varying concentrations of CO_2 between 0 and 140 μM.

For analysis of oxygen parameters, runs were carried out in vials purged with variable oxygen concentrations for different assays (0, 21, 40, and 60% vol/vol) mixed with nitrogen using Wostoff gas-mixing pumps (Whitney and Sharwood, 2007; Whitney et al., 2011). To measure the rate of $^{14}CO_2$ fixation, activated protein extract was added to the reaction mix to make a total reaction volume of 0.5 mL. After a known time (between 2-3 minutes) the reaction was stopped with 25% (v/v) formic acid and the vials were left on hot plates (80°C) to dry. Dried samples were resuspended in 0.5 mL H_2O and 1 mL scintillation cocktail, vortexed to mix and left to count in the scintillation counter (Sharwood et al., 2008; Whitney and Sharwood, 2007).

Data was fitted to curves according to the Michaelis-Menten equation and the Michaelis constant K_m for CO_2 (K_c) was determined from the curve (Bird et al., 1982). Examples of plots of rate of the carboxylation reaction versus CO_2 substrate for pooled samples are shown for a range of species in Figure 3-6. Standard deviations for replicates measured for the species *P. lutheri*, *P. carterae*, *I.* sp. and *P. tricornutum* are 0.02, 0.01, 0.03 and 0.02, respectively. The K_m for O_2 (K_o) was calculated from the relationship $K_{c,(45\%O2)} = K_{c,(0\%O2)} \times (1 + [O_2]/K_o)$ (Sharwood et al., 2008). The concentration of O_2 in the assay medium was calculated assuming the solubility at a partial pressure equivalent to one standard atmosphere (101.32 kPa) to be 256 μM at 25°C. For each sample the maximum rate of catalysis (V_c) was extrapolated from the Michaelis-Menten fitted data and normalized to number of Rubisco-active sites measured with [^{14}C]CABP binding (methods outlined in the following section).

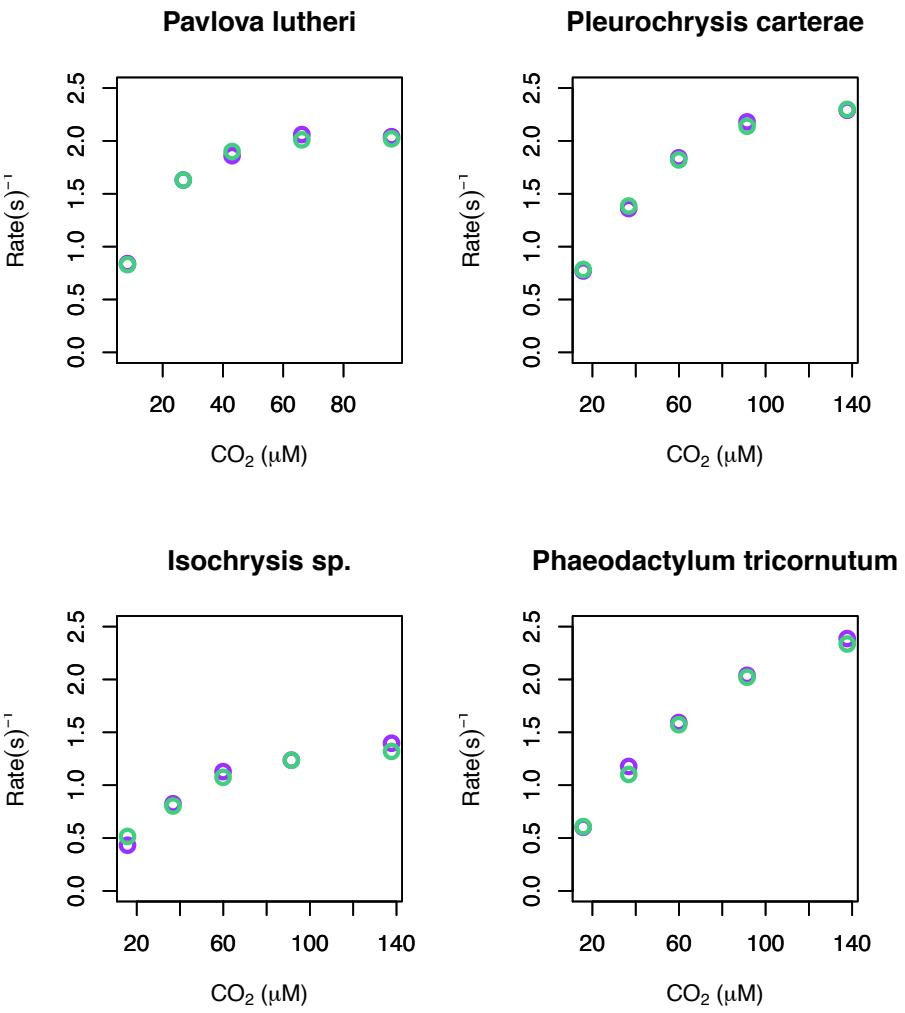

Figure 3-6: Plots of rate (s^{-1}) against substrate concentration (CO_2 μM) of data produced at ANU from radioactive kinetic assay. Colors represent technical replicates. Standard deviations for replicates measured for the species *P. lutheri*, *P. carterae*, *I.* sp. And *P. tricornutum* are 0.02, 0.01, 0.03 and 0.02, respectively.

The specificity of Rubisco for CO_2 versus O_2 ($S_{c/o}$) was measured at ANU from extracts purified by ion exchange chromatography (5 mL Q-sepharose column Sigma Aldrich) equilibrated with column buffer [50 mM Hepps-NaOH, pH 8.0, 1 mM EDTA]. Proteins were eluted over a 0 to 400 mM NaCl gradient over 150 mL elution buffer (5 mL min^{-1} flow rate) and the fractions containing peak Rubisco activities (measured by $^{14}CO_2$ fixation) were pooled and collected. Peak fractions were dialyzed for 15h at 4°C against

1 L of storage buffer [24 mM Hepps-NaOH, pH 8.0, 1 mM EDTA, 20% (v/v) glycerol] (Sharwood et al., 2008; Whitney and Sharwood, 2007). Purified Rubisco was used to measure CO_2/O_2 specificity according to Kane et al. (1994). All assays were run in duplicate or triplicate if initial replicates were insufficient. Kinetic data measured in two different laboratories were compared for the model diatom *Phaeodactylum tricornutum* and tobacco. Consistency across the data suggests that small differences in technique did not skew either measurement.

3.2.4 Quantification of Rubisco

3.2.4.1 Western blots and ImageJ (University of Oxford)

Relative quantification of Rubisco enzyme as a percentage of total protein was carried out in the Earth Sciences Department, University of Oxford on total protein extracts. Extracts were measured for total protein content using a standard Bradford protein quantification assay, a colorimetric assay based on a dye that binds to proteins present in an extract (Bradford, 1976). A standard curve was prepared using a range of concentrations of bovine serum albumin (BSA) (Sigma-Aldrich) in extraction buffer. 1.5 ml of Bradford reagent (Sigma-Aldrich) was added to standards and samples. Samples were vortexed and left to incubate for 45 minutes to allow the dye to bind to the protein. After 45 minutes the samples were transferred into spectrophotometer cuvette and measured for absorbance at 595 nm. Total protein in each sample was quantified against the standard BSA curve.

Using the protein quantification measurements from the Bradford assay, the extract was equally loaded into a SDS-PAGE gel (Mini-PROTEAN Any kDa Biorad). Samples were

run alongside a series of three to five RbcL Rubisco protein standards (Agrisera). SDS-PAGE gel was run at ~25A for 1 h. Proteins were transferred onto a polyvinylide fluoride (PVDF) membrane (100 mA) in transfer buffer [200ml methanol, 3 g Tris, 14.4 g glycine, 3 ml 10% (v/v) SDS in 1L DI water] for 1-1.5 h. Membrane was visually checked for ladder transfer and briefly, membrane was blocked with BSA-milk buffer [5% w/v non-fat milk powder, 1% w/v BSA, 0.75% v/v Tween20] and incubated with primary antibody (polyclonal global anti-RbcL form I antibody, Agrisera) in blocking buffer overnight. Primary antibodies are designed against peptide tags that are conserved across all oxygenic photosynthesizers so that no bias in affinity is expected (Campbell et al., 2003). Finally the membrane was incubated in a secondary antibody (alkaline phosphate-coupled goat anti-rabbit IgG antibody, Sigma-Aldrich 1:1000) in blocking buffer without milk for 1 h. Membrane was washed and colorimetric determination of bound proteins was performed with nitroblue tetrazolium chloride/5-bromo-4-chloro-3-indolyphosphate p-toluidine (NBT/BCIP, Promega). Picomole measurements of RbcL were quantified by comparing the intensity of the sample bands with the loaded standards using ImageJ software (Schneider et al., 2012) (Figure 3-7). Rubisco concentration was calculated using stoichiometric estimates of the large and small subunits from their relative molecular weights (Baker et al., 1975).

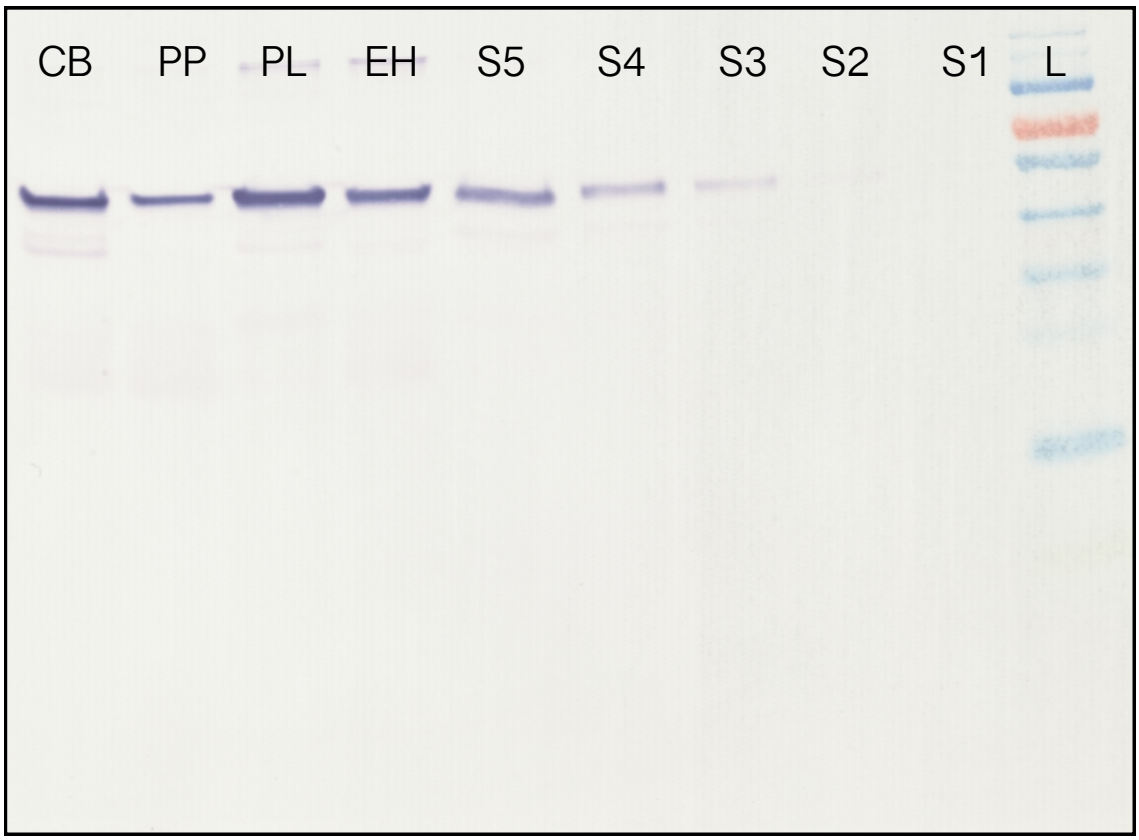

Figure 3-7: Example of Western blot image with species *Coccolithus braarudii* (CB), *Pleurochrysis placolithoides* (PP), *Pavlova lutheri* (PL), and *Emiliania huxleyi* (EH). Standards are shown on the right with 0.132 µg (S5), 0.07 µg (S4), 0.033 µg (S3) Agrisera RbcL Rubisco standard. Standards S2 and S1 were too low for detection in this blot. The final lane on the right is the ladder. For more Western blot images see appendix S-4 and S-5.

3.2.4.2 [^{14}C]carboxyarabinitol bisphosphate (CABP) binding (ANU)

Rubisco active sites were quantified using [^{14}C]CABP binding columns at the Research School for Biological Sciences and Medicine at ANU. Algal protein extracts were incubated at room temperature with [^{14}C]CABP binding solution [2.43 mM ^{14}C-CABP in extraction buffer with 20 µM $NaHCO_3^-$] for approximately 15 minutes and then spun down at 8000 rpm for 10 minutes to remove any residual debris. 100 µl of sample was loaded and gel filtration carried out according to Russka et al. (1998) and Whitney and

Andrews (2011b). Sample peaks were collected sequentially for quantification of background, sample and finally unbound ^{14}C. Scintillation fluid was added to collected samples, vortexed, and run in the scintillation counter to quantify the bound Rubisco.

3.2.5 Identification of pyrenoid morphology and CCM characteristics

Pyrenoid morphology and other aspects of the carbon concentrating mechanisms for the species in this study were identified either by PhD student Maeve Eason-Hubbard or compiled from the literature for this study (Allen et al., 2011; Bendif et al., 2011). Other aspects of the algal CCM for the species in this study were compiled including internal C_i pools and carbonic anhydrase activity (Badger et al., 1998). The presence/absence of δ-CA in select algal species was determined in our laboratory by Dr. Renee Lee. Briefly, PCR was performed on isolated genomic DNA template, using a pair of degenerate primers. The identity of each fragments produced (~370 bp) was further confirmed by sequencing. A BLAST search was also carried out on the full genome of *P. tricornutum* to further confirm the absence of this gene where no band was seen on the gel.

3.3 Results and Discussion

3.3.1 Part One: K_c and the pyrenoid

First we outline CO_2 affinity (K_c) measured and compiled in this study from 20 species of chromalveolate algae. K_c values across these species range from a high of 65 μM in the diatom *Thalassiosira weisflogii* to a low of 8 μM in the Pavlovale *Rebecca salina*. Table 3-4 shows K_c values of species measured in this study separated into *Bacillariophyceae,*

or diatoms, and Haptophyta, which are further divided into the classes *Pavlovophyceae* and *Calcihaptophycidae*. In Table 3-4, we note that the *Pavlovophyceae* and *Calcihaptophycidae* have a relatively lower range from 8-41 μM, with the *Pavlovophyceae* displaying lower K_c values than the *Calcihaptophycidae*. The *Bacillariophyceae* have a higher range from 23-65 μM. For sake of discussion, we will group the K_c values into three categories: low (>20 μM), middle (20-40 μM) and high (>40 μM). We observe that the *Pavlovophyceae* have K_c values only in the low group, *Calcihaptophycidae* have representatives in the low and middle group, and *Bacillariophyceae* K_cs fall into middle and high group.

Affinity of Rubisco for CO_2 (K_c) (µM)				
Higher plants (C_3)	Spinach		14/11	this study; Badger et al., 1998
Higher plants (C_4)	Maize		32	Badger et al., 1998
Cyanobacteria	*Synechococcus*	sp.	185	Badger et al., 1998
Pavlovophyceae				
	Pavlova	*lutheri*	10	Young, thesis
	Rebecca	*salina*	8	this study
	Exanthemacrysis	*gayraliae*	18?	this study
Calcihaptophycidae				
	Pleurochrysis	*carterae*	11	Young, thesis
	Pleurochrysis	*placolithoides*	18/14	this study; Young, thesis
	Coccolithus	*braarudii*	36	this study
	Isochrysis	*galbana*	30	Badger et al., 1998
	Isochrysis	sp.	17	this study
	Phaeocystis	sp.	30?	Badger et al., 1998
	Emiliania	*huxleyi*	39/40/41	this study; Young, thesis; Webster, thesis
Bacillariophyceae				
	Thalassiosira	*pseudonana*	31	this study
	Thalassiosira	*weisflogii*	65	this study
	Thalassiosira	*oceania*	65	this study
	Pheodactylum	*tricornutum*	36/41/56	this study; Badger et al., 1998
	Cylindrotheca	*closterium*	39	this study
	Cylindrotheca	*fusiformis*	36	Badger et al., 1998
	Chaeotoceros	*mulleri*	25/30	this study
	Chaeotoceros	*calcitrans*	23	this study
	Cyclotella	sp.	30	Badger et al., 1998

Table 3-4: Table of K_c values in the chromalveolate algae measured in this study (blue) and compiled from the literature (black). Cyanobacteria and higher plant values are shown for reference. We note that some species measured in this study were cultures at Princeton University by Dr. Jodi Young and therefore are not outlined in the culturing section above.

A Rubisco with a low K_c value, high affinity, can reach half of the maximum velocity of the carbon fixation reaction with a relatively low concentration of substrate. In the case of our groups of K_c values, the high group will require approximately 5 times the concentration of substrate in order to reach $½V_{max}$ than the low group. However, the actual fixed carbon output depends on the concentration of Rubisco as well as the other kinetic parameters.

In higher plants there is also a distinct separation of high and low Rubisco K_c values between C_3 and C_4 plants. C_4 plants tend to have higher K_c values in the range of 25-40 μM while C_3 plants tend to have K_cs between 10 and 20 μM (reference values in Table 3-4). Generally, a higher K_c value is thought to represent the presence of a CCM in both higher plants and other algal species (Badger et al., 1998). C_3 plants, with a low K_c, rely on passive diffusion of CO_2 from the atmosphere into the chloroplast stroma (von Caemmerer et al., 1994). On the other hand, the high requirement for carbon in C_4 plants is explained by active concentration and storage of carbon near the site of carbon fixation (Sage, 2004).

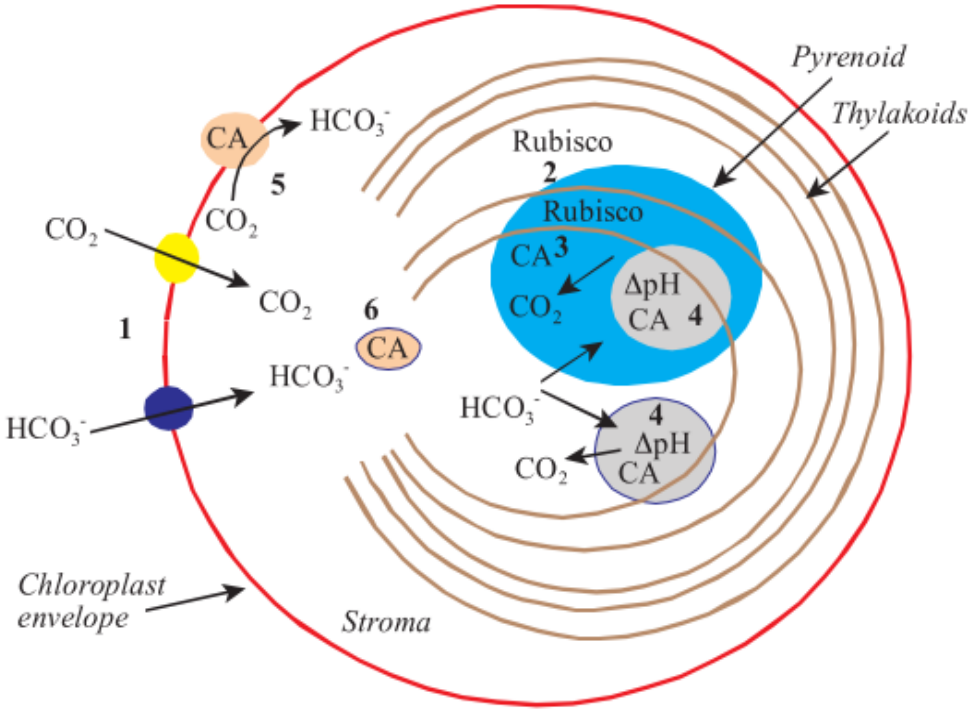

Chloroplast property	Type 1[a]	Type 2[b]	Type 3[b]	Type 4[c]	Type 5[c]
Rubisco kinetics K_m (CO_2)	Lower K_m	Higher K_m	K_m?	Higher K_m	K_m?
Rubisco localization	Stromal	Pyrenoid	Stromal	Pyrenoid	Stromal
Stromal CA	Yes	No	Yes	No	No
Pyrenoid CA	No	Yes	No	No	No
Pyrenoid thylakoid CA	No	No	No	Yes	No
Stromal thylakoid CA	?	No	No	No	Yes
Envelope CA	No	Yes/no	No	Yes/no	Yes/no
Active HCO_3^- transport	No	Yes	Yes	Yes	Yes
CO_2 diffusion barrier	No	Yes	Yes	Yes	Yes
C_i pool	Passive	High pool	Medium pool	Lower pool	Lower pool

[a]Passive.
[b]Active transport, no thylakoid CA.
[c]Active transport, thylakoid CA.

Figure 3-8: Model of possible elements of the algal chloroplast CCM. 1, chloroplast envelope Ci transporters; 2, pyrenoid or stromal Rubisco; 3, pyrenoid CA; 4, thylakoid CA (pyrenoid or stromal thylakoids); 5, envelope CA; 6, stromal CA (taken from Badger et al., 1998). Not all elements are discussed in the present study.

Table 3-5: Table showing potential algal chloroplast types illustrated by figure 3-8 (taken from Badger et al., 1998).

In their study of the diversity of Rubisco and chloroplast-based CO_2 concentrating mechanisms, Badger et al. (1998) model different elements of algal CCMs dividing them into possible CCM "types" and characterizing the related attributes resulting from the CCM elements in each type (Figure 3-8 and Table 3-5). One overall trend elucidated by these models is that CCM types with a pyrenoid structure have higher Rubisco K_c. They observe that a pyrenoid-based CCM appears to be the most effective in elevating the internal CO_2 pool around a smaller area of concentrated Rubisco. As a result, the Rubisco in these species is experiencing a higher concentration of CO_2 as reflected in their Rubisco CO_2 requirement or K_c. Here we use our dataset to illustrate this relationship modelled in Badger et al. (1998) between Rubisco K_c values and the presence/absence of a pyrenoid using observations specifically in the haptophyte algae with diverse pyrenoid morphologies. In the diatoms, pyrenoid structures have been observed across most species. Pyrenoid diversity is complicated slightly in diatoms as they tend to vary more in plastid number, especially across the centric species (Matsuda et al., 2011). We omit discussion of the diatom pyrenoid in this section as we have not fully characterized the diatom pyrenoid and plastid number.

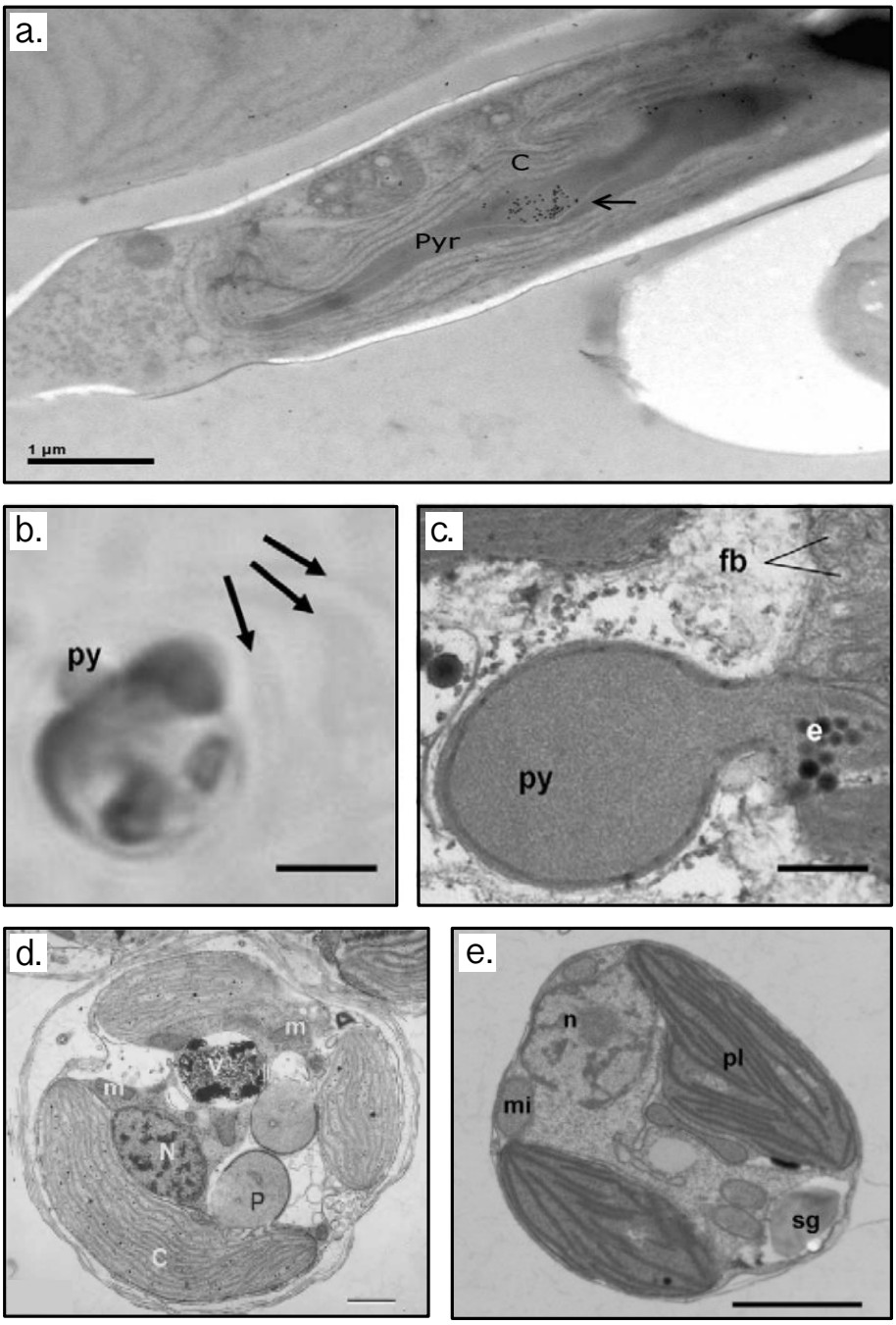

Figure 3-9: Images of pyrenoid morphologies present across the haptophytes and the model diatom species *Phaeodactylum tricornutum* compiled from Allen et al. (2011); Bendif et al. (2011); Fresnal and Billard (1991). The immersed pyrenoid in *P. tricornutum* (a.) is typically lens shaped and completely embedded within the chloroplast. Bulging pyrenoids can either protrude outward toward the cell periphery as shown in *Exanthemachrysis gayraliae* (b. and c.) or inward toward the center of the cell in *Ochrosphaera neapolitana* (d.). Bulging pyrenoids can form a stalk (c.) in which case the pyrenoid is almost completely isolated from the chloroplast only connected by the stalk. Finally, a cell lacking a pyrenoid is shown in *Pavlova viridis* (e.) and exhibits no distinct body in or related to the chloroplast structure. Scale bars: a.) 1 µm, b.) 5 µm, c.) 500 nm, d.) 1 µm and e.) 1 µm.

Across the haptophyte phylogeny, there is significant diversity in pyrenoid morphology (Figure 3-9). Maeve Eason-Hubbard (unpublished data) classifies pyrenoids in the haptophytes as (1) immersed (Figure 3-9a), a spherical or sub-spherical body embedded within the chloroplast, usually more or less centrally located (Griffiths 1970) (2) bulging to the cell interior (Figure 3-9d), a projecting body toward the center of the cell, sometimes connected by a short stalk (3) bulging to the cell periphery (Figure 3-8b;c), a projecting body toward the exterior or cell wall or (4) absent (Figure 3-9e), a cell lacking a pyrenoid structure of any kind. The divisions across the haptophyte phylogeny coincide with divisions in pyrenoid morphology (see phylogenetic tree Figure 1-2). The class *Pavlovophyceae* is dominated by the absence of a pyrenoid (4) with some species exhibiting a pyrenoid bulging to the periphery (3). In the *Calcihaptophycidae*, a pyrenoid is present across the entire lineage with pyrenoid types (1) immersed and (2) internally bulging.

In this study we find a relationship between Rubisco K_c and pyrenoid morphology across the haptophytes (Figure 3-10). As predicted by Badger et al. (1998), species lacking a pyrenoid have a low K_c (~10 μM). Cells with a bulging pyrenoid, either to the periphery or the interior, maintain K_c values slightly higher but close to the values of cells lacking a pyrenoid. Algal cells with an immersed pyrenoid have K_c values approximately 3-5 times that of the algal cells lacking a pyrenoid (a range around 35 μM). This relationship suggests that the immersed pyrenoid in marine haptophytes plays a role in determining the CO_2 kinetics of Rubisco and supports the model in Badger et al. (1998) (Figure 3-8).

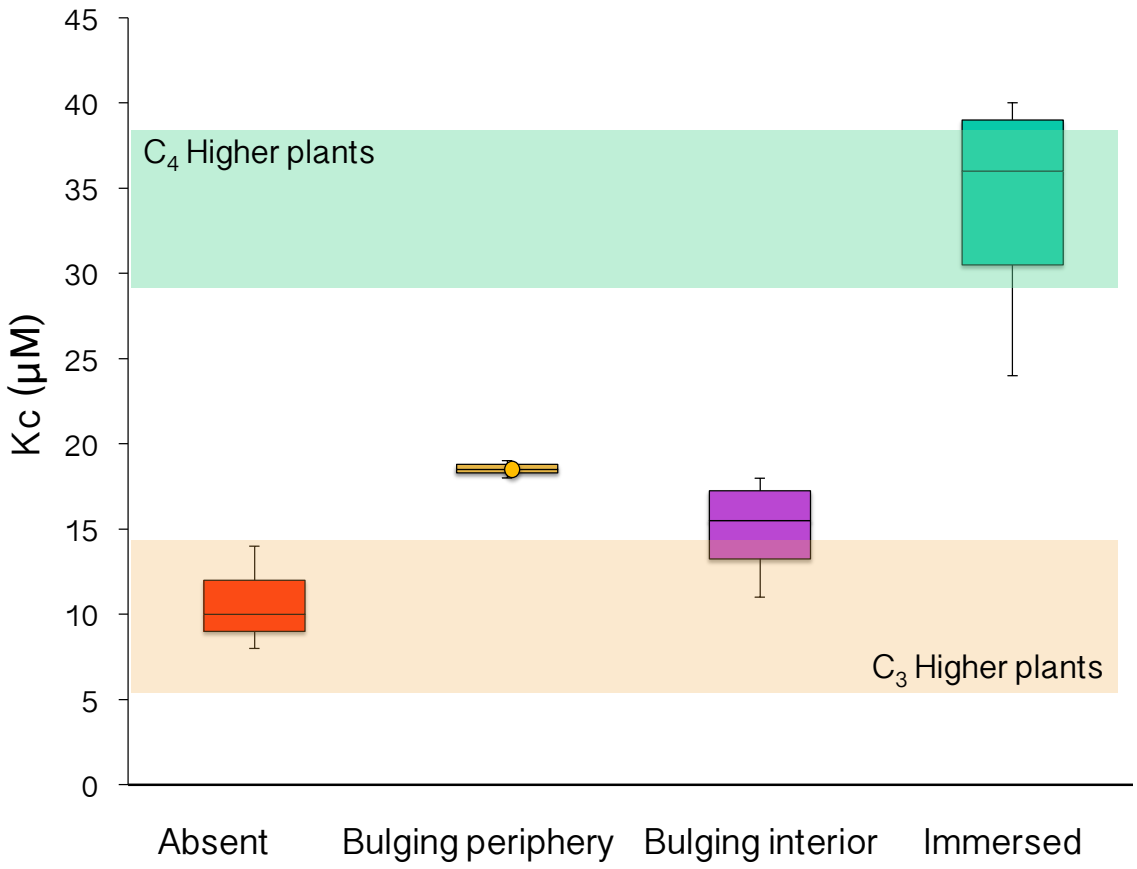

Figure 3-10: Spread of Rubisco K_c values across the range of haptophyte pyrenoid types measured in this study (Table 3-4). This figure highlights the relationship between pyrenoid type and Rubisco CO_2 kinetics. Cells with immersed pyrenoid show a significantly higher range of K_c values than all other species measured here. The bulging pyrenoid values are within error of the K_c values of cells with an absent pyrenoid.

As previously proposed (Badger et al., 1998), it seems that the pyrenoid is extremely effective in creating a higher CO_2 environment for packed Rubisco and this is evident in the diversity of CO_2 affinity we see across these algal species. From this data, we suggest that specifically an immersed pyrenoid controls the [CO_2] environment for algal cells and cells lacking a pyrenoid have adapted a higher affinity Rubisco that can cope with ambient [CO_2] and likely higher [O_2] acquired by diffusion. The implications of a bulging pyrenoid are more difficult to interpret. The K_c values of cells with a bulging pyrenoid are only incrementally higher than cells lacking a pyrenoid completely. This data suggests that a pyrenoid that is bulging either into the cell or to the cell periphery is less effective at

increasing [CO_2] than an immersed pyrenoid. The role of different pyrenoid morphologies and the impact on Rubisco kinetics will be discussed in more detail in the following section.

3.3.2 Part Two: A closer look at kinetics across distinct pyrenoid morphologies

In this section we scrutinize the kinetics of Rubisco from four species of marine algae in the chromalveolate kingdom representing three diverse pyrenoid morphologies to assess how different morphologies influence the subcellular environment for Rubisco. These species (outlined in Table 3-6) include the haptophytes *Pavlova lutheri*, *Pleurochrysis carterae* and *Isochrysis sp.* as well as the model diatom *Phaeodactylum tricornutum*. Table 3-6 also compiles data on known CCM parameters or physiological adaptations for each species in this study.

Species	Pyrenoid type	Inhibition by CA inhibitors	Light-stimulated CA	δCA	Ci pool	Rubisco % TSP
Pavlova lutheri	Absent			-		11.4%
Pleurochrysis carterae	Bulging internally	AZA+, EZA+		+		3.0%
Isochrysis sp.	Immersed	EZA+	++	+	6-fold	3.5%
Phaeodactylum tricornutum	Immersed	EZA+	++	-	5-6 fold	3.2%

Table 3-6: This table outlines known carbon concentrating mechanisms in the species represented in this study. The pyrenoid type is characterized from TEM images either from work in our lab or compiled from the literature. Inhibition by CA inhibitors for 3 of the 4 species presented here was measured by Burns and Beardall (1987). Light-stimulated CA is found in the species *Isochrysis sp.* and *Phaeodactylum tricornutum* by Badger et al. (1998). Presence/absence of δ -CA was determined in our laboratory. The fold increase of the internal Ci pool is presented for 2 species (Badger et al., 1998). Finally, the Rubisco quantity as a percentage of total soluble protein (TSP) was measured in this study.

3.3.2.1 Carbonic anhydrase

The carbonic anhydrase (CA) enzyme plays an integral role in the carbon concentrating mechanism of photosynthetic organisms as it catalyzes the reversible interconversion between carbon dioxide and water to bicarbonate and protons. Without CA, this process would take place too slowly to support the kinetic throughput of carbon fixation (Badger and Price, 1994). To assess the presence/absence and relative activity of CAs in our algal species, we compile evidence of inhibition by CA inhibitors (Burns and Beardall, 1987), light-stimulated CA activity (Badger et al., 1998), and presence of δ-CA in the genome (Renee Lee, unpublished data).

The effects of two CA inhibitors, the relatively impermeable acetazolamide (AZA) inhibitor and membrane permeable ethoxyzolamide (EZA) inhibitor, are shown in Table 3-6 as either presence of effect (+) or absence of effect (-) on the affinity of photosynthesis for C_i (Badger et al., 1998; Burns and Beardall, 1987; Okazaki et al., 1992). It has been observed that algal species grown in the presence of EZA significantly reduce their affinity for external C_i during photosynthesis. This effect (EZA+) is interpreted as evidence for CA involved in the CCM (Badger et al., 1998). The relative effect of AZA, an external CA inhibitor, is more difficult to interpret. AZA+ indicates the presence of a CA allowing the cell to utilize external HCO_3^-, but CAs compensating elsewhere in the cell may mask the signal. The effect of CA inhibitors has only been measured in 3 of the species in this study, indicating a reduction of external C_i affinity (EZA+) for *Isochrysis sp.* and *Pheodactylum tricornutum*, and both EZA+ and AZA+ for *Pleurochrysis carterae*,

the cells with a pyrenoid structure. Unfortunately, this parameter has not been measured in *Pavlova lutheri*, the species lacking a pyrenoid.

Light-stimulated CA activity (Table 3-6) indicates the uptake of external inorganic carbon into the CA containing cell that is energized by light. This parameter is measured as described in Badger et al. (1998), by monitoring the exchange of ^{18}O from C_i species to ^{16}O labelled water on a mass spectrometer. The method tracks the decreasing ^{18}O post-enrichment as a result of internal CA accessing external C_i when the light is switched on. The pattern should be reversed in the dark for cells with light-stimulated CA activity. This pattern was observed in the species *Isochrysis galbana* and *Pheodactylum tricornutum* (Badger et al., 1998), but was not measured in *Pavlova lutheri* or *Pleurochrysis carterae*.

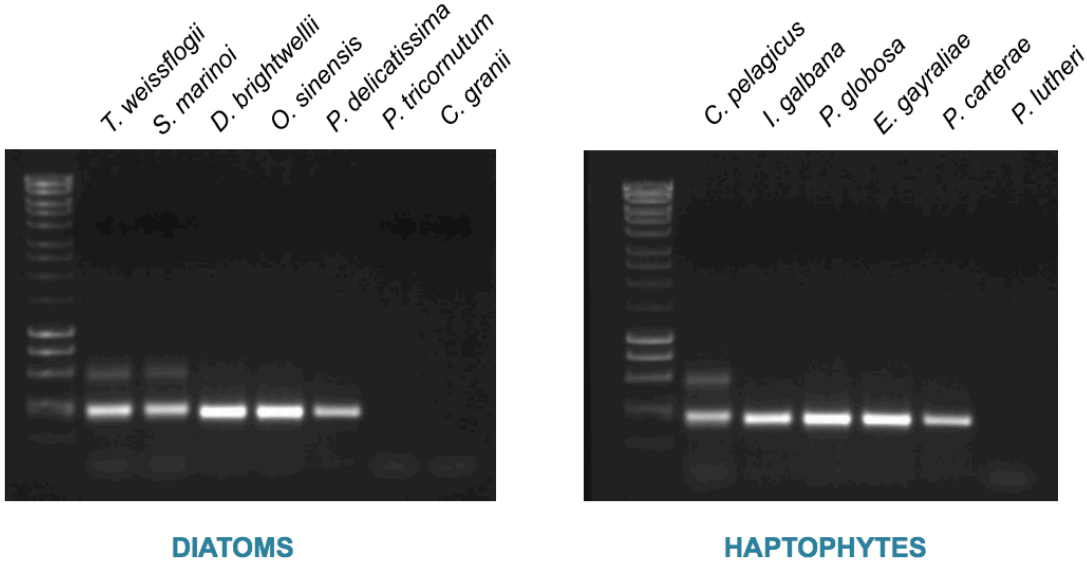

Figure 3-11: Determination of presence/absence of δ-CA across various diatom and haptophytes. Presence is indicated by the visualization of a band (370 base pairs) and absence is indicated by the lack of bands. PCR was performed on isolated genomic DNA template, using a pair of degenerate primers, fragments shown here. The species *P. tricornutum*, *C. granii* and *P. lutheri* are shown to lack δ-CA (Lee et al., unpublished).

Finally, the presence or absence of the δ-CA was determined within the genome of each species (Renee Lee, unpublished). δ-CA has been identified as an external carbonic

anhydrase in marine dinoflagellates (Lapointe et al., 2008) and has also been found specifically in eukaryotic marine algae (Lee et al., 2013; Soto et al., 2006). We find that *P. lutheri*, the species lacking a pyrenoid, also lacks δ-CA. The presence of a δ-CA was detected in the other two haptophytes (Figure 3-11). Although we do not identify a δ-CA in the diatom species *P. tricornutum*, other studies have identified a number of CAs, including pyrenoid localized CAs, that likely satisfy the need for CA activity in this species (Tachibana et al., 2011). Although all of the CA parameters were not measured across all species in this study, the data available suggests that all haptophyte cells with a pyrenoid, either bulging or immersed, also express CAs or CA activity. From this data we can only conclude that the species lacking a pyrenoid, *P. lutheri*, also lacks a δ-CA, but from this data we cannot conclude that it lacks CA activity altogether. We can preliminarily suggest that the presence of a pyrenoid is coincident with the presence/absence of significant CA activity, functioning as a component of the CCM, in marine algae.

3.3.2.2 Internal carbon pools and Rubisco content

Table 3-6 shows measured values of the internal C_i pools or the ratio of internal C_i accumulated in the cell versus the carbon pool predicted as a result of passive diffusion alone (Badger et al., 1998; Burns and Beardall, 1987; Coleman and Rotatore, 1995), as a direct measure of how much the cell is concentrating carbon. Measurements of this parameter have only been performed for two species from this study, *Isochrysis galbana* and *Phaeodactylum tricornutum*. Both species exhibit an internal carbon pool ~6 times the expectation from passive diffusion alone.

Also shown in Table 3-6 is a measure of the Rubisco content as a percentage of total soluble protein (TSP) across our species via [^{14}C]CABP binding. This parameter can provide insight into the CCM as it reveals the amount of Rubisco available to carry out carbon fixation. However, depending on the relative kinetics and activity of the Rubisco, the amount of Rubisco may not be directly related to the amount of carbon a cell can fix. We note that Rubisco quantity in the species lacking a pyrenoid is higher than the others in this study. It has also been observed that higher plants lacking a CCM, have a lower turnover rate of carboxylation but tend to compensate by making more Rubisco as a percentage of TSP (Ku et al., 1979; Long, 1999). The species with a pyrenoid maintain 3-3.5% Rubisco while *P. lutheri* has 11.4% TSP. This suggests that one possible mechanism for a cell lacking a pyrenoid to maintain an effective rate of carbon fixation without CA or an internal CCM structure is to produce more Rubisco enzyme.

3.3.2.3 Kinetics

Now we turn to the kinetic data to determine if our current assessment of the CCM across the algal species outlined in this study is supported by the kinetics of the Rubisco enzymes, assuming kinetic optimizations can shed light on intracellular [CO_2]:[O_2]. Table 3-7 shows the suite of kinetic parameters measured across these species.

3.3.2.4 Carboxylation

The parameters K_c and K_c^{cat} in Table 3-7 describe the affinity for and rate of the carboxylation reaction carried out by each Rubisco enzyme. Across the species, we note

significant variation relative to the known range of these parameters in higher plants and non-green algae (Badger et al., 1998). CO_2 affinity (K_c) varies as we might predict with the species lacking a pyrenoid, *Pavlova lutheri*, exhibiting the highest CO_2 affinity (lowest K_c). We presume that in this cell, without a pyrenoid structure and/or other active CCM parameters (i.e. CAs), Rubisco resides in an environment with relatively low access to CO_2 and a lower $[CO_2]$:$[O_2]$ ratio. As a result, this species requires a stronger ability to distinguish between the two substrates to carry out carboxylation.

Species	**Pyrenoid type**	**K_c** (µM)	**K_c^{cat}** ($s^{-1}site^{-1}\mu M^{-1}$)	K_o (µM)	K_o^{cat} ($s^{-1}site^{-1}\mu M^{-1}$)	**$S_{c/o}$**
Pavlova lutheri	Absent	14.4	2.48	1146	1.57	125
Pleurochrysis carterae	Bulging internally	17.6	3.29	366	0.67	102
Isochrysis sp.	Immersed	24.1	2.24	799	0.83	89
Phaeodactylum tricornutum	Immersed	41.1	3.35	663	0.47	115

Table 3-7: Table of the suite of kinetic data measured in this study. Michaelis-Menten constants (K_c and K_o) for CO_2 and O_2, catalytic turnover rates (K_c^{cat} and K_o^{cat}) for carboxylation and oxygenation and specificity for CO_2 substrate versus O_2 ($S_{c/o}$). Average standard errors for K_c and K_o are 2.95 and 167, respectively. Standard deviations for K_c^{cat} and $S_{c/o}$ are 0.5 and 2.1, respectively. K_o^{cat} was calculated from other 4 measured parameters.

The other cells studied all exhibit a lower CO_2 affinity (higher K_c) than *Pavlova lutheri* with a gradient from highest to lowest affinity from immersed to internally bulging to absent pyrenoid, respectively (Table 3-7). *Phaeodactylum tricornutum* and *Isochrysis* sp. with immersed pyrenoids have the lowest CO_2 affinity. This result follows the line of reasoning that this cell with an effective pyrenoid structure, high CA activity and higher internal carbon pool allows for a relative relaxation of the CO_2 affinity of its Rubisco enzyme.

Looking at the rate of carboxylation (K_c^{cat}), we can investigate how the relative relaxation of the CO_2 affinity in a cell impacts the catalytic turnover rate of the reaction. According to the hypothesis in Tcherkez et al. (2006) and Savir et al. (2010), a decrease in CO_2 affinity will result in an increased catalytic turnover rate of carboxylation. However, the trend we observe across these species is not so clear. While the species with the lowest CO_2 affinity (*P. tricornutum*) does indeed have the highest K_c^{cat}, the lowest K_c^{cat} is exhibited by *Isochrysis sp.*, which has the second highest K_c. This K_c^{cat} value, however, may be an outlier as the other two values fall in the predicted order. *P. tricornutum* has a K_c^{cat} of 3.35 $s^{-1}site^{-1}\mu M^{-1}$, similar to 3.29 for *P. carterae*. This value is significantly lower for *P. lutheri* at 2.48 $s^{-1}site^{-1}\mu M^{-1}$. When plotted against each other, Figure 3-12 illustrates the relative relationship between the variables. One other noteworthy observation from these two variables is that while *P. lutheri* and *P. carterae* have similar K_c values (14.4 μM and 17.6 μM respectively), *P. carterae* has a much higher K_c^{cat} (3.29 $s^{-1}site^{-1}\mu M^{-1}$) than *P. lutheri* (2.48 $s^{-1}site^{-1}\mu M^{-1}$) which may suggest a more effective overall carboxylation ability of the *P. carterae* Rubisco. We observe that cells with a more relaxed affinity for CO_2 substrate have a higher catalytic turnover rate for carboxylation, however the relationship is not strictly linear (Figure 3-12).

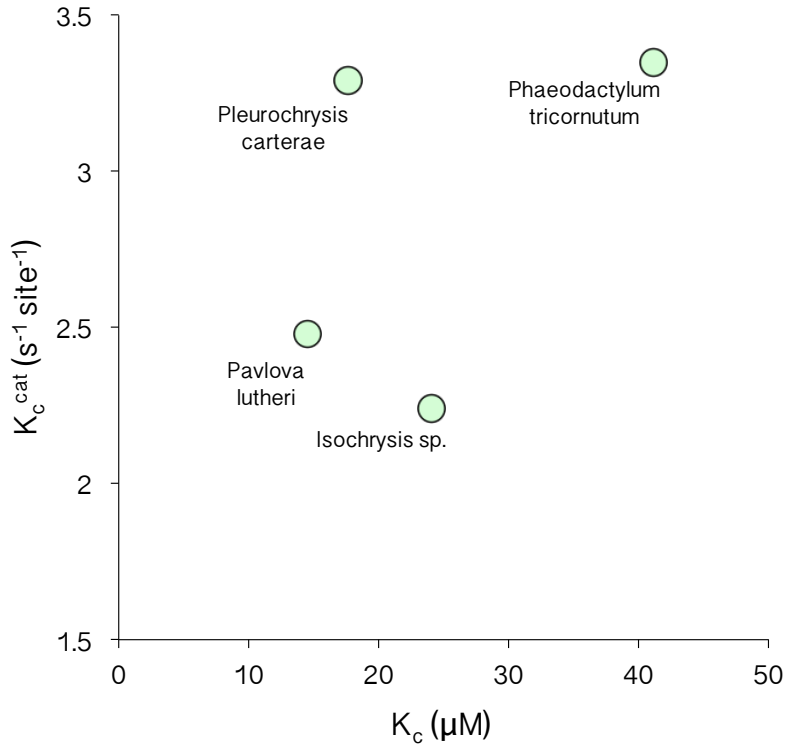

Figure 3-12: Rubisco affinity for CO_2 (K_c) plotted against the turnover rate of carboxylation (K_c^{cat}) for the species measured in this study.

3.3.2.5 Oxygenation

The kinetic parameters of the oxygenation reaction of Rubisco are generally overlooked as some studies suggest that the contribution of the oxygenation reaction for marine algae is much smaller than in higher plants (Beardall 1989; Burns and Beardall 1987; Johnston 1991; Raven et al., 1990). Measurements performed in cyanobacteria and diatom enzymes show only little potential for the oxygenation reaction even under 21% oxygen and limiting CO_2 (Badger et al., 1998). For the species *P. tricornutum* and *I. galbana*, they find that O_2 uptake in light-stimulated algae is only 7% of CO_2-saturated electron transport while in higher plants it is up to 30% (Canvin et al., 1980; Gerbaud and Andre 1980).

Here we consider the variation in the O_2 affinity (K_o) and turnover rate of the oxygenation reaction (K_o^{cat}) assuming the [O_2] concentration in the subcellular environment varies between different pyrenoid morphologies. We aim to explore the ability of the pyrenoid to alter internal [O_2] as well as [CO_2] to aid in increased carboxylation over oxygenation. Table 3-7 shows the variability in kinetics for the oxygenation reaction. The affinity of the different enzymes for O_2 is drastically different between the four species. Most notably the species lacking a pyrenoid, *P. lutheri*, has an extremely low affinity for O_2 (1146 μM) even when compared to other measured primary producers to date (Badger et al., 1998). This low O_2 affinity may be an indicator of a subcellular environment for Rubisco with a high concentration of O_2 that requires the enzyme to relax its affinity for the substrate. *Isochrysis sp.* and *P. tricornutum* have a K_o around 700 μM and *P. carterae* has the highest affinity at 366 μM. We suggest that the higher affinities in the species with a pyrenoid may not cause a problem for the enzyme as the pyrenoid is providing a relatively low O_2 environment. Specifically, for *P. carterae*, with an internally bulging pyrenoid, the central location of Rubisco provides a long pathlength for the diffusion of O_2. This diffusional distance may make the internally bulging pyrenoid structure ideal for the exclusion of oxygen as indicated by its low K_o.

The trend we observe here with the cell lacking a pyrenoid-based CCM having the lowest O_2 affinity while the other cells have a higher affinity is opposite to that observed in higher plants. It is possible that this is how algae manage to minimize the oxygenation reaction to 7% versus ~20% in higher plants (Badger et al., 1998), but should be investigated further. If we follow the same logic as for CO_2 affinity, the low O_2 affinity signifies high [O_2] around the *P. lutheri* Rubisco enzyme, as is hypothesized for a cell lacking a pyrenoid.

Cells with a pyrenoid and a higher O_2 affinity, may benefit from the subsequent decrease in the catalytic rate of the damaging oxygenation reaction.

In the turnover rate of oxygenation (K_o^{cat}), we again note the most significant difference is in *P. lutheri* with a higher K_o^{cat} at 1.57 $s^{-1}site^{-1}\mu M^{-1}$ compared to values of 0.67, 0.83, and 0.47 $s^{-1}site^{-1}\mu M^{-1}$ for species *P. carterae*, *Isochrysis sp.*, and *P.tricornutum* respectively. Figure 3-13 shows the linear relationship between the two parameters. The higher O_2 affinity for species with a pyrenoid, may be a means of ultimately decreasing the turnover rate of oxygenation to slow down the contribution of this inhibitory reaction for the cell.

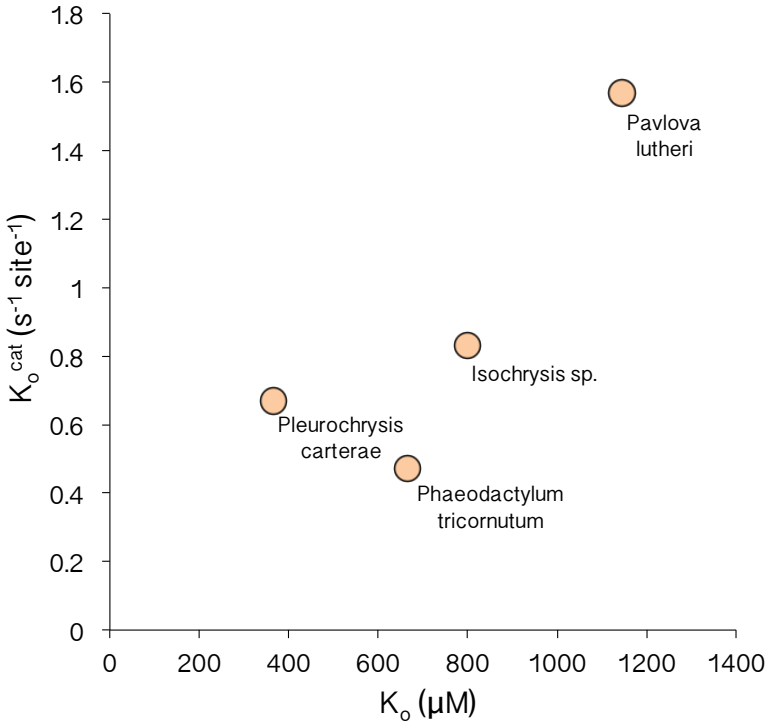

Figure 3-13: Rubisco affinity for O_2 (K_o) plotted against the turnover rate of oxygenation (K_o^{cat}) for the species measured in this study.

Another overarching relationship that stands out across the kinetic parameters discussed so far is the trade-off between turnover rates for carboxylation and oxygenation (Table 3-

7). This means that as Rubisco has a set number of active sites, if one substrate is being rapidly turned over, the enzyme likely cannot physically keep up with the other catalytically. *P. tricornutum* with an immersed pyrenoid has the highest turnover rate for CO_2 and the lowest turnover rate for O_2. *P. lutheri* which has a very low CO_2 turnover rate has a much higher rate for O_2. This suggests that the pyrenoid may overall aid in the relatively rapid turnover rate of carboxylation over oxygenation in lieu of a relative low affinity for CO_2 versus O_2. A high affinity for CO_2, however, becomes less necessary in the high $[CO_2]$:$[O_2]$ environment provided by the macromolecular structure.

3.3.2.6 Catalytic efficiency under different O_2 conditions

Finally, we look at a ratio between the catalytic turnover rate for carboxylation (K_c^{cat}) and the affinity for CO_2 (K_c) as a measure of the overall effectiveness of carboxylation in the Rubisco enzyme at two different oxygen concentrations (0% and 21% O_2). A higher value represents a more effective enzyme for carboxylation. Figure 3-14 shows that this ratio is consistently higher at 0% oxygen versus 21% oxygen, as expected since the presence of oxygen will result in turnover of O_2 in the place of CO_2. In addition to this signal, we note that there is a larger difference between the two O_2 treatments in the species *P. carterae* of about 50 mM s^{-1} when compared to a change of about 20 mM s^{-1} for the other species. Under the 21% oxygen condition, the carboxylation efficiency of *P. carterae* is most detrimentally affected. We hypothesize that *P. carterae*, with an internally bulging pyrenoid, is most sensitive to the presence of oxygen. As mentioned previously, kinetics suggests that the internally bulging pyrenoid is the most effective at maintaining a low O_2

environment for Rubisco. This finding of high O_2 sensitivity in *P. carterae* supports the idea that a cell can tolerate a high affinity for O_2 in a low O_2 environment.

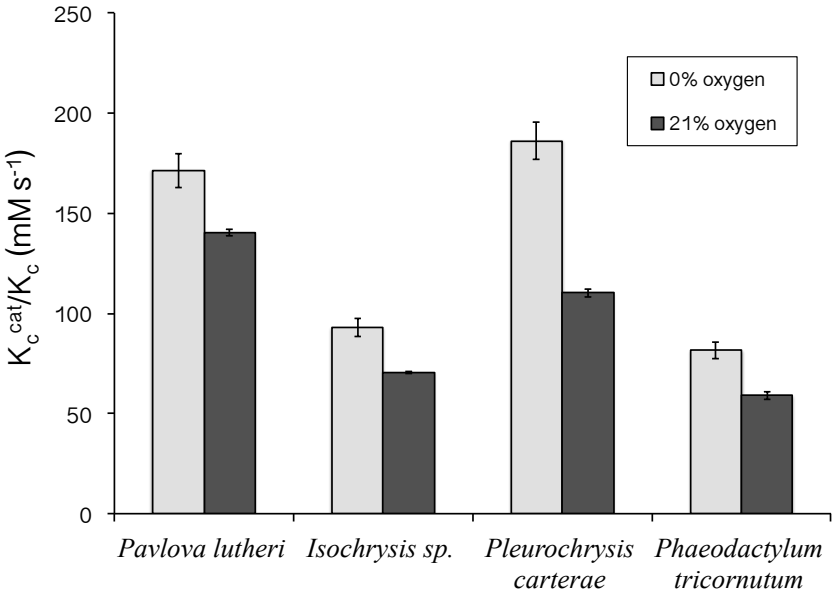

Figure 3-14: The ratio of catalytic turnover rate for carboxylation (K_c^{cat}) and the affinity for CO_2 (K_c) across the 4 species assayed at 0% oxygen (light gray) and 21% oxygen (dark gray). The difference between this ratio with increased oxygen provides insight into the effect of oxygen on the relative efficiency of the carboxylation reaction.

3.3.3 Part Three: Trade-offs in the cell - kinetic vs. whole cell strategies

3.3.3.1 Kinetic trade-offs

Here we present data from all of the species in which we have measured the whole suite of kinetic parameters (Table 3-8). In the remainder of this chapter we explore the broader relationships and correlations between kinetics variables as well as other measures of carbon concentrating mechanisms across these species. Previous studies have looked at these correlations from literature compilations of widely diverse photo- and chemosynthetic organisms (Tcherkez et al., 2006; Savir et al., 2010). In this study we look at the same relationships in closely related eukaryotic algae and observe unique trends.

Species		K_c (µM)	K_c^{cat} (s^{-1})	K_o (µM)	K_o^{cat}(s^{-1})	$S_{c/o}$
Pavlovophyceae						
Pavlova	*lutheri*	14	2.48	1146	157	125.5
Prymnesiophyceae						
Pleurochrysis	*carterae*	17	3.29	366	0.67	102.3
Isochrysis	*sp.*	24	2.24	799	0.83	89.1
Bacillariophyceae						
Thalassiosira	*weisflogii*	65	3.19	2031	1.28	78.5
Thalassiosira	*oceania*	65	2.35	954	0.43	79.8
Fragilariopsis	*cylindrus*	64	3.51	667	0.48	76.7
Phaeodactylum	*tricornutum*	56	3.38	2267	1.25	108.7
Phaeodactylum	*tricornutum*	41	3.35	663	0.47	115.9
Phaeodactylum	*tricornutum*	36	3.22	592	0.49	107.9
Chaeotoceros	*mulleri*	23	2.39	425	0.46	95.6
Chaeotoceros	*calcitrans*	25	2.62	412	0.75	56.7
Chaeotoceros	*calcitrans*	30	3.45	490	0.73	75.4

Table 3-8: Suite of kinetic data measured in select species from this study.

The correlations we observe between kinetic parameters in marine algae measured in this study are generally weak according to r^2 and p-values (presented in Figure 3-15) when compared to the linear trends reported by Tcherkez et al. (2006) and Savir et al. (2010). We find significant relationships between K_c vs K_c^{cat} (r^2=0.378, p=0.044) and K_o vs K_o^{cat} (r^2=0.494, p=0.011), however the trends between other variables plotted in Figure 3-15 are not statistically significant. When plotted against the data from Tcherkez et al. (2006) (Figure 3-16), our data shows either a different trend or a lack of trend altogether compared against the diverse species in their study. The direct trade-offs caused by a more product like transition state may be obscured in marine algal kinetics as a result of the variable CCM components and ability to up and down-regulate different aspects of the CCM.

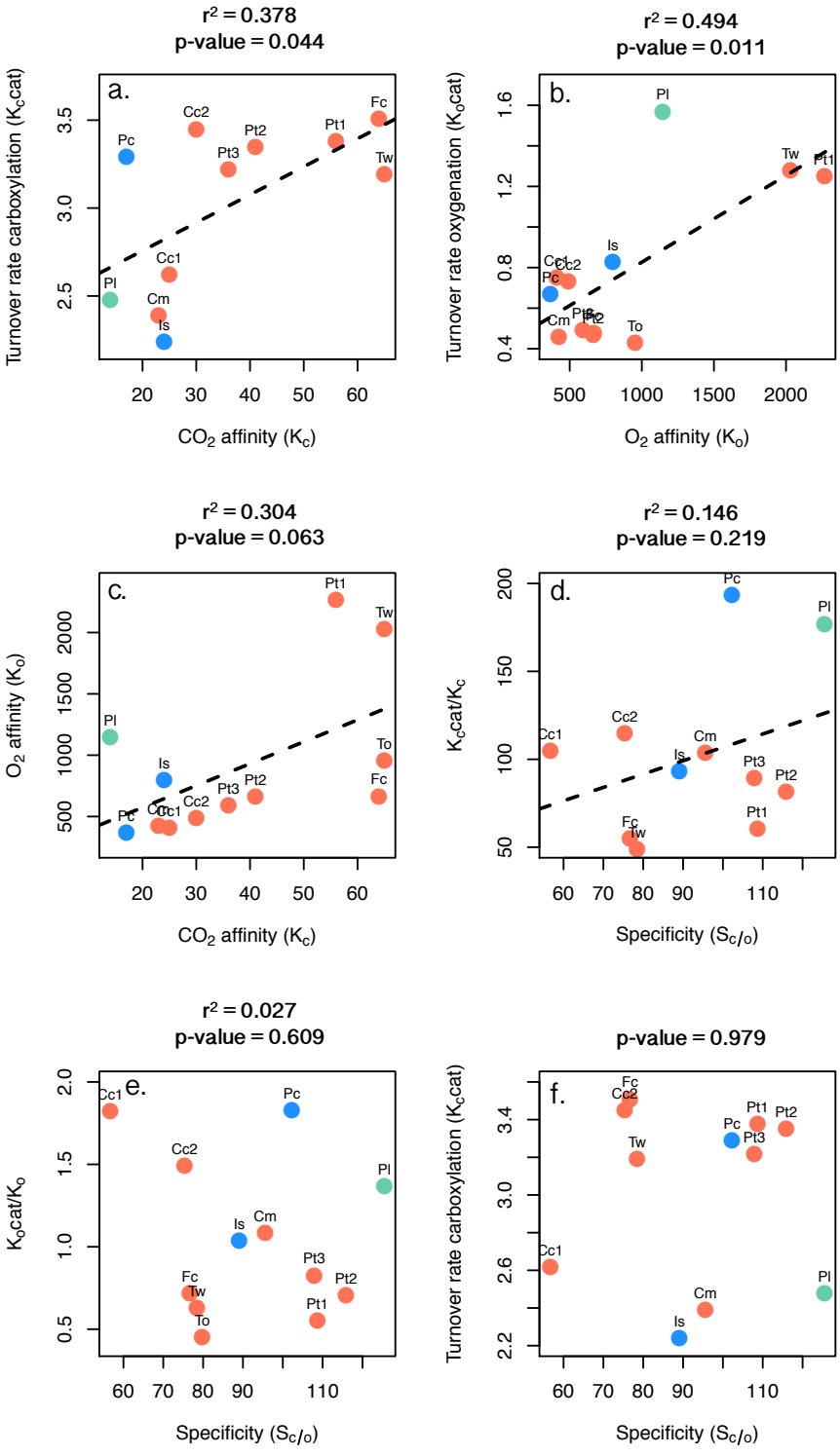

Figure 3-15: Plots showing relationships between key kinetic variables across all of the species outlined in Table 3-8 and the statistical relationship between the variables (r^2 and p-value). The *Pavlovophyceae* species is in green, *Prymnesiophyceae* in blue and the *Bacillariophyceae* in coral. The black dotted line shows the linear regression between the variables on each plot. A regression between plots e. and f. is not shown because there is no relationship between the two variables.

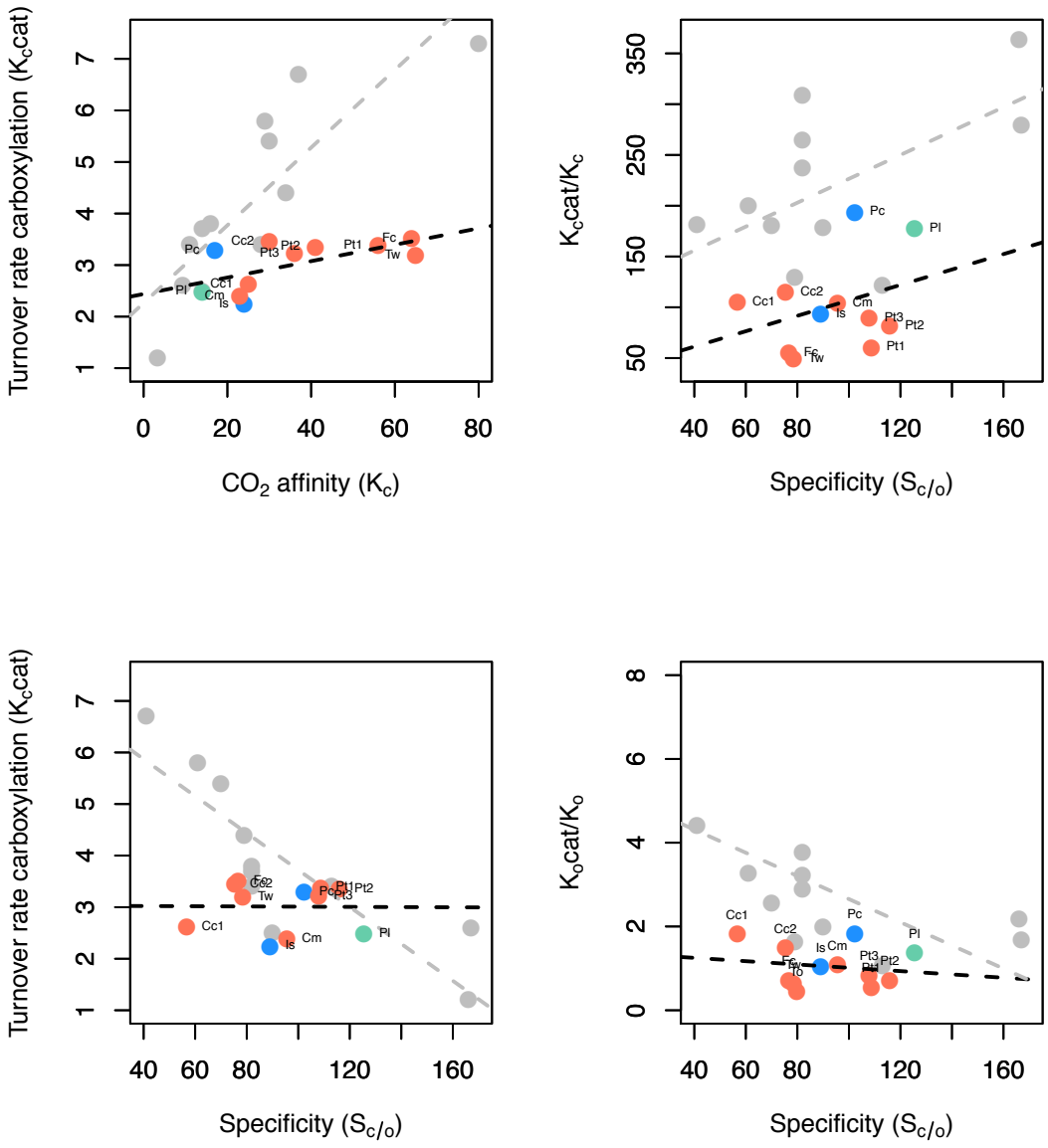

Figure 3-16: Plots of the data from this study plotted with the data from Tcherkez et al. (2006) (shown in grey). The regressions between the variables are shown in grey from Tcherkez's data and in black for this study. The trends are different between the two datasets. The plots in the bottom panels show no significant trend in our data with a linear relationship reported by Tcherkez et al. (2006).

In the closely related marine algae investigated in this study, we find that cells are using a combination of various strategies to meet their carbon needs and to avoid oxygen. For example, we know that algae have distinct pyrenoid morphologies, structures, and membrane components (or lack thereof). A pyrenoid bulging into the center of a cell may provide a longer path length for gases to diffuse into than a pyrenoid bulging to the periphery. While an internally bulging pyrenoid appears to provide a lower O_2 environment, an immersed pyrenoid acts to increase CO_2 at the site of Rubisco. Other parameters also define the unique CCM character in marine algae including carbonic anhydrase, bicarbonate transporters (Burkhardt et al., 2001; Trimborn et al. 2007). Together these factors will greatly vary the subcellular environment for Rubisco. This variability in strategies for carbon fixation many explain why trends observed by Tcherkez et al. (2006) are obscured in our study of kinetic variables in marine algae (Figures 3-15 and 3-16).

3.3.3.2 $K_m(CO_2$ photosynthesis) : $K_m(CO_2$ Rubisco) and Rubisco %TSP

Here we investigate further the CCM character of different marine algae and how it plays out in cell physiology. As another measure of presence/absence of a CCM across these species we compare the affinity of photosynthesis for external CO_2 ($K_{m(photosynthesis)}$) (measured in our lab by Dr. Benjamin Rae) to that of the affinity of its Rubisco ($K_{m(Rubisco)}$). The ratio $K_{m(photosynthesis)}$:$K_{m(Rubisco)}$ close to or higher than 1 suggests that the Rubisco enzyme requires approximately the same amount or less substrate than is provided by the cell, thus a CCM is not necessary to meet the demand. However, if

$K_{m(photosynthesis)}$:$K_{m(Rubisco)}$ is low, i.e. $K_{m(Rubisco)}$ is higher than $K_{m(cell)}$, we might assume that the pool of substrate available for Rubisco is higher than what is being taken up by the cell alone. Cells with a low $K_{m(photosynthesis)}$:$K_{m(Rubisco)}$ likely employ a CCM to achieve this ratio. With a few exceptions, most Chrysophyta and Chlorophyta algae measured to date are estimated to have low ratios between <1:30 and <2:30 (Badger et al., 1998) suggesting the presence of a CCM in these species.

Using the $K_{m(Rubisco)}$ values measured in this study and $K_{m(photosynthesis)}$ measured by Dr. Ben Rae using the oxygen electrode as well as additional values collected from the literature, we calculate $K_{m(photosynthesis)}$:$K_{m(Rubisco)}$. We observe a wider range of $K_{m(photosynthesis)}$:$K_{m(Rubisco)}$ across these species than shown in Badger et al. (1998). To assess the implications of this diversity, we consider the effects of this ratio and the presence of a CCM on the cell. Here we explore the trade-off between a CCM and the quantity of Rubisco produced by the cell (measured by Western blot). For reference, Figure 3-17 displays the established relationship in higher plants between $1/K_{m(Rubisco)}$ and the Rubisco as a percentage of total protein (Badger et al., 1998; Ku et al., 1979; Long et al., 1999).

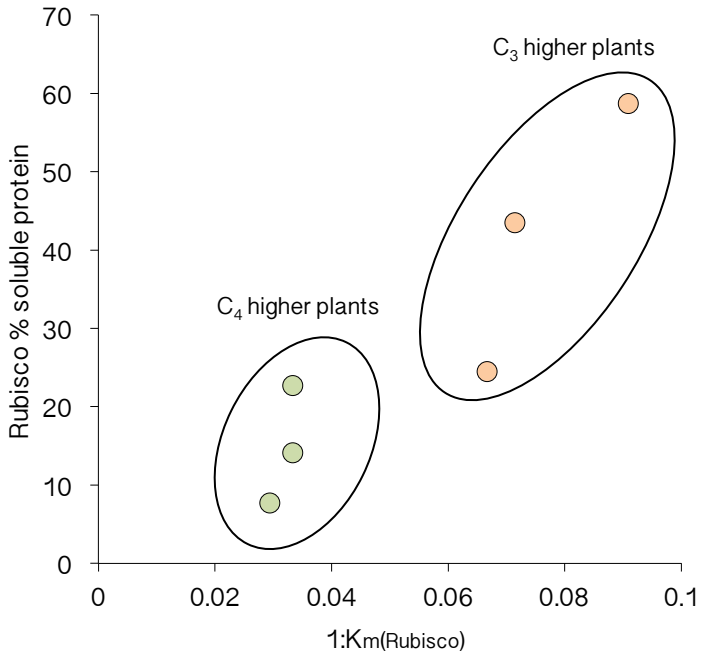

Figure 3-17: Plot of $1/K_{m(Rubisco)}$ versus Rubisco as a percentage of soluble protein. The figure shows a relationship between the two parameters with C_3 plants (lacking a CCM) exhibiting higher Rubisco percentage and lower $K_{m(Rubisco)}$. C_4 plants exhibit lower Rubisco percentage with higher $K_{m(Rubisco)}$ (Ku et al., 1979).

Figure 3-18 shows $K_{m(photosynthesis)}$:$K_{m(Rubisco)}$ plotted against Rubisco quantity (measured by Western blot and ImageJ quantification in the Earth Sciences Department, Oxford) as a proportion of total protein for species in this study where all three necessary parameters were measured. We observe a linear relationship in both the haptophytes (Figure 3-18a) and the diatoms (Figure 3-18b). This relationship supports the hypothesis that producing more Rubisco is a potential mechanism by which cells lacking a CCM may compensate to maintain the production of biomass as observed in C_3 higher plants. We must note that Rubisco quantity data presented in Figure 3-18 is different than values measured by [^{14}C]CABP binding, and discuss the differences in more detail in the conclusions section.

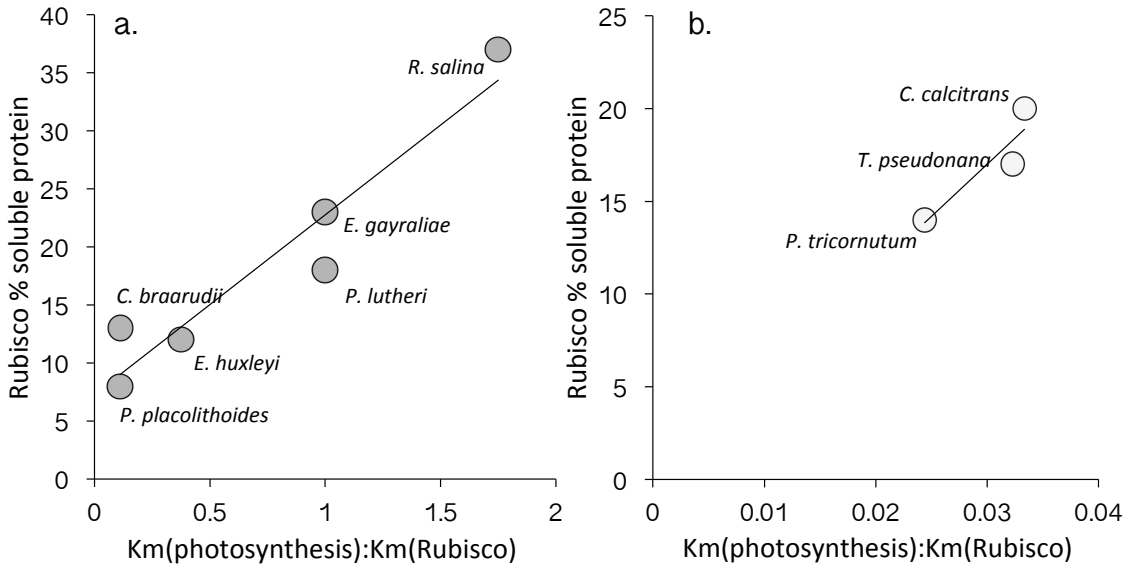

Figure 3-18: Plots of Km(photosynthesis):Km(Rubisco) versus Rubisco % per total soluable protein in (a.) the haptophytes (r^2=0.91) and (b.) the diatoms from this study.

Finally we plot $K_{m(photosynthesis)}$:$K_{m(Rubisco)}$ against cell size in the haptophytes to illustrate the role of size as a CCM (Figure 3-19). We observe that cells lacking a CCM according to this ratio are smaller while cells with a CCM tend to be bigger, with the exception of *E. huxleyi* with a strong CCM signal as well as a small cell size. There seems to be a threshold of CCM where without any carbon concentrating abilities, and presumably high Rubisco content, cells are unable to grow in biovolume. Only in cells with a CCM do we observe cell sizes over 4-5 μm.

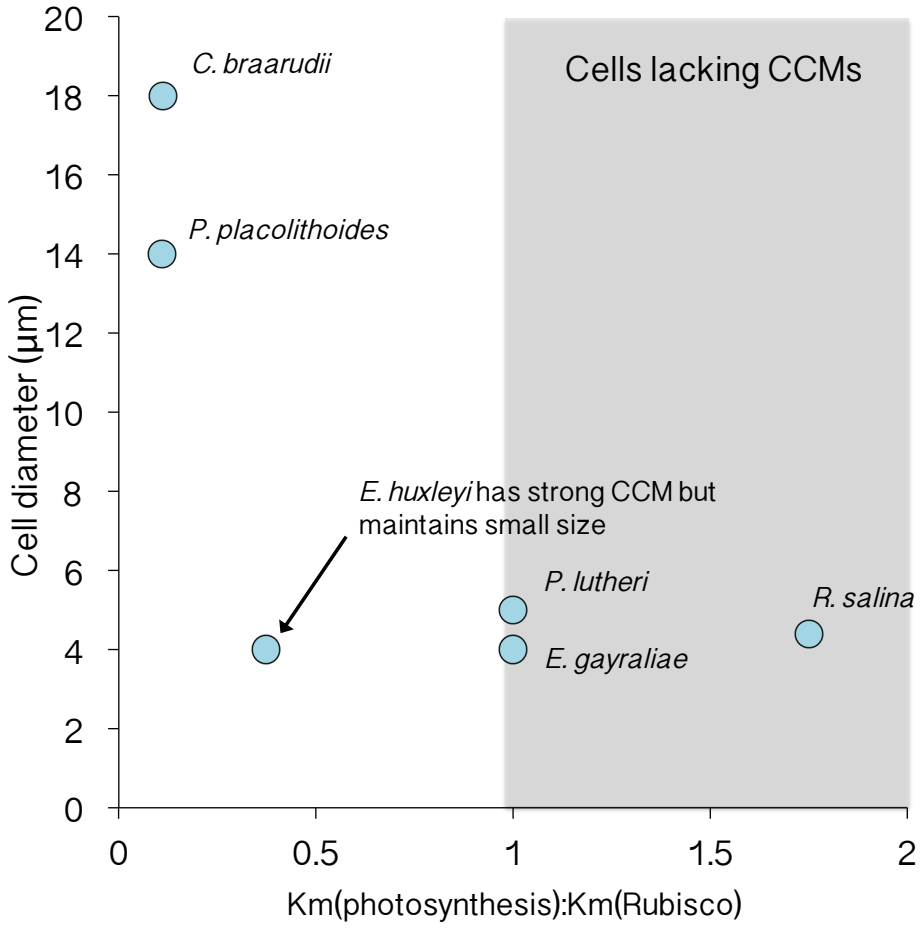

Figure 3-19: Km(photosynthesis):Km(Rubisco) as a measure of CCM ratio plotted against cell diameter. We can see that cells lacking a CCM (grey shaded area) tend to have the smallest cell diameters and highest Km(cell):Km(Rubisco) ratios. *Emiliania huxleyi* is an anomaly as it exhibits CCM characteristics but also has the smallest diameter.

3.3.4 Limitations

The interpretation of this data must take into account that the measurements in this study were performed in two different laboratories with slightly different methodologies. Our discussion of K_c is more complete than our discussion of other kinetic variables as we have more measurements of K_c completed at Oxford while other kinetics were only measured at the Australian National University. We also note the differences in Rubisco quantification via Western blot and via [^{14}C]CABP binding. While the absolute values

vary between the two methods, the trends are generally the same. We hypothesize that this discrepancy is due to differences in growth conditions in the two labs as well as other slight differences in methodologies of the Bradford assay between the two labs. Finally, we note a limitation of this dataset is the variability in parameters measured in some species but not in others. Again this is due to what species we had available in each department.

3.4 Conclusions

We conclude from this three-part study that the pyrenoid-based CCM provides an "Archaean-like" subcellular environment for the Rubisco enzyme to ease its inability to differentiate between CO_2 and O_2 as substrates. This is achieved it two ways, (1) by actively concentrating CO_2 and (2) by decreasing O_2 at the site of Rubisco, as evidence by contrasting Rubisco affinities. In the species measured here, we find that the activity of the enzyme carbonic anhydrase, facilitating the interconversion between HCO_3^- and CO_2, corresponds to the presence of a pyrenoid, but we do not identify major differences in CA activity between different pyrenoid morphologies. In cells with an immersed pyrenoid and active CA measured by at least two methods, the internal carbon pool was measured to be ~6-fold higher than the external C_i pool (Badger et al., 1998).

We find significant variation in the affinity of Rubisco for CO_2 substrate, overall kinetics and other coincident CCM parameters across eukaryotic marine algae. As predicted, we find that CCMs in marine algae broadly fall into groups as outlined by Badger et al. (1998). The CCM "types" observed in this study fall under the modelled type 1 and type 2 CCM

(outlined in Figure 3-8 and Table 3-5 taken from Badger et al. [1998]), with and without a pyrenoid with high and low K_c values, respectively. Our dataset confirms modelled assumptions about diversity in the CCM of marine algae, but suggests that the story might be even more complex than assumed from reviews of the algal CCM system (Badger et al., 1998; Reinfelder et al., 2011; Tcherkez et al., 2006, 2013) when considering the diversity in strategies for increasing CO_2 fixation within these unicellular eukaryotes.

The suite of kinetic parameters measured in this study provides new and telling insight into the subcellular environment provided by the pyrenoid in marine algae. The relationships, however, are not entirely straightforward. The high CO_2 and low O_2 Rubisco affinity of *P. lutheri*, the cell lacking a pyrenoid, suggests a low $[CO_2]$:$[O_2]$ environment at the site of the enzyme. The species exhibits the highest overall specificity, which we presume is a necessary adaptation for a cell with the most O_2 around the site of Rubisco. As a result of its requirement for high CO_2 affinity, the cell detrimentally has the lowest turnover rate for carboxylation and the highest for oxygenation, making it the slowest at fixing carbon for photosynthesis. In conclusion, the inability to increase the $[CO_2]$:$[O_2]$ ratio around Rubisco forces it to increase specificity and decrease turnover for CO_2. We hypothesize that to compensate for this slow rate, cells without a pyrenoid-based CCM increase Rubisco production, and in turn can only support a small cell (Figure 3-19).

The reduction of O_2 as a competitive substrate for Rubisco allows enzymes within a pyrenoid to relax their CO_2 affinity and specificity, and as a result increase the catalytic turnover rate of the carboxylation reaction over oxygenation. These cells, more rapidly fixing carbon are able to downregulate Rubisco production. This overall efficiency and

downregulation may free up resources for the cell to use elsewhere and allow them to live in environments limited by essential resouces such as nutrients, trace metals, light etc.

When we plot kinetic parameters against each other, we observe different or no significant trends in the marine algae from this study when compared to trends observed across diverse primary producers in Tcherkez et al. (2006). We conclude that this variability is a result of the diverse components of the CCM system in marine algae, each playing a different role to benefit the function and carbon fixation of the cell. As a result of these varied components with each species utilizing them to different degrees, the kinetics have not evolved a simple trade-off between high and low $[CO_2]$:$[O_2]$ environments.

3.4.1 Trade-offs in the CCM system

Although our study in marine algae suggest that kinetic parameters do not experience such distinct trade-offs as hypothesized by Tcherkez et al. (2006), we suggest that the CCM system in marine algae is still using trade-offs to achieve a sufficient amount of carbon fixation to sustain life. One major trade-off highlighted in this study is between the affinity of Rubisco for CO_2 substrate and the packaging of the Rubisco in an immersed pyrenoid structure. In marine haptophytes we conclude that although the exact function of the pyrenoid remains contentious, the presence/absence of a pyrenoid has played a role in the resultant kinetics of the Rubisco enzyme. The pyrenoid may benefit the cells in other ways in addition to the relaxation of CO_2 affinity. Some examples include ordered packing, increase activation, and the presence of pyrenoid CA within an ordered Rubisco environment providing a constant supply of CO_2 while also preventing leakage (Badger

et al., 1998). The packaging of Rubisco, and potentially CAs, in the pyrenoid is an interesting avenue for future work.

Another trade-off we observe is between the presence of a CCM and the amount of Rubisco synthesized by the cell. The more the cell concentrates carbon or higher the $K_{m(photosynthesis)}$:$K_{m(Rubisco)}$, the less Rubisco we find per total protein. We suggest that a cell with higher internal $[CO_2]$:$[O_2]$ ratio, decreased affinity and higher turnover rate of carboxylation needs fewer Rubiscos to produce the same amount of fixed carbon. Another explanation for the decreased Rubisco with higher CCM is that in a high CO_2 environment, more Rubisco is active. With a higher percentage of active Rubisco, the cell may similarly need less of the enzyme to achieve the same end result. However, it is important to note that Rubisco is extremely nutrient expensive so its upregulation may not be a viable option for all cells. This illuminates how each cell may be adapted to fix carbon efficiently in its selected environment.

Looking more broadly across all kinetic parameters measured in this study, we suggest that the *P. carterae* Rubisco may be the most "effective" overall with a high CO_2 affinity, high carboxylation rate and low oxygenation rate, evidence against Tcherkez's hypothesis that there *must* be a trade-off between K_c and K_c^{cat}. This does not disprove that Rubisco enzymes are perfectly adapted to their environment, however does argue against the hypothesis by Tcherkez et al. (2006) that every optimization in affinity has a corresponding negative trade-off in turnover rate. This finding may be important in the search for optimal Rubisco present in the natural world.

3.4.2 The role of the CCM in determining success and habitats in marine algae

In higher plants, the C_4 photosynthetic pathway is thought to have evolved as an adaptation to arid climates, high temperature and high light intensity (Edwards et al., 2010). C_4 plants have independently evolved more than 50 times from C_3 angiosperms, suggesting a relative simplicity of the genetic pathway (Muhaidat et al., 2007). The relative frequency of the evolution of this pathway is explained by the finding that each step toward the C_4 pathway is thought to lead to an evolutionary benefit for the organism, even before establishment of the full C_4 pathway. C_4 plants have undergone biochemical and anatomical modifications that ultimately increase the concentration of CO_2 at the site of Rubisco and prevent the loss of water during gas exchange when the stoma is open. As a result of the higher CO_2 concentration, Rubisco in C_4 plants works more efficiently and subsequently less enzyme is required (Gowik et al., 2011). Plants with a developed C_4 pathway have a higher rate of photosynthesis per unit nitrogen and as a result have better nitrogen-use efficiency compared to C_3 plants (Oaks, 1994). The dual benefit of increased photosynthetic rate per unit nitrogen and decreased water loss during carbon fixation primes C_4 plants for life in taxing environments.

Although marine algae do not have to struggle against arid conditions, there are a number of other obstacles for survival in the ocean. In the modern open ocean, algae are faced with nutrient limitation, high light, CO_2 limitation and trace metal limitation. One salient feature of the diversity of algae in this study is that they reside in drastically diverse marine environments. While the *Pavlovophyceae* tend to live in coastal or benthic environments, the coccolithophorids as well as the *Bacillariophyceae* are generally found in the open

ocean. In conclusion to this study we suggest that the CCM may act to streamline carbon fixation, increasing nutrient-use efficiency and priming these algae for life in the open ocean (DeVargas et al., 2007). From a first order, we conclude that the species in this study with a strong CCM reside mainly in the open ocean or are hypothesized to have moved out and back to the coast during their evolutionary history (Liu, 2010; Eason-Hubbard, unpublished data). Cells lacking a pyrenoid-based CCM are limited to coastal environments.

We conclude in this study that species with a CCM are, like C_4 plants, reducing Rubisco production and thus also optimizing their nitrogen use efficiency compared to cells without a CCM. This benefit alone gives cells with a CCM an advantage. Another yet unknown parameter is how much energy/resources cells invest in the actual production of the CCM in marine algae. Although more work must be done, we conclude that the role of a CCM for marine algae is not simply to increase carbon fixation and growth rate, but also a strategy for filling an available niche where species lacking a CCM cannot.

Chapter 4: Assessing physiological responses of marine algae to elevated CO_2

Contributions: This work was carried out and written by myself. I would like to thank Dr. Renee Lee for instruction and help with method development and implementation. Also Alan Wainman for his help and expertise with the confocal microscope. Cell size data was measured by 4th year student Ian Chan supervised by Dr. Michael Hermoso and myself.

4.1 Introduction

The diversity of evolutionary solutions for overcoming the limitations of the Rubisco enzyme (as outlined in Chapter 1) is great in aquatic eukaryotic organisms due to their relatively complex structural and genetic systems (Badger et al., 1998; Reinfelder 2010). However, a large proportion of work to date on the functional diversity of the carbon fixation reaction is focused on the more basic system in prokaryotic organisms, such as cyanobacteria (Price & Badger, 2008; Rae et al., 2014) and in higher plants (Ehleringer & Monson, 1993; Long et al., 1999; Muhaidat, 2007; Sage, 2014). This study aims to build our understanding of evolutionary solutions for efficient primary production in marine eukaryotes as their role in the environment is of great ecological and geological importance. So far in this thesis we have omitted one important dimension in carbon fixing strategies: plasticity, or the organism's ability to rapidly respond to changing environmental conditions.

One of the major environmental applications of marine eukaryotic algae material is the fractionation of carbon isotopes ($\delta^{13}C$) recorded in organic material as Rubisco fixes CO_2 into biomass (as shown in Chapter 2). However, in order to use organic $\delta^{13}C$ from marine algae as a proxy to interpret carbon dioxide changes in the geological record, the chemical signal must be calibrated under controlled conditions (Pagani, 2014; Zhang et al., 2013). To do so, algal producers of specific organic compounds are grown in media calibrated in variable carbon chemistry and subsequently the compound of interest is analyzed for $\delta^{13}C$. This value plotted against the carefully controlled carbon system parameters can then be used as a calibration for $\delta^{13}C$ measured in ancient samples where the CO_2 is unknown.

Throughout this thesis we have aimed to elucidate some of the controls on and variability in the machinery that in turn controls this process. In this chapter we go a step further to look at the plastic response of this machinery in cells grown at variable CO_2 concentrations in culture.

While models and calibrations of carbon fractionation for the application of biological proxies provide useful estimates of the fluxes in and out of the cell (Francois et al., 1993; Laws et al., 1995, 1997; Pagani et al., 2011; Popp et al., 1998), they do not fully consider biological or physiological responses occurring coincidentally in response to changing CO_2. A plastic change in carbon fixing strategy may alter the subcellular environment around carbon fixation, changing the baseline for isotopic fractionation of the organic compounds and ultimately complicating the interpretation of $\delta^{13}C$. The more thoroughly we understand the cell's photosynthetic machinery, as well as its response to changing CO_2, the more effectively we can interpret signals recorded in $\delta^{13}C$ from ancient organic material.

In this chapter, we review and discuss reported measurements of carbon anhydrase (CA) transcript levels (Tachibana et al., 2011) as an indicator of CCM, nitrogen use and C:N ratios (Wang et al., 2015) in marine eukaryotes in response to variable CO_2 conditions in the laboratory. With this data for context, we present new measurements of Rubisco location and quantity at high and low CO_2 in select well-studied species of marine algae. This information brings this thesis full circle from Chapter 2 where we used $\delta^{13}C$ in marine diatoms as a proxy for CO_2, to Chapter 3 which built an understanding of the diversity of photosynthetic machinery in marine haptophytes and diatoms, and finally to this chapter

looking at short term changes in this machinery in response to varying CO_2. This final chapter will not only again inform our interpretation of carbon isotopes from marine phytoplankton, but will additionally try to answer some of the unanswered questions from the previous chapter about variation in nutrient requirement and enzyme production with differences in physiology. These three chapters together should provide a holistic picture of evolutionary solutions that aid photosynthesis in eukaryotic marine algae, clarify our understanding of the function of the algal CCM and ultimately illuminate oversights in the current application of $\delta^{13}C$ from organic compounds in marine algae for the interpretation of CO_2 in the geological record.

The physiological response of the CCM to CO_2 has been well documented in cyanobacteria and green algae (Dionisio-Sese et al., 1990; Marcus et al., 1983; Matsuda et al., 2011; Matsuda and Colman, 1995a, b; Mayo et al., 1986). While in prokaryotic algae the CO_2 response is primarily in the regulation of available metabolite, eukaryotic algae have been found to directly alter the mechanisms for CO_2 uptake (Matsuda and Colman 1995b). Previous work looking at marine algae communities has shown increased growth at high CO_2, increased photosynthetic efficiency and suggests energy savings from the down-regulation of the CCM (Hopkinson et al., 2010; Sobrino et al., 2014). The present study provides insight into the mechanistic response of eukaryotic algae to changes in the carbon system. Although the cell will not be able to change genetically determined characters such as the kinetics of the Rubisco enzyme (Chapter 3), we show in this study that a eukaryotic cell can quite effectively adapt its physiological parameters to variation in its external CO_2 environment.

From the data measured and compiled in the present study, we find that at elevated CO_2, pyrenoid based carbonic anhydrase is downregulated and we observe the migration of Rubisco out of the pyrenoid. While these CCM parameters are being suppressed, we show that the amount of Rubisco synthesized by the cell increases along with the reported increase in nitrogen uptake per cell. In these experiments at high [CO_2], and importantly nutrient replete conditions, the cells forego CCM use potentially freeing resources and increasing protein production. However, under limited CO_2 or nutrient conditions, eukaryotic algal cells use CCM mechanisms to optimize their nutrient use efficiency and streamline carbon fixation. The availability of resources may strongly dictate the cell's ability to make these changes. This study has great implications for understanding differences in lifestyle and habitats in marine algae as well as the interpretation of biological markers for estimates of paleo-atmospheric CO_2.

4.2 Methods

4.2.1 Culturing and altering carbon chemistry

Culturing was carried out in the Rickaby microbiology laboratory in the department of Earth Sciences at Oxford University. For species and culturing details refer to Chaper 3 methods and table 3-1.

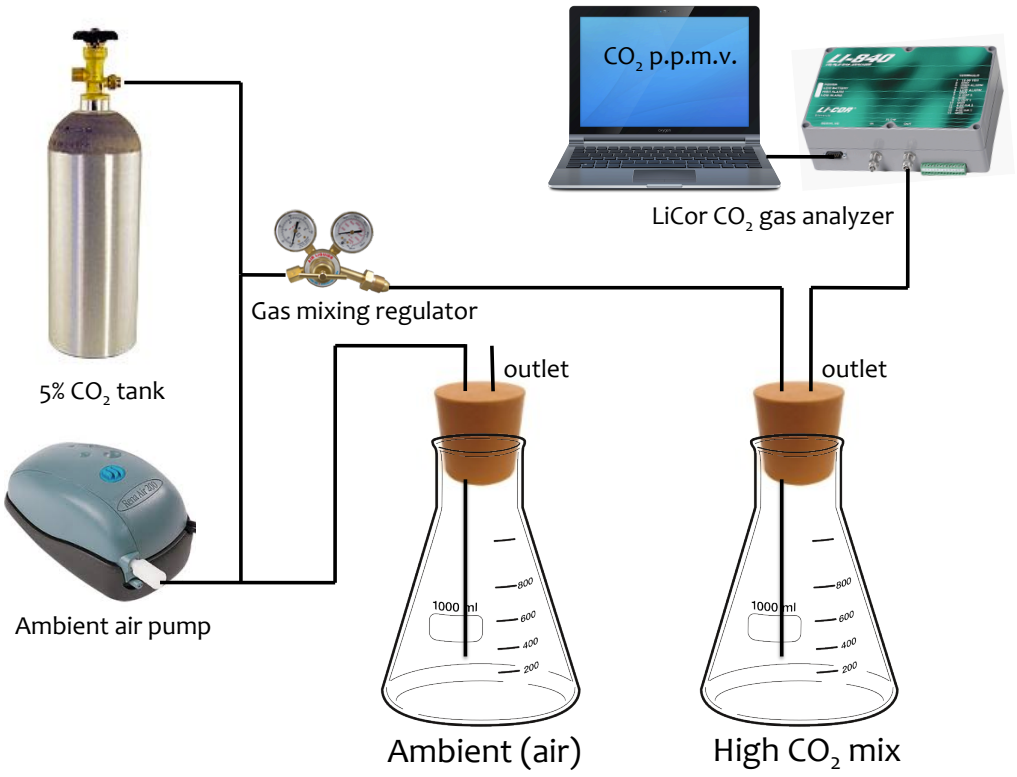

Figure 4-1: Schematic of experimental set up for bubbling cultures with ambient (390 p.p.m.v.) and high CO_2 gas. Conical flasks were kept in incubators throughout growth. Ambient air and CO_2 from 5% CO_2 tank were mixed with a gas regulator (Cole palmer) and bubbled for the high CO_2 mix cultures. The ambient cultures were bubbled with air pumped from the laboratory. High CO_2 cultures were monitored twice daily. Gas leaving the outlet was connected to the LiCor CO_2 gas analyzer and measured in p.p.m.v.

Carbon chemistry was altered in this study using bubbling set up with conical flasks and rubber stoppers with an inlet and an outlet gas exchange (Figure 4-1). Gas was pumped in through a sterile plastic inlet mixed to the desired CO_2 concentration from a 5% CO_2 tank and ambient air pumped from the laboratory. The concentration of CO_2 entering the flasks and leaving the outlet was monitored twice daily during the course of the experiment using a LiCor (LI-820 CO_2/H_2O gas analyzer). Samples were acclimatized to CO_2 conditions for 10 generations, harvested during exponential growth and immediately frozen until analysis.

4.2.2 Rubisco localization using confocal microscopy

Slides for Rubisco localization were prepared by incubating coverslips in 1% (v/v) PEI (P3143 Sigma) for approximately 30 minutes. Coverslips were rinsed with DI water and left to dry in a petri dish. Once dry, a suspension of desired culture was applied to fully immerse slip and left to settle for ~15 minutes, then the supernatant was removed. Cells were fixed at room temperature (RT) in 4% (v/v) PFA in 1x PBS buffer [137mM NaCl, 2.7 mM KCl, 10 mM Na_2PO_4, 1.8 mM KH_2PO_4 in MilliQ H_2O autoclaved sterile] or K/2 media for 30 minutes (Table 4-1). Next, cells were permeabilized with 0.5% Tween20 in 1x PBS for 15 minutes. Slides were incubated in blocking buffer [1% w/v BSA in 1x PBS] for 30 minutes before incubation in blocking buffer with Rabbit anti-RbcL (Sigma) primary antibody (1:800) for 1 hour at RT (again see table 4-1 for different treatments). Finally, slides were incubated in blocking buffer with Alexa Fluor 488 goat anti-Rabbit IgG (H + L) (Molecular probes) secondary antibody (1:1000) for 1 hour at RT. Between each incubation step slides were rinsed 3x in 1x PBS. Treatments varied slightly depending on the species (see Table 4-1). Coverslip was mounted on slide with mounting buffer (Vectashield mounting medium for fluorescence) and sealed with clear nail varnish. Slides were stored in the dark until visualization. To visualize the cells, we used the light confocal microscope system (Fluoview FV1200 IX83; Olympus) with a 60x/1.4 NA oil objective, a 488 nm excitation wavelength and FV10-ASW software (Olympus) with help from Alan Wainman in the Dunn School Imaging Facility, University of Oxford.

Species	Fixation solution	Permeabilization solution	Primary antibody concentration	Secondary antibody concentration
Emiliania huxleyi	4% PFA in K/2	0.5% Tween-20 in 1x PBS	1:250	1:200
Pleurochrysis placolithoides	4% PFA in K/2	0.5% Tween-20 in 1x PBS	1:250	1:200
Phaeodactylum tricornutum	4% PFA in 1x PBS	1.5% Tween-20 in 1x PBS	1:800	1:1000
Thalassiosira pseudonana *Thalassiosira weisflogii* *Chaeotoceros calcitrans* *Rhizosolenia setigera*	4% PFA in 1x PBS	1.5% Tween-20 in 1x PBS	1:800	1:1000

Table 4-1: Outline of treatments used in preparation of confocal slides. Treatments were varied on a trail and error basis to get best results for each species.

4.2.3 Rubisco quantification

Immoblots carried out according to methods outlined in Chapter 3. Three replicates were performed for each species under both CO_2 treatments.

4.3 Results and Discussion

4.3.1 Reported carbonic anhydrase (CA) in response to changing CO_2

Briefly, CAs were identified in the marine diatoms *Phaeodactylum tricornutum* and *Thalassiosira pseudonana* by searching the genome sequences for CA-encoding genes. Quantification was achieved using semi-quantitative reverse transcription PCR performed on mRNA (Figure 4-2). Immunostaining transmission electron microscopy was used to show relative localization of CAs in the cell. In their study, Tachibana et al. (2011) find

that when grown under high CO_2 conditions, transcript levels of plastid localized CAs (PtCA1 and PtCA2) are decreased in *P. tricornutum* and some cytosol localized CAs (CA1, 3, and 7) in *T. pseudonana*. Their findings, supported by data from Satoh et al. (2011), Harada et al. (2005) and Harada and Matsuda (2005), additionally demonstrate that other CA isoforms did not respond to variation in CO_2. The downregulation of chloroplast and pyrenoid CAs under high CO_2 allows the cell to control the influx and efflux of C_i because without CA activity, the resistance to diffusion is great (Tachibana et al., 2011). At low CO_2, the activity of CA in the chloroplast/pyrenoid will draw the C_i flux inward, effectively increasing [CO_2] in the plastid. More work must be done to clarify these mechanisms, but these results support the downregulation of a CCM in the two diatom species presented here under high CO_2 conditions.

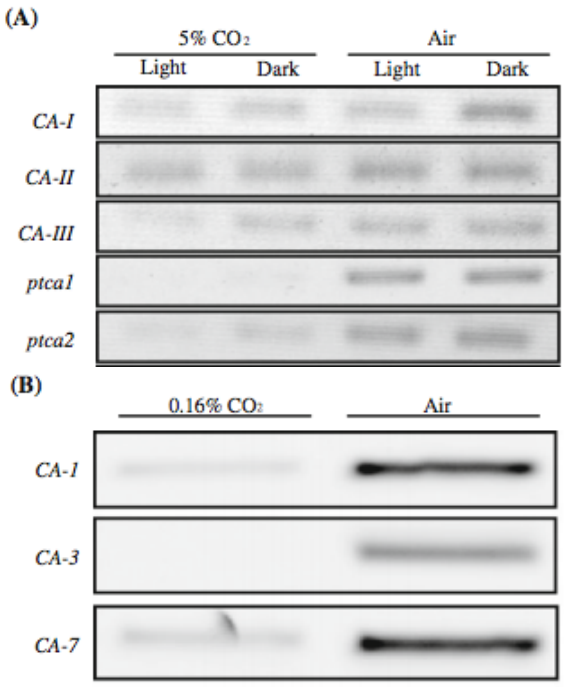

Figure 4-2: Transcript levels of diatom CAs in *P. tricornutum* (A) and *T. pseudonana* (B) under different CO_2 conditions. Diatom *P. tricornutum* was grown at 5% CO_2 and atmospheric air (Air). *T. pseudonana* was grown at 0.16% CO_2 and atmospheric air (Air) with continuous illumination (taken from Tachibana et al., 2011).

4.3.2 Changes in Rubisco: location and quantity

In this study we characterize changes in the location and quantity of the Rubisco enzyme under high and low CO_2. The localization of Rubisco, achieved by immunolocalization was difficult to optimize in many of the species attempted in this study as they have biomineral layers separating the cells from the environment causing difficulty in penetrating the barrier for antibody diffusion. After attempting various treatments, we were able to successfully penetrate the membrane and visualize the haptophyte species *Emiliania huxleyi* and *Pleurochrysis placolithodes* and the model diatom species *Phaeodactylum tricornutum*. We experimented with the diatom species *Thalassiosira pseudonana*, *Thalassiosira weisflogii*, *Chaeotoceros calcitrans* and *Rhizosolenia setigera*, but were unable to get the antibody to penetrate the cell. Across the samples we visualized, the location of the Rubisco enzyme was not uniform. We hypothesize, as suggested by Lin and Carpenter (1997) in *Chlamydomonas reinhardii*, that Rubisco location is never uniform across the community of cells in a given sample. In this section, we have identified the Rubisco localization most representative of cells in each treatment.

Results from *Emiliania huxleyi* grown at low (ambient or ~390 p.p.m.v) and high (0.16% or 1,600 p.p.m.v.) CO_2 are shown in Figure 4-3. This high CO_2 treatment was chosen as it is environmentally relevant (estimated Eocene [CO_2]) and also has been used in other relevant studies such as Tachibana et al. (2011). In cells where the antibody has penetrated and bound within the cell, we find that at low CO_2 the Rubisco seems to be localized to one or two small semi-circular areas within the cell. We hypothesize that this area is a pyrenoid structure. In the cells grown under high CO_2, we observe Rubisco dispersed

across a larger area in the cell. In this treatment, we observed immunolocalized Rubisco (green) overlain with chlorophyll autoflouresence (red), suggesting that the Rubisco is spread throughout the chloroplast where chlorophyll resides. From visual observation alone, it looks as though there is more antibody-bound Rubisco in the cells grown at high CO_2, however these observations are not quantitative. The general trend observed in cells from low to high CO_2 treatments is the movement of Rubisco from a localized spherical area to spreading throughout the chloroplast.

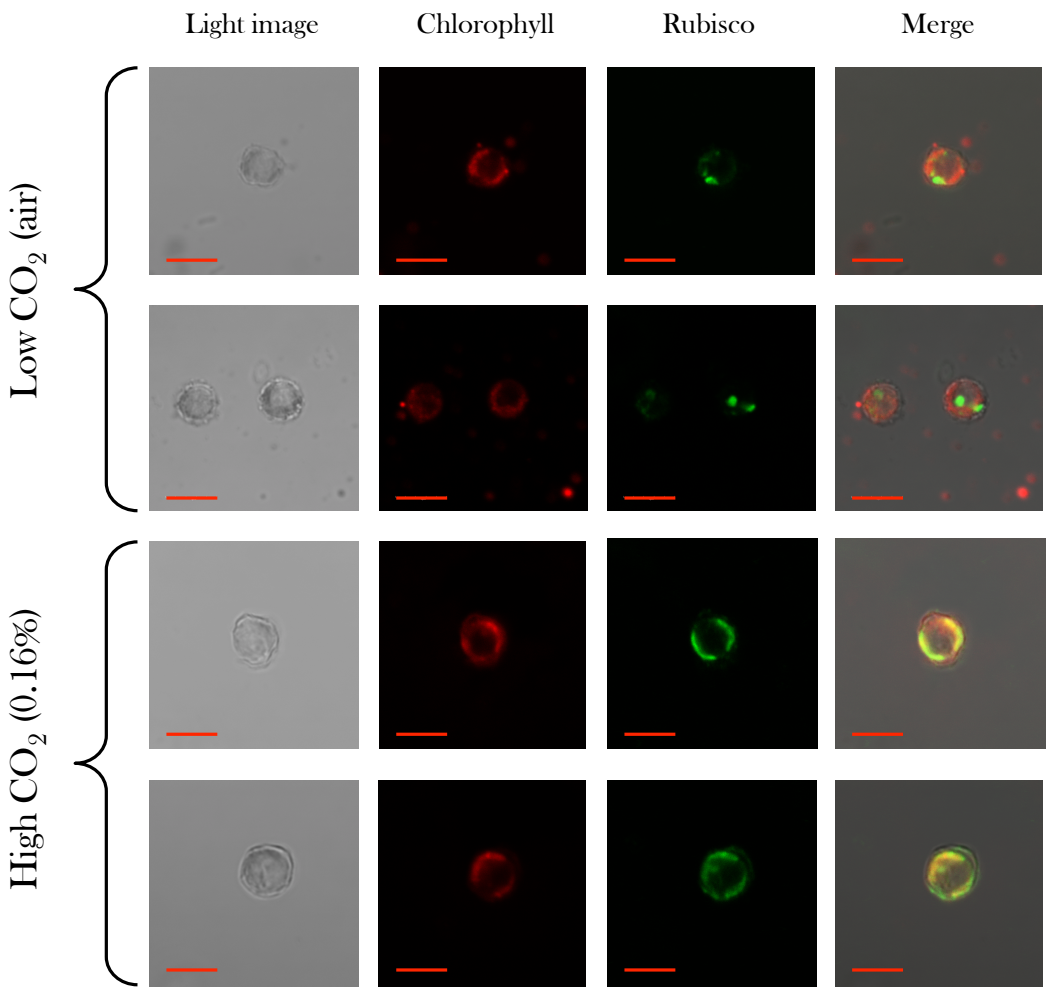

Figure 4-3: Confocal images of the haptophyte *Emiliania huxleyi*. The first column shows transmission light microscope images. The second represents chlorophyll autoflorescence (red) and the third column is immunolocalized Rubisco (green). The final column of images shows the merged channels. The top two panels are cells grown at low (ambient) CO_2 concentrations and the bottom two panels are cell grown at high CO_2 (0.16%). The scale bars represent 5 μm.

In the diatom species *Phaeodactylum tricornutum*, we find a similar trend between the two CO_2 treatments (Figure 4-4). In the low CO_2 treatment, we find the Rubisco antibody (green) concentrated in the dark elongate area in the center of the autoflouresence (red). We assume that this area, lacking chlorophyll, is the Rubisco dense pyrenoid for this species as shown in Tachibana et al. (2011). Cells were grown in two high CO_2 treatments (0.16% and 5% CO_2), to compare with the CA measurements at 5% CO_2 in Tachibana et al. (2011). In the high CO_2 treatments, we do not find Rubisco limited to this darkened area and in some cases it seems to be present in the chloroplast but *not* in the area presumed to be the pyrenoid (white arrow Figure 4-4). In both species, Rubisco is localized to a smaller area, that we hypothesize to be the pyrenoid, in low CO_2 treatments. We observe greater dispersion of Rubisco in the high CO_2 treatments, generally throughout the chloroplast. In one example in *P. tricornutum*, we observe Rubisco leaving the pyrenoid structure completely and only located in the chloroplast.

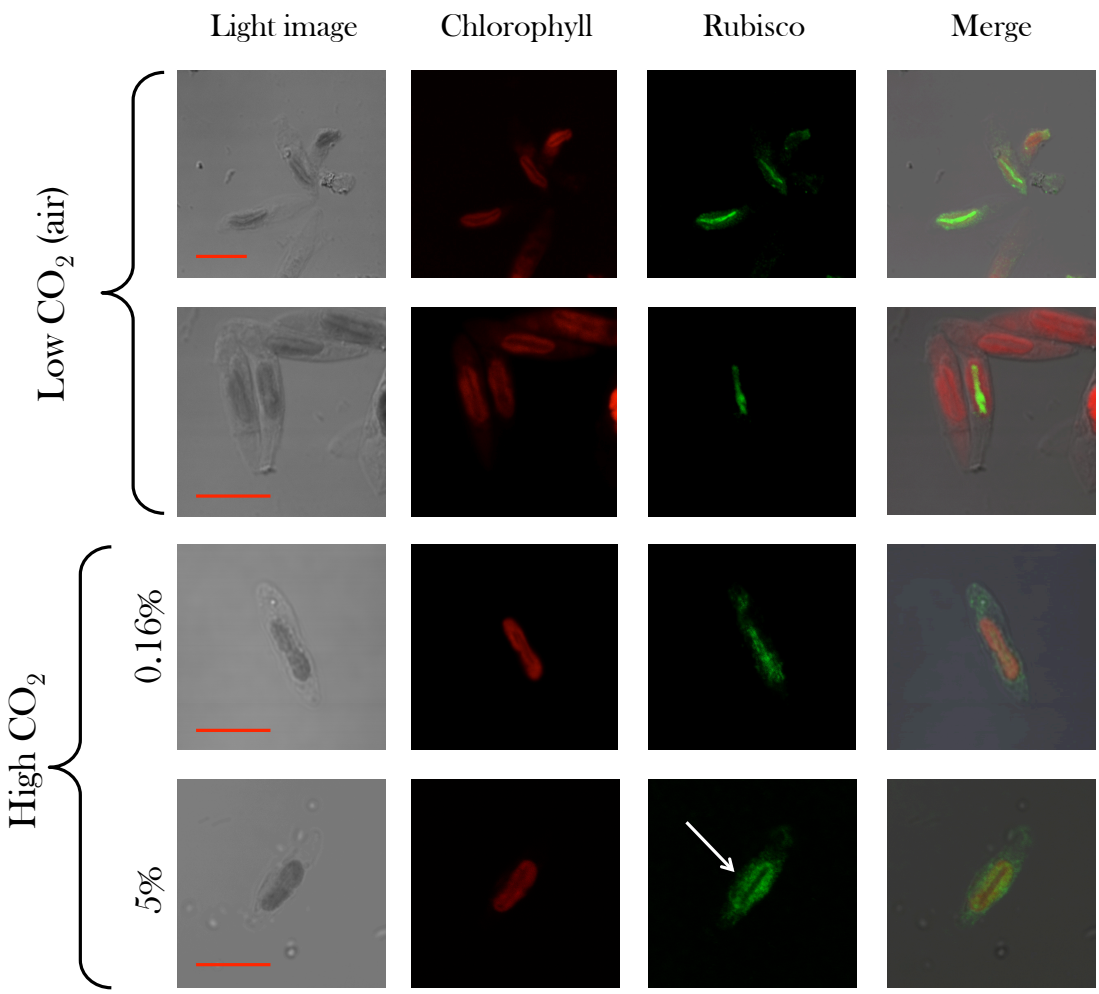

Figure 4-4: Confocal images of the diatom *Phaeodactylum tricornutum*. The first column shows transmission light microscope images. The second demonstrates chlorophyll autoflorescence (red) and the third column is immunolocalized Rubisco (green). The final column of images shows the merged channels. The top two panels are cells grown at low (ambient) CO_2 concentrations and the bottom two panels are cell grown at high CO_2 (0.16% and 5%). White arrow highlights example of Rubisco moving out of the pyrenoid structure completely. The scale bars represent 5 μm.

In the species *Pleurochrysis placolithoides*, we were able to get antibody into the cell, however we observed possible cell damage as a result of the treatment and preparation of the slides. We observed similar damage in other diatom species, including distinct autoflorescence artifacts where we suggest the chloroplast structure may have burst releasing chlorophyll in concentrated leaks in the cell (Figure 4-5), however the cells still demonstrate some degree of preservation of cell structure. In both the low and high CO_2 treatments presented in Figure 4-5, we can see the internally bulging pyrenoid structure. In Figure 4-5 we present the best examples of a preserved cell with antibody binding. These examples suggest that Rubisco is actually more dispersed in the low CO_2 treatment than in the high treatment where Rubisco seems to be limited to the perimeter of the pyrenoid structure, opposite to what we observed in the two other species. We do not put as much weight on these results due to the potential damage of the cell, however include them as they show an interesting trend of Rubisco localization at the pyrenoid perimeter which has not been observed before in any species of aquatic primary producer.

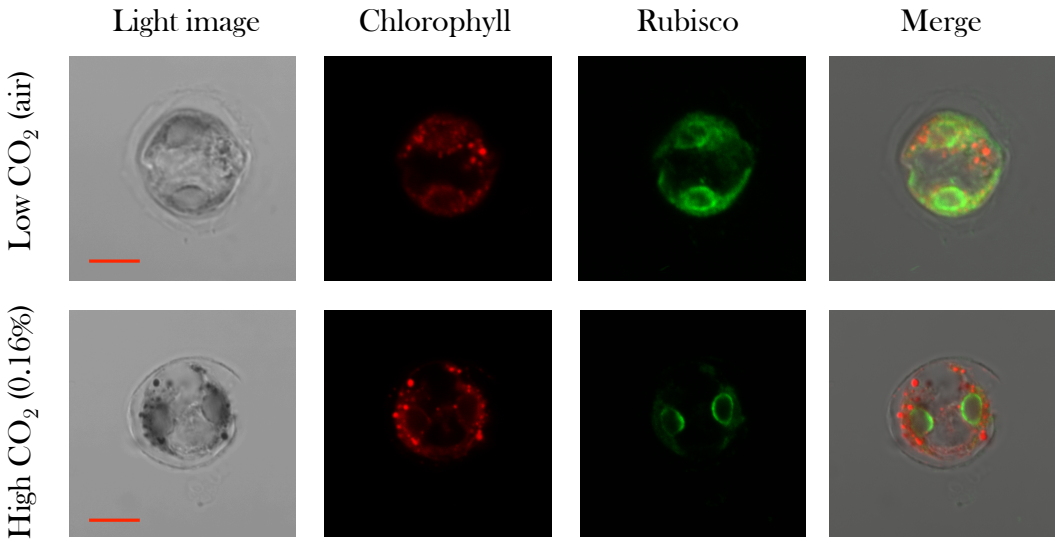

Figure 4-5: Confocal images of the haptophyte *Pleurochrysis placolithoides*. The first column shows transmission light microscope images. The second demonstrates chlorophyll autoflorescence (red) and the third column is immunolocalized Rubisco (green). The final column of images shows the merged channels. The top panel is cells grown at low (ambient) CO_2 concentrations and the bottom panel is cells grown at high CO_2 (0.16%). The scale bars represent 5 μm.

We note that these images of *P. placolithoides* are preliminary as we need to replicate the treatments to confirm the trend. We observe a non-uniform signal and often had difficulty in achieving penetration by the antibody. These are general limitations for this type of data. Here we present the most representative antibody localization across the samples in our study. More work on the localization of Rubisco across the community will provide another dimension to this data.

In this study we quantified the amount of Rubisco produced in two species of diatom, *Phaeodactylum tricornutum* and *Thalassiosira pseudonana*, at ambient and high (0.16%) CO_2. The data produced, presented in Figure 4-6, shows that across three replicates for each treatment, cells grown under the high CO_2 conditions produce more Rubisco as a percentage of total soluble protein. *In P. tricornutum*, Rubisco %TSP increased from

~14±2 to 23±1% and in *T. pseudonana* the amount increased slightly less from ~17±1.5 to 21±1%.

This finding is supported by measurements done by McCarthy et al. (2012) in the diatom *Thalassiosira pseudonana* and the haptophyte *Emiliania huxleyi*. They measure Rubisco (molecules RbcL $cell^{-1}$) and find that both species experience an increase in the amount of Rubisco in the 750 p.p.m.v. treatment versus the 390 p.p.m.v. treatment. In *E. huxleyi*, they observe an increase of over an order of magnitude. These findings suggest that under high CO_2, the cells increase their capacity for carbon fixation by increasing Rubisco production. This result, however, is likely limited to cells living or grown in nutrient replete conditions. Under nutrient limited conditions, the cells may not have the resources to support additional Rubisco production. Other studies, including Losh et al. (2013) and Levitan et al. (2010), show the opposite trend or no change between different CO_2 treatments. The discrepancy may be a result of variable growth conditions (i.e. nutrients) because of the high requirement of Rubisco for nitrogen. While our study and McCarthy et al. (2012) grow cultures in nutrient replete conditions, cultures in Losh et al. (2013) are grown under much lower nitrogen and phosphorus conditions.

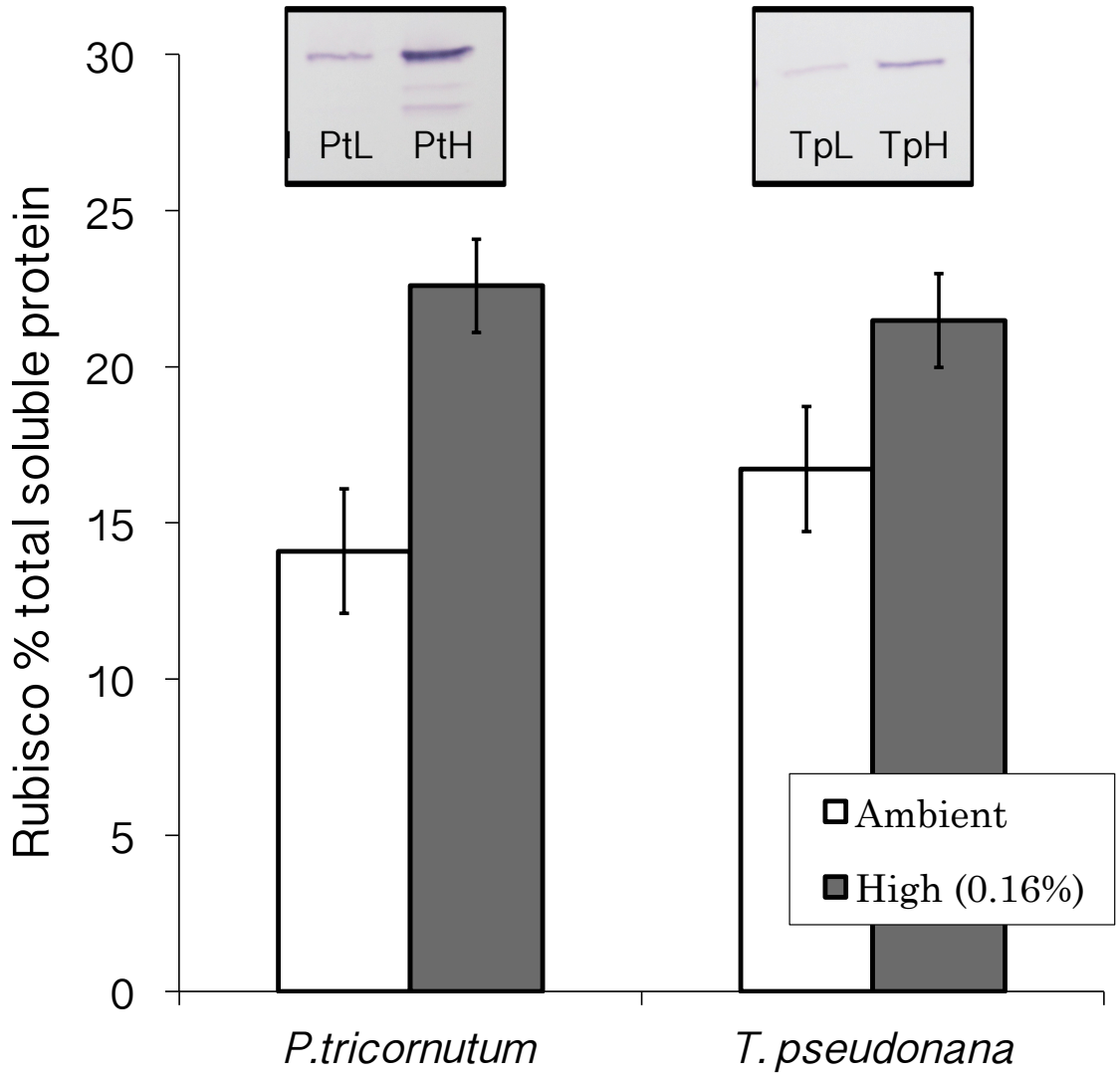

Figure 4-6: Quantification of the Rubisco enzyme as a percentage of total soluble protein in two species of marine diatom *Pheodactylum tricoruntum* (Pt) and *Thalassiosira pseudonana* (Tp). Cells grown at low (ambient) CO_2 are shown in white and cells grown at high (0.16%) CO_2 are shown in dark grey. Both species show increased Rubisco %TSP when grown under high CO_2 conditions. Panels above plot show equally loaded Western blot bands run simultaneously for both species at low (L) and high (H) CO_2. Full blots and replicate images can be found in the appendix.

In this study we find that both the quantity and location of the Rubisco enzyme changes in 4 species of eukaryotic algae in response to an increased concentration of CO_2 when grown in culture. The important implication for this change is that the fractionation of carbon by Rubisco is from the pool of CO_2 at the site of Rubisco ($[C]_{Rubisco}$) described in

Eqn 4-1. If the location of the Rubisco enzyme moves from the pyrenoid to the chloroplast, the enzyme will be exposed to a different substrate environment. The location of Rubisco also determines the volume holding the CO_2 substrate (Vol) described in Eqn. 4-1.

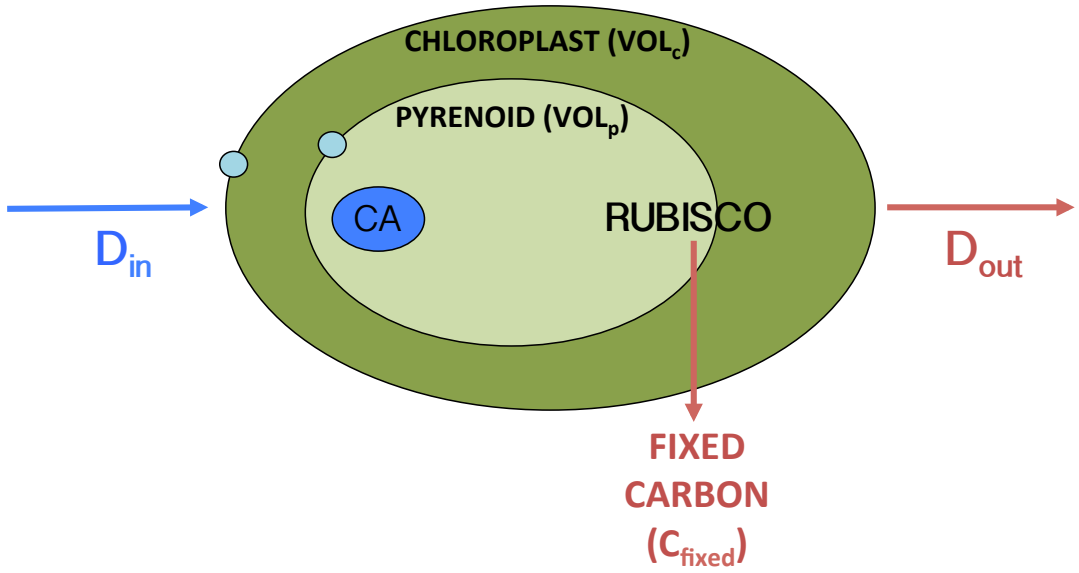

$$[CO_2] \text{ around RUBISCO } ([C]_{Rubisco}) = C_{source} - C_{sink}/VOL_{(p/c)} \quad (4\text{-}1)$$

$$C_{source} \approx D_{in} + CA + transporters \quad (4\text{-}2)$$

$$C_{sink} \approx D_{out} + C_{fixed} - CA \quad (4\text{-}3)$$

Figure 4-7: Illustration of how the variables discussed in this chapter will alter the concentration of carbon around the Rubisco enzyme. Equations represent a simplified view of the fluxes of carbon in and out of the chloroplast or pyrenoid structure.

Where $[C]_{Rubisco}$ is the concentration of carbon around the Rubisco enzyme. C_{source} describes the parameters determining the inward fluxes of the carbon pool, C_{sink} describes the outward flux and C_{source} - C_{sink} is divided by the volume (Vol) depending on if the enzyme is in a pyrenoid or chloroplast structure to estimate the concentration of carbon around Rubisco. C_{source} described in Eqn. 4-2 depends on diffusion into the cell (D_{in}), carbonic anhydrase (CA) overcoming the resistance to diffusion, and HCO_3^- and CO_2 transporters actively moving carbon inwards. C_{sink}, or the removal of carbon from the

internal carbon pool, is determined by leakage/diffusion (D_{out}) and removal of carbon fixed by Rubisco. C_{sink} can be reduced if CA is preventing the leakage of C from either the pyrenoid or the chloroplast.

If the quantity of Rubisco enzyme changes, this impacts the amount of carbon fixed (C_{fixed}) therefore changing $C_{sink.}$ C_{fixed} is a function of the rate of the carboxylation versus the oxygenation reaction multiplied by the amount of Rubisco enzyme (Eqn 4-4).

$$C_{fixed} = \int \left({K_c}^{cat} - {K_o}^{cat} \right) \times Rubisco\ quantity \qquad (4\text{-}4)$$

We show here that variation in quantity and location of the Rubisco enzyme can alter the CO_2 concentration experienced by the enzyme. If changing CO_2 is driving the movement of the enzyme, this may complicate the signal from which Rubisco is fractionating. Our study finds that at high CO_2 both C_{fixed} and Vol increase, which from these equations will result in a decrease in $[C]_{Rubisco}$. However, if the external CO_2 increases then diffusion of CO_2 into the cell (D_{in}) will increase, having the opposite effect on $[C]_{Rubisco}$, possibly cancelling each other out. This study highlights the importance of changing Rubisco quantity and location with CO_2 for the internal carbon pool. With this knowledge, parameters that impact the concentration of carbon at the site of Rubisco can be added to models of whole cell isotopic fractionation.

4.3.3 Nutrient use changes in response to changing CO_2

In their study of four coccolithophore strains (2 *Emiliania huxleyi* and 2 *Gephyrocapsa oceanica*), Wang et al. (2015) measure response to changing [CO_2] and pH. For measurement of carbon and nitrogen content, samples were filtered onto precombusted Watman GF/F fiters and stored at -20°C. Filters were fumed over HCl to remove inorganic carbon and then packed into solvent-rinsed tin sample boats. Particulate organic carbon (POC), particulate organic nitrogen (PON) and total particulate carbon (TPC) were measured with a Vario EL III automatic elemental analyzer.

In this study, Wang et al. (2015) report that all strains increase their nitrogen uptake with increasing CO_2 up to 2000 μatm. The four strains exhibited increases between 48 and 33% in nitrogen uptake. Jin et al. (2013) also find nitrogen uptake increased in coccolithophores and found upregulation in the gene for nitrate reductase under elevated CO_2. Various studies have proposed a redistribution of energy under ocean acidification conditions (Beaufort et al., 2011; Raven et al., 2011; Wang et al., 2015). Generally, they find that cells have a preference for nitrogen uptake and production of PON at high CO_2. Seeing as the production of Rubisco has a high nitrogen requirement, this data supports our findings that Rubisco production increases under high CO_2 and nutrient replete conditions.

4.3.4 Cell size

Measurements of coccosphere size (a measure of the cell including external $CaCO_3$ layer) in response to varying dissolved inorganic carbon (DIC) with the addition of bicarbonate

were carried out in our lab by Ian Chan in his 4th year project under the supervision of Dr. Michael Hermoso and myself. Calculated CO_2 changes across experimental DIC levels (2-12 mM) range from ~290 to 1,500 p.p.m.v. (Ian Chan, unpublished data). Across this range of carbon system variation, we observe an increase in coccosphere (cell size plus layer of coccoliths) size with increasing DIC and nutrient replete conditions (Figure 4-8). Here we present data from the two species showing a small but clear increase in coccosphere diameter (μm) with increasing DIC from 2 to 12 mM. Other evidence for increasing cell size with increasing [CO_2] comes from Beaufort et al. (2011) and Iglesias-Rodriguez et al. (2008). We hypothesize from these results that with ample CO_2 and nutrients, the cells are allocating energy away from CCM machinery, towards protein production and cell growth.

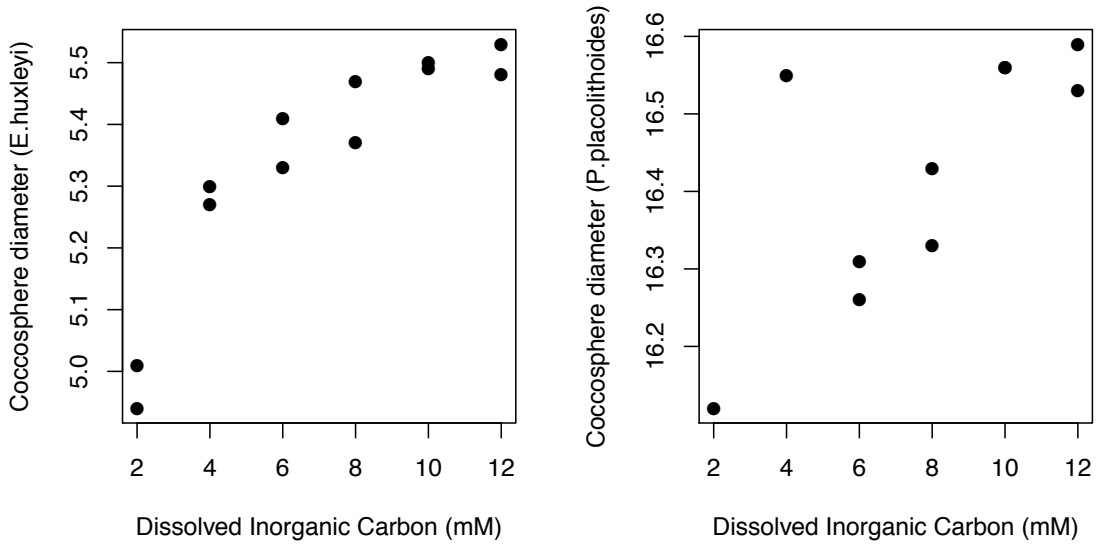

Figure 4-8: Coccosphere diameter (μm) in the species *Emiliania huxleyi* and *Pleurochrysis placolithoides* across a range of dissolved inorganic carbon concentrations from 2-12 mM.

We hypothesize from the compilation of all the data presented in this study that an increase in external CO_2 triggers the downregulation of CCM machinery (i.e. carbonic anhydrase

and localization of Rubisco in the pyrenoid) and increases Rubisco production and nitrogen uptake. When the resources are available, the cell uses them to produce more protein and ultimately increase cell size, albeit only by a small amount (Figure 4-8). Bach et al. (2013) show CCM induction at low CO_2 in *Emiliania huxleyi* via the physiological and transcriptional response to carbonate system parameters. The relative timing and [CO_2] at which each stage of CCM induction takes place cannot be entirely illuminated by this study as the reported CA and Rubisco quantity are taken at "high" and "low" CO_2 control points. If there is indeed a CO_2 threshold where the cell is able to allocate its resources toward a different carbon fixing strategy, this could have large implications for the interpretation of $\delta^{13}C$ in geological periods characterized by high CO_2 conditions.

4.4 Conclusions

In this final chapter we bring together the work we have done implementing an algae-based CO_2 proxy and the studies characterizing carbon concentrating mechanisms and Rubisco kinetics across diverse biomineralizing marine algae. In this study we have reviewed known physiological responses in marine algae to changes in the carbon system. By looking at these physiological changes together, we can build a more complete picture of the cell's response to changing CO_2 and how this might impact what is recorded in the carbon isotopic signature.

From our studies we conclude that in addition to evolutionary adaptation in enzymatic function (i.e. Rubisco kinetics) marine algae undergo significant plastic change in response to short term changes in CO_2. These plastic changes, including the regulation of

Rubisco quantity, Rubisco location, reported CA activity and nutrient uptake, have great implications for the carbon pool around Rubisco. From the data measured and compiled in the present study, we conclude that under high CO_2 conditions, aspects of the CCM are downregulated including the downregulation of pyrenoid based carbonic anhydrase as well as the migration of Rubisco out of the pyrenoid structure. As the CCM is suppressed, we observe a coincident increase in Rubisco quantity along with reported nitrogen uptake per cell. The increased quantity of Rubisco and likely other proteins allows the cell to increase in size with higher [CO_2]. The present study also supports our hypothesis from previous chapters that there is a trade-off between Rubisco production and active CCM machinery (Figure 4-9). This trade-off though, is likely determined by the habitat and lifestyle of different species. The physiological changes illustrated in Figure 4-9 are importantly only representative of cells living in nutrient rich environments.

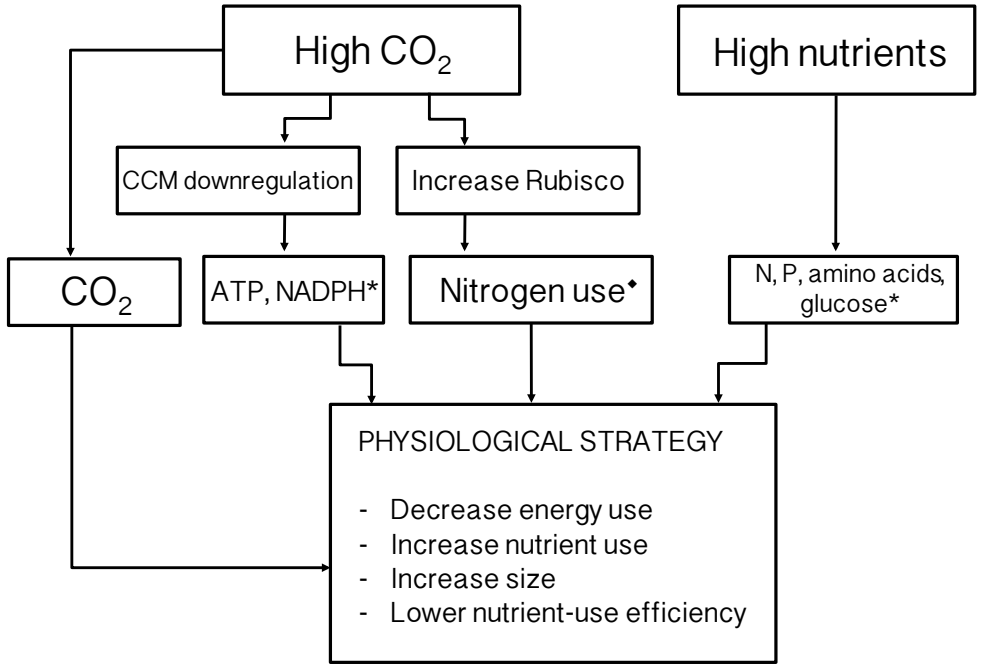

Figure 4-9: Conceptual model illustrating the effects of CO_2 and high nutrients on the physiology illuminated by this study. Conclusions from Wang et al. (2015) are labelled with a diamond (◆) and information from model in Sobrino et al. (2014) is marked with an asterisks (*).

The set of equations discussed in this study demonstrate how with increased external $[CO_2]$ and resultant increase in Rubisco production and movement of the enzyme out of the pyrenoid, the $[C]_{Rubisco}$ or concentration of carbon experienced by Rubisco may remain constant. More work must to done to quantify how Rubisco and internal carbon pools vary across a gradient of CO_2, while this study only looks at the end members of the carbon system. The ability of complex eukaryotic cells to alter their physiology at high CO_2 concentrations highlights the importance of using caution when interpreting algal organic $\delta^{13}C$ from periods of high environmental $[CO_2]$ and presents new parameters to incorporate into models of carbon fixation in eukaryotic algae.

Chapter 5: Conclusions

This interdisciplinary thesis gives a multifaceted look at carbon fixation in eukaryotic marine algae both from a paleo-climatological and biological perspective. Our approach to looking at these complex and cosmopolitan organisms from various angles has resulted in new insights and perspectives on their function and chemical markers. This D.Phil project began with the investigation of carbon isotopes from ancient marine diatoms preserved in ocean sediments. These extremely well-preserved fossil shells dating back to the Oligocene presented us with the opportunity to apply a well-understood proxy to a novel source. Additionally, the preservation of organic material inside the silica frustule allows us to simultaneously measure carbon isotopic signature with the size of the cell, two parameters used in the reconstruction of paleo-CO_2. In this study we concluded that diatom-bound organic carbon isotopes have the potential to provide a useful source of paleo-CO_2 information that should be further investigated in future studies. We also emphasize the merit in the use of multiple proxies for reliable estimates of paleo-CO_2.

In this initial investigation, however, we noticed a number of limitations in the proxy as a result of assumptions made about carbon fixation in marine algae. One main flaw in our interpretation of $\delta^{13}C$ from eukaryotic marine organisms is that most of the information we have on photosynthetic mechanisms comes from terrestrial plants or aquatic prokaryotes. For the calibration of paleo-proxies, most studies assume that fractionation by the Rubisco enzyme is consistently between ~25 and 28‰ (Bijl et al., 2010; Pagani et al., 2011; Zhang et al., 2013). However, it has been shown that enzyme fractionation varies significantly between organisms and with the kinetic parameters of individual Rubisco enzymes (Badger et al., 1998; Boller et al., 2015; Tcherkez et al., 2006; this study). We concluded from our application of this proxy that understanding the individual controls

on carbon fixation in marine phytoplankton is extremely important for the interpretation of $\delta^{13}C$ paleo-proxies. In the remaining chapters we aimed to elucidate controls on carbon fixation in geologically relevant marine algae.

In Chapter 3 we investigate diversity in the kinetics of the Rubisco enzyme and their relationship to other strategies for achieving more efficient carbon fixation in the cell. We find a large amount of kinetic diversity in relatively closely related eukaryotic marine algae from the haptophyte and diatom groups. We look closely at the Michaelis-Menten constant for carboxylation (K_c) across 20 species of marine algae. These values show a definite relationship with the presence/absence of a pyrenoid structure. We conclude that, assuming K_c is a measure of the relative [CO_2] at the site of Rubisco, an immersed pyrenoid effectively increases [CO_2] inside the pyrenoid, allowing for the relaxation of the affinity of Rubsco for CO_2 substrate. Cells lacking a pyrenoid, with a higher affinity for CO_2, are the earliest branching *Pavlovales* and seem to be constrained to coastal ecosystems. This constraint could be a result of their increased production of Rubisco enzyme to compensate for their lack of CCM. The affinity for CO_2 in cells with a bulging pyrenoid is only slightly lower than cells lacking a pyrenoid, suggesting that bulging pyrenoids are less effective at increasing CO_2 at the site of Rubisco than immersed pyrenoids.

We elaborate on this overview of 20 species by investigating the entire suite of kinetic parameters (K_c, K_o, K_c^{cat}, K_o^{cat}) across 4 algal species with 3 different pyrenoid morphologies: absent, bulging internally, and immersed. From this study we conclude that the internally bulging pyrenoid may not provide a significantly higher CO_2 environment,

but instead may provide a lower oxygen environment for the Rubisco enzyme as a result of its central position with a long diffusional path length for substrate. Cells with a bulging pyrenoid are thought to have moved to the open ocean and back to the coast, thus this morphology may facilitate an adaptable lifestyle.

One key finding of these studies is that across the marine algae, we do not observe the same kinetic trade-offs found by Tcherkez et al. (2006) between kinetic parameters. Tcherkez's hypothesis, that the improvement of affinity is a result of a more product-like transition state and therefore slows down the catalytic throughput of a given reaction, is supported by data from the diverse photosynthetic organisms in his study. However, when we investigated this relationship in the more closely related haptophyte and diatom algae, the direct kinetic trade-off is not so clear. We suggest that in marine algae the spectrum of complexity in physiology and macromolecular structures play a role in increasing the variability of kinetic parameters, thus obscuring the trade-offs observed in the kinetic system.

A correlation we observe consistently throughout these studies, however, is between various measures of CCM (i.e. K_c, $K_{m(Rubisco)}$:$K_{m(cell)}$, presence of a pyrenoid and carbonic anhydrase) and Rubisco quantity. It seems that marine algae have developed two distinct ways to increase the amount of carbon fixed by the cell: changing the subcellular environment for Rubisco or increasing the production of Rubisco. Both methods seem to allow the cell to carry out a sufficient amount of carbon fixation in the modern low CO_2 world. While upregulating Rubisco production seems to be a more straightforward strategy for a cell, it is extremely energy and nutrient intensive and thus not viable for

many organisms (Parry et al., 2003). We hypothesize that investing in creating an efficient CCM system provides a more streamlined mechanism to achieve efficient carbon fixation for organisms limited by nutrients and energy. We outline the three distinct lifestyles proposed in this study in table 5-1. Using higher plants as an analogy, we note that C_3 plants, lacking the ability to concentrate CO_2 around the Rubisco enzyme, upregulate Rubisco production. However, C_4 plants which increase the [CO_2] around Rubisco produce less enzyme and are therefore more tolerant of extreme conditions and survive in nutrient poor/arid regions (Edwards et al., 2010; Gowik et al., 2011; Oaks, 1994).

Pyrenoid type	Ecology	Size	Rubisco character	Internal [CO_2]:[O_2]
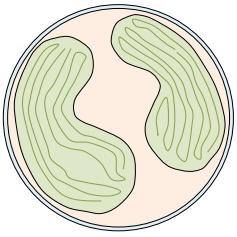	Coastal High nutrients 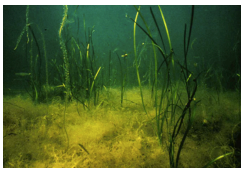	~5µm 	↑ CO_2 affinity ↓ O_2 affinity ↓ Rate carboxylation ↑ Rate oxygenation	↓
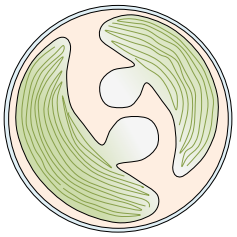	Move between coast/open ocean 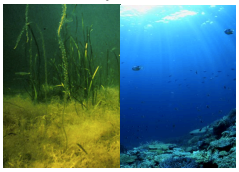	8-12µm 	↑ CO_2 affinity ↑O_2 affinity ↑ Rate carboxylation ↓ Rate oxygenation	↑ (Low O_2)
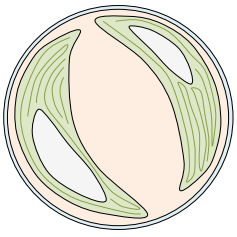	Open ocean Low nutrients 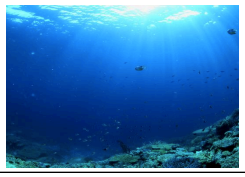	Variable 5-15µm 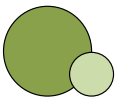	↓ CO_2 affinity ? O_2 affinity ↑ Rate carboxylation ? Rate oxygenation	↑ (High CO_2)

Table 5-1: Different types of eukaryotic marine algae outlined by this thesis in terms of CCM type, ecology, size, Rubisco character and their relative internal [CO_2]:[O_2].

Finally, in Chapter 4 we investigate physiological changes in the photosynthetic machinery of select marine algae to changing CO_2. In this study we find a response across

all measured parameters both reviewed in the literature and measured in our study to variable [CO_2] or [DIC] growth conditions. We find that under high CO_2 conditions, the production of pyrenoid localized CAs is downregulated in two marine diatoms and the Rubisco enzyme is shown to move out of the pyrenoid in both a diatom and haptophyte species. Coincident with the downregulation of these CCM parameters, we show increased production of Rubisco enzyme together with reported increased nitrogen uptake by the cell (McCarthy et al., 2011; Wang et al., 2015). All of these findings are from studies carried out under nutrient replete conditions and we emphasize that the results will likely differ in nutrient-limiting conditions.

At high CO_2 and nutrient replete conditions, we find that cells increase in size. This suggests that cells may allocate their resources away from CCMs when they aren't necessary and toward Rubisco and protein production. These findings further support our hypothesis that CCMs are a means of streamlining carbon use efficiency and cells only upregulate Rubisco production when they have the means (i.e. nutrients and CO_2 substrate) to do so. We hypothesize that there could be a saturation point at which Rubisco production is upregulated and therefore the enzyme to substrate ratio remains constant causing a stabilization of the internal pool of substrate. We use a set of equations to illustrate the role of different parameters in altering the concentration of carbon observed by the Rubisco enzyme. We conclude that the increase in external CO_2 will raise the internal pool, however subsequent increase in Rubisco quantity, movement out of the pyrenoid and downregulation of the CCM will have the opposite effect. These opposing impacts on internal C_i may keep the amount of carbon at the site of Rubisco constant under increasing CO_2 conditions.

This dichotomy between carbon fixation strategies from low to high CO_2 could have significant implications for determining the habitats of different organisms as well as for carbon fractionation during periods of atmospheric [CO_2] at the higher end of our experimental conditions. These studies together have illuminated both uses and limitations of the application of biomineralizing algae in ancient sediments. The outputs of this thesis can be used to refine the application of paleo-proxies as well as better characterize the role of primary production in different marine environments, both in the geological past and the modern ocean. The data presented here are additionally of great importance for the growing interest in Rubisco diversity and potential for optimization of primary production on Earth. This thesis provides an unprecedented amount of data on photosynthetic mechanisms in eukaryotic marine algae, information with the potential to broaden and develop our understanding of their role across a wide-range of disciplines.

Future work:

This thesis highlights countless avenues for future research both in the fields of paleoclimatology and algal cell physiology. In our first study, Chapter 2 of this thesis, our findings prove the suitability of organic material preserved in diatom frustules as a chemical marker in ancient sediments. This yet untapped reservoir of organic material provides a further dimension to studies of paleo-CO_2, i.e. cell size directly associated with the chemical marker. This material has the potential to provide another proxy of ancient atmospheric CO_2 as a check on current proxy estimates and should be applied in future work.

Chapter 3 of this thesis greatly contributes to our current understanding of the diversity of photosynthetic mechanisms in eukaryotic marine algae, but again lends itself to a plethora of future studies. This work is in a unique place scientifically because so much of the framework for understanding photosynthesis has been lain down by the investigation of vascular plants, yet relatively little is known about eukaryotic marine organisms. The body of research has the potential to develop significantly in the coming years and bridge the important gaps between our understanding of climate, ocean systems and biology.

One main limitation of this study, as identified in the chapter, is that we were not able to create a complete dataset of all parameters measured across all species. Future work should fill in these gaps, especially in the measurement of the whole suite of kinetic data across eukaryotic marine algae. Another area of future work that this work would greatly benefit from is the investigation of Rubisco genes to see if we can pinpoint genetic footprints of the optimizations we observe in kinetic parameters in this study. Identifying the genetic controls on kinetic variability has huge implications for the possible improvement of the Rubisco enzyme and for understanding the evolutionary history of these organisms.

Another important avenue for future work is the investigation of nutrient budgets and requirements of different physiological changes and creating a better understanding of nutrient-use efficiency in marine primary producers. One key factor that we were not able to address in this thesis is the cost of having a CCM. While we know that the production of Rubisco has a high nutrient requirement for the cell, we do not know the

energetic “price” of a CCM. An important first step towards this goal will be to better characterize the CCM components, specifically the make up of the pyrenoid structure as shown in Chlamydomonas by Engel et al. (2015).

Our final chapter was experimental in testing new techniques for better understanding the cell’s response to changing CO_2. We noted throughout the chapter the extreme difficulty we encountered treating the cells for immunolocalization. Further optimization of these techniques should be pursued in the future, as the results of our preliminary work are very encouraging. Another option for further investigation of the location of Rubisco in these cells is in situ localization via TEM.

Building on the work in this thesis, we have begun to investigate how Rubisco is packed inside the pyrenoid. We are investigating the use of mass spectra and high resolution TEM of the pyrenoid and enzyme complexes to uncover additional components, namely carbonic anhydrase, packed within the pyrenoid. This project is still at the development stages and we hope to push it forward in the coming months. Overall, our datasets and novel observations provide an important stepping-stone for future work on the carbon fixation systems in eukaryotic marine algae.

Appendix:

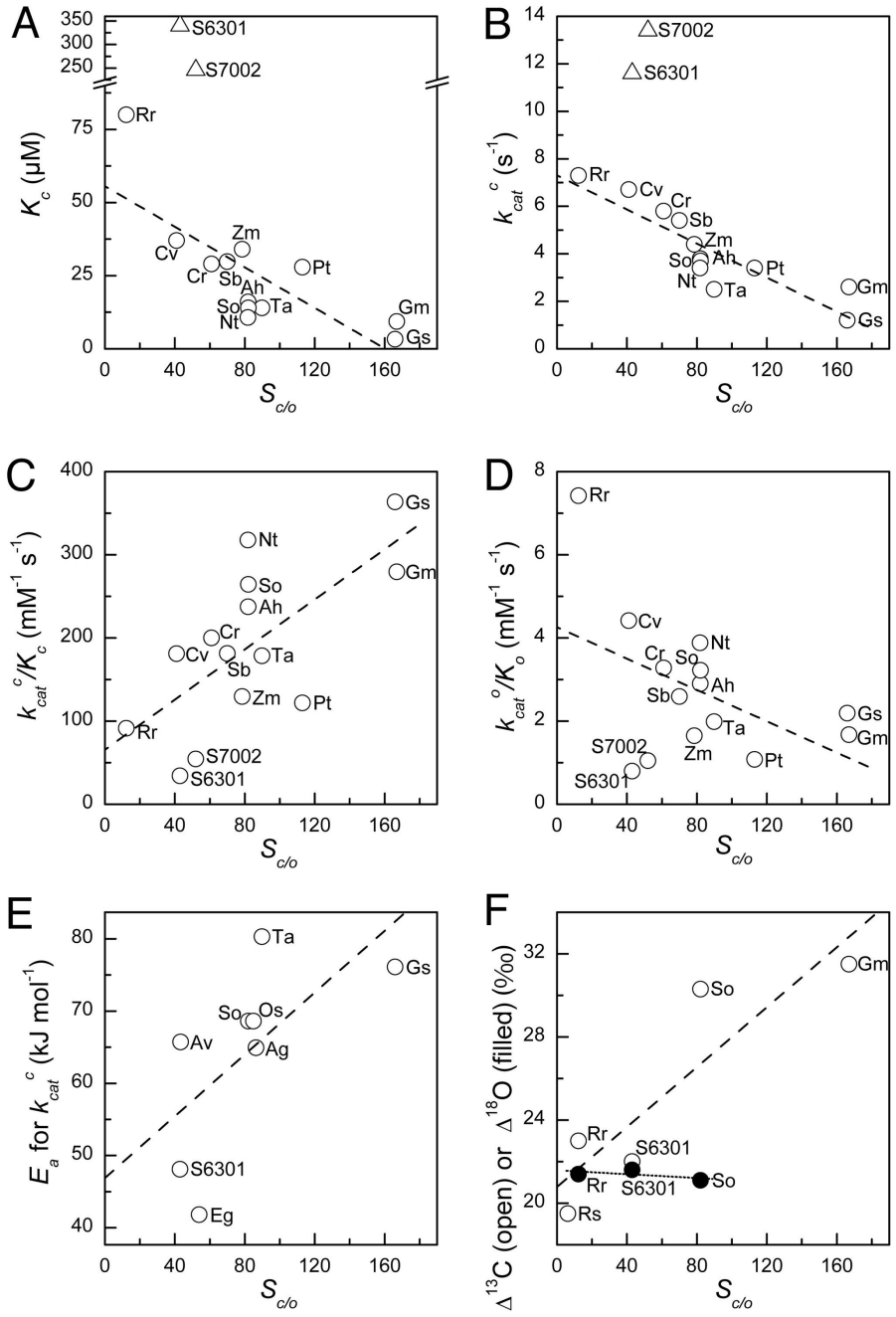

Figure S-1: Variation and relationships in the kinetic properties of Rubisco *in vitro* at 25°C. Rubisco isolated from the organisms: Ag, *Atriplex glabriuscula* (C_3 dicot); Ah, *Amaranthus hybridus* (C_4 dicot); Av, *Anabaena variabilis* (cyanovacterium); Cr, *Chlamydomoas reinhardtii* (green alga); Cv, *Chromatium vinosum* (bacterium); Eg, *Euglena gracilis* (green alga); Gm, *Griffithsia monilis* (red alga); Gs, *Galdieria sulfuraria* (red alga); Nt, *Nicotiana tabacum* (C_3 dicot); Os, *Oryza sativa* (C_3 monocot); Pt, *Phaeodactylum triconutum* (diatom); Rr, *Rhodospirillum rubrum* (bacterium); Rs, the bacterial symbiont of the tubeworm *Riftia pachyptila*; Sb, *Sorghum bicolor* (C_4 monocot); So, *Spinacia oleracea* (C_3 dicot); S6301, *Synechococcus* PCC 6301 (cyanobacterium); S7002, *Synechococcus* PCC 7002 (cyanobacterium); Ta, *Triticum aestivum* (C_3 monocot); and Zm, *Zea mays* (C_4 monocot). E_a is the activation energy of the carboxylation reaction. Dashed and dotted lines are linear regressions through all of the data except or the cyanobacterial outliers (triangles) in A and B, which were excluded (taken from Tcherkez et al., 2006).

	Rubisco CO_2:O_2 environment	$S_{c/o}$	K_c, μM [pH]	k_{cat}^c, s^{-1}	E_a for k_{cat}^c, kJ mol^{-1}	Δ ^{13}C,* ‰	$\Delta^{18}O$,* ‰	CABP release, $t_{0.5}$, d
Bacteria								
Riftia pachyptila symbiont	Anaerobic	6.2 (42)				19.5 (42)		
Rhodospirillum rubrum	Anaerobic	12.3 (43)	80 [7.8] (44)	7.3 (44)		23.0 (25)	21.4 (25)	1.4 (45)
Chromatium vinosum	Anaerobic	41 (46)	37 [8.0] (46)	6.7 (46)				
Cyanobacteria								
Anabaena variabilis	CCM† present	43 (47)			65.7 (47)			
Synechococcus 7002	CCM present	52 (48)	246 [7.8] (48)	13.4 (48)				
Synechococcus 6301	CCM present	43 (49)	340 [7.8] (49)	11.6 (49)	48.1 (50)	22.0 (25)	21.6 (25)	
Green algae								
Euglena gracilis	CCM present	54 (9)			41.8 (51)			
Chlamydomonas reinhardtii	CCM present	61 (9)	29 [8.3] (9)	5.8‡				
C_4 higher plants								
Amaranthus hybridus	CCM present	82 (9)	16 [8.3] (9)	3.8§				
Sorghum bicolor	CCM present	70 (10)	30 [8.3] (10)	5.4 (52)				
Zea mays	CCM present	79 (43)	34 [8.3] (9)	4.4 (52)				
C_3 higher plants								
Triticum aestivum	CCM absent	90 (43)	14 [8.0] (50)	2.5 (50)	80.3 (50)			
Oryza sativa	CCM absent	85 (43)			68.6 (53)			
Spinacia oleracea	CCM absent	82 (43)	14 [8.3]) (9)	3.7 (52)	68.6 (50)	30.3 (25)	21.1 (25)	530 (15)
Atriplex glabriuscula	CCM absent	87 (54)			64.9 (54)¶			
Nicotiana tabacum	CCM absent	82 (55)	11 [8.3] (55)	3.4 (55)				
Nongreen algae								
Phaeodactylum tricornutum	CCM present	113 (55)	28 [8.3] (55)	3.4 (55)				
Griffithsia monilis	CCM absent?	167 (55)	9.3 [8.3] (55)	2.6 (55)		31.5‖		
Galdieria sulfuraria	CCM absent?	166 (55)	3.3 [8.3] (55)	1.2 (55)	76.1**			

Unless otherwise specified, the data apply to 25°C. Where necessary, $S_{c/o}$ and K_c values were adjusted using the Henderson–Hasselbalch equation to a common pK_a of 6.25 for the CO_2/HCO_3^- equilibrium.

*Unless stated otherwise, the ^{13}C and ^{18}O isotope fractionations were measured with the isolated enzymes *in vitro*. The limited data for $\Delta^{18}O$ are supported by a recent observation of 21.3‰ for the $\Delta^{18}O$ of the oxygenase reaction of *Pisum sativum* Rubisco (56).

†CCM, CO_2 concentrating mechanism that increases the CO_2 concentration in the subcellular environment of Rubisco by 10^1- to 10^3-fold above ambient, either by accumulation of CO_2 or HCO_3^- directly or by intermediate accumulation and decarboxylation of C_4 dicarboxylic acids.

‡Determined at 30°C (57) and adjusted to 25°C using the E_a listed for *Euglena gracilis*.

§For Rubisco isolated from the related species, *Amaranthus retroflexis* (52).

¶E_a for temperatures >15°C.

‖Inferred from the carbon-isotope fractionation at saturating CO_2 of whole tissues of another temperate floridiophycean macrophyte, *Lamanea mamillosa* (58).

**For Rubisco isolated from the closely related species *Galdieria partita* (33).

Table S-1: Kinetic data for Rubisco from various bacteria, algae, and higher plants (taken from Tcherkez et al., 2006).

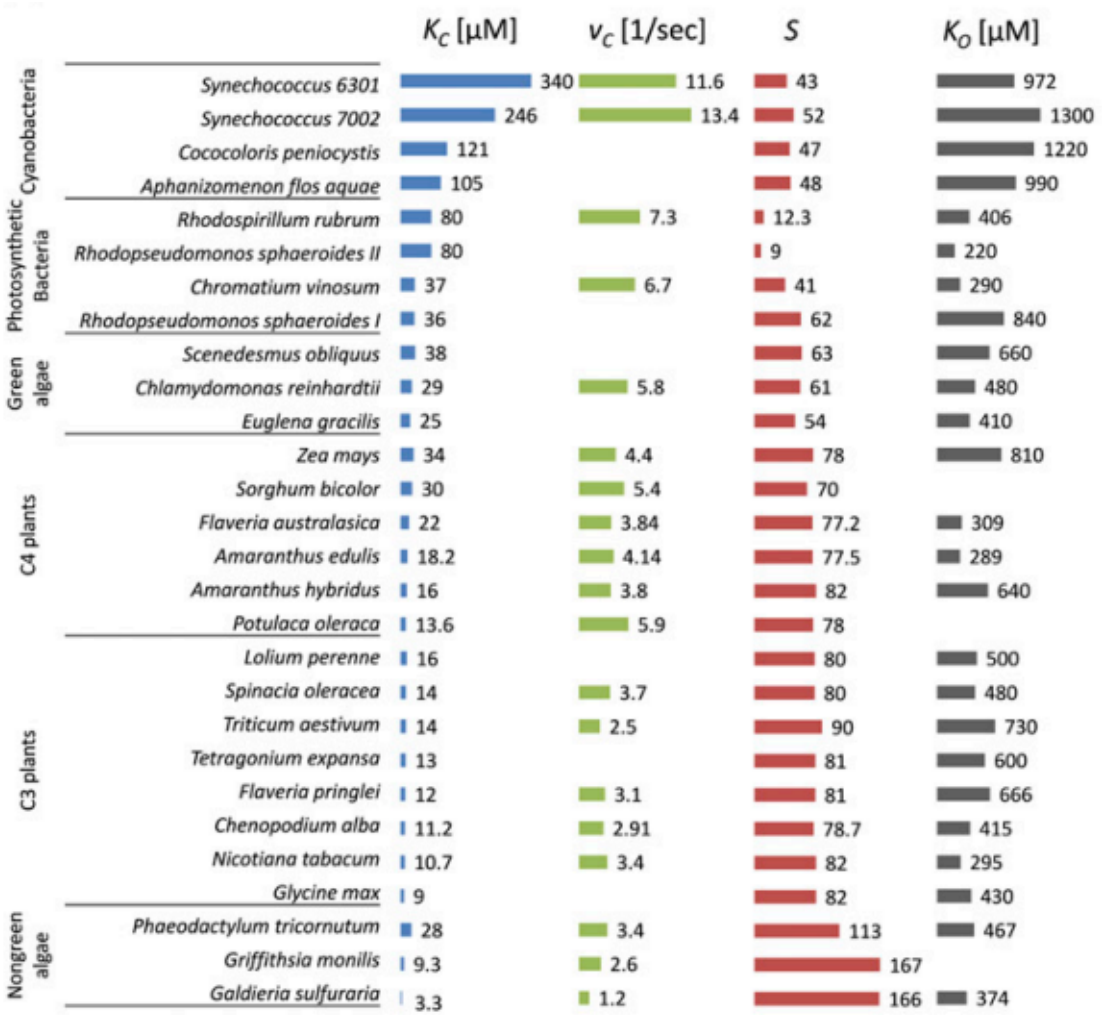

Figure S-2: Visual data representation of four kinetic parameters from 28 Rubisco enzymes isolated from 27 species on primary producers compiled in Savir et al. [2010]. All four paramters were only available for 16 of the 27 species in this study. Parameters outlined in this study include affinity for CO_2 (K_c), the maximal carboxylation rate v_c [1/s], the specificity (S) and the effective affinity for O_2 (K_o).

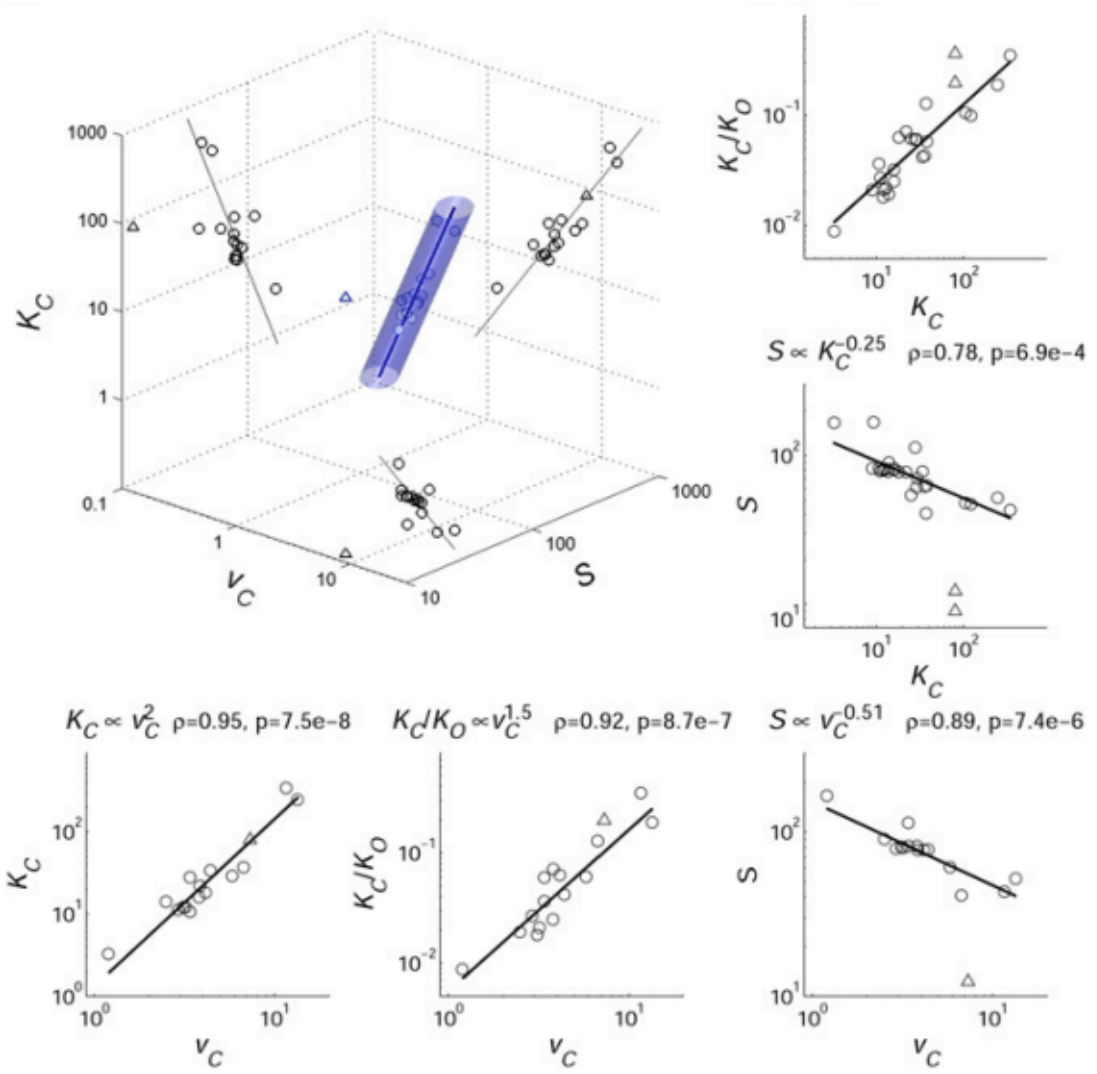

Figure S-3: A 3D projection of the 4D kinetic parameter data. Data from the 16 species for which all four kinetic parameters are available are graphed in logarithmic scale. The plot depicts the PCA result that the radius is the standard deviation from the axis. Total least-squares fit of the data from all 28 Rubiscos to a 1D power law model (black lines). The correlation coefficient, p, and P value, p, are shown.

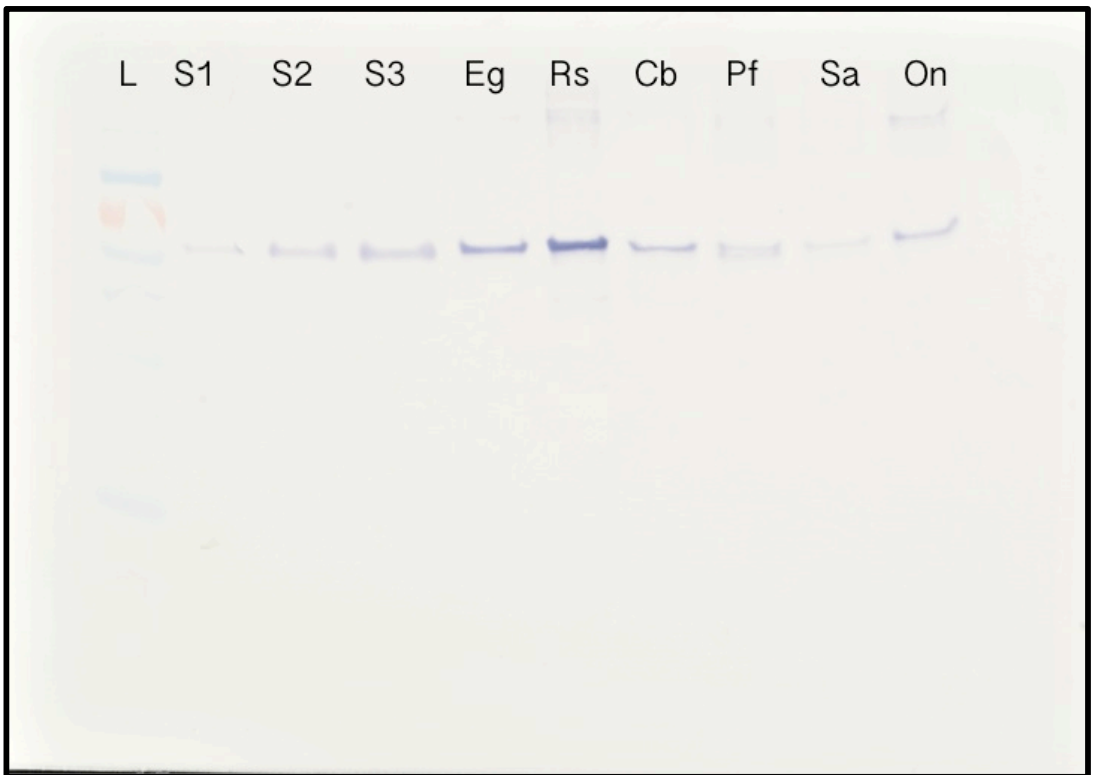

Figure S-4: Western blot imagine of species *Exanthemachrysis gayraliae* (Eg), *Rebecca salina* (Rs), *Coccolithus braarudii* (Cb), *Prymnesium faveolatum* (Pf), *Scyphosphaera apstenii* (Sa) and *Ochrosphaera neopolitana* (On). Standards in micrograms of Rubisco are 0.033ug (S1), 0.066ug (S2) and 0.132ug (S3). L represented the ladder.

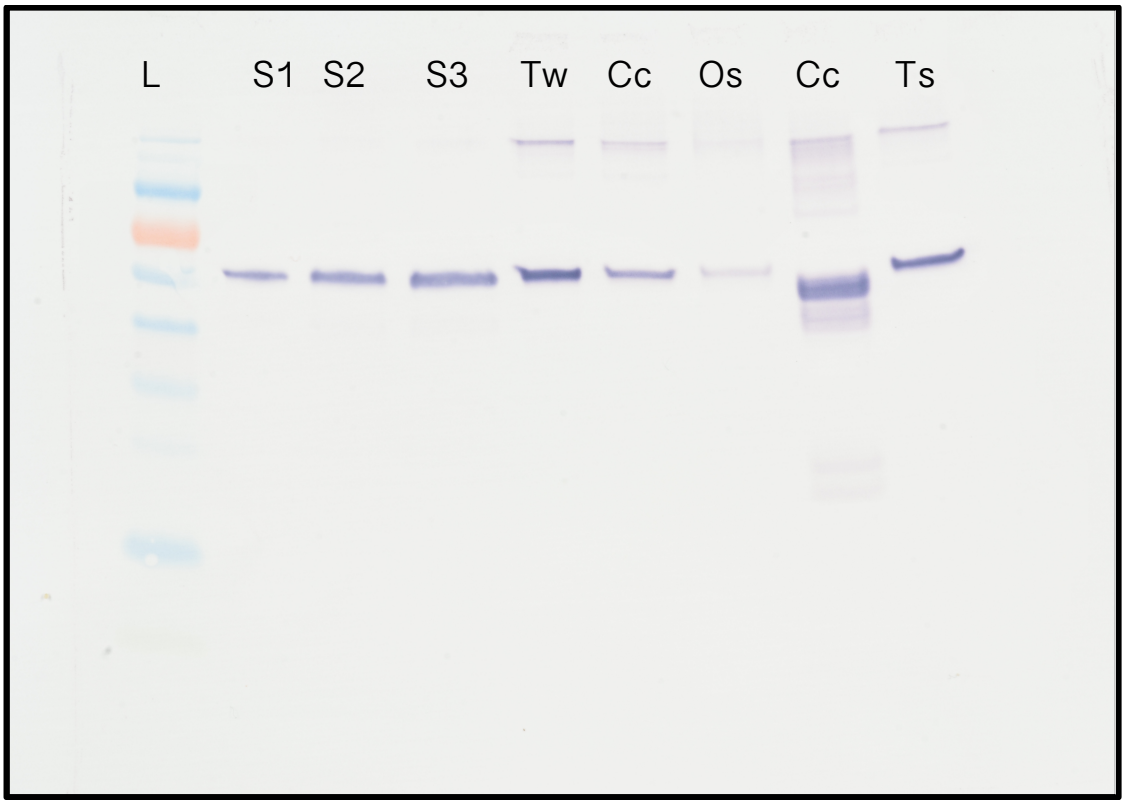

Figure S-5: Western blot imagine of species *Thalassiosira weisfloggi* (Tw), *Cylindrotheca closterium* (Cc), *Odontella sp.* (Os), *Chaetoceros calcitrans* (Cc) and *Thalassiosira pseudonana* (Ts). Standards in micrograms of Rubisco are 0.041ug (S1), 0.083ug (S2) and 0.12ug (S3). L represented the ladder.

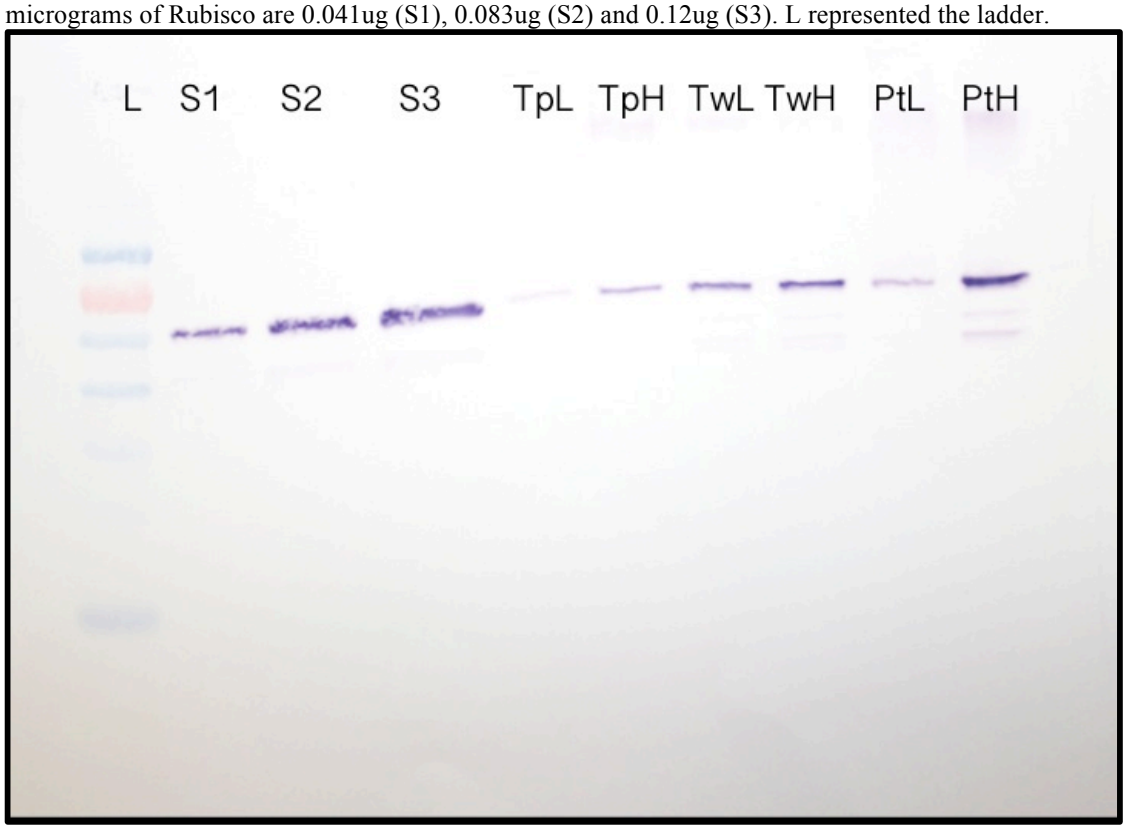

Figure S-6: Western blot image of species *Thalassiosira pseudonana* (Tp), *Thlassiosira weisflogii* (Tw) and *Phaeodactylum tricornutum* (Pt) grown at low (ambient) and high (0.16%) CO_2. Standards in micrograms of Rubisco are 0.041ug (S1), 0.083ug (S2) and 0.12ug (S3). L represented the ladder.

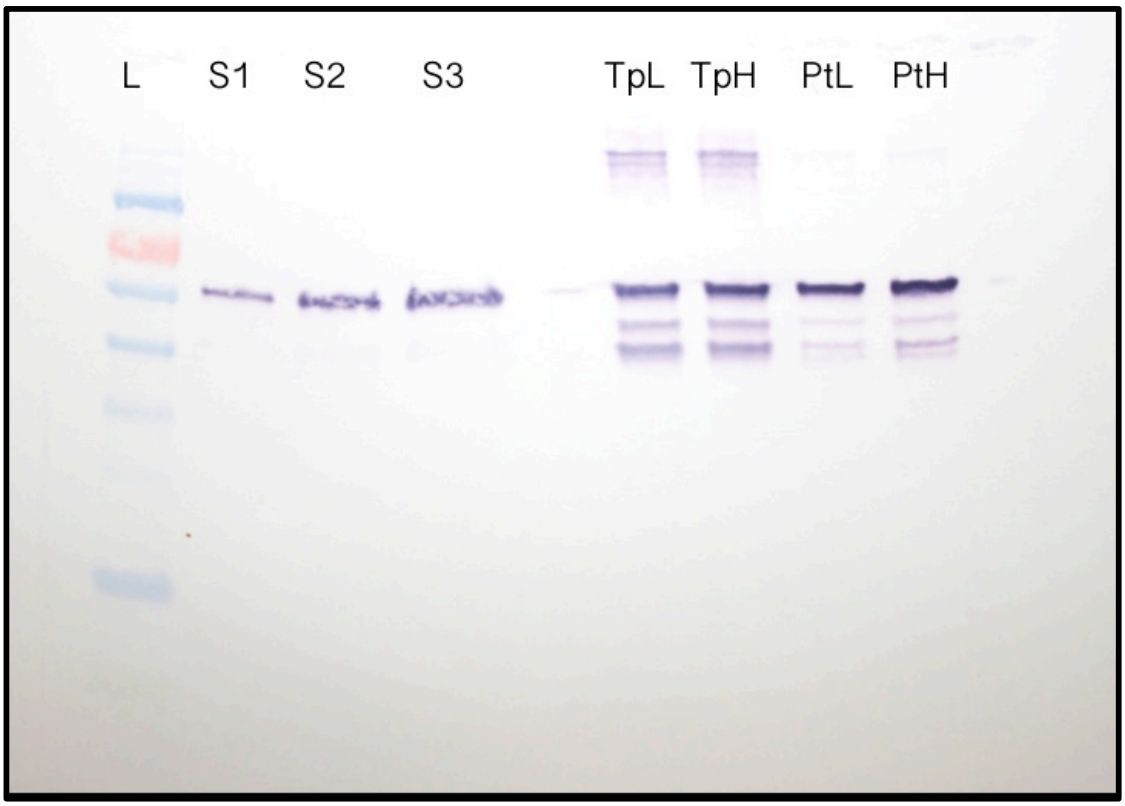

Figure S-7: Western blot image of species *Thalassiosira pseudonana* (Tp) *and Phaeodactylum tricornutum* (Pt) grown at low (ambient) and high (0.16%) CO_2. Standards in micrograms of Rubisco are 0.041ug (S1), 0.083ug (S2) and 0.12ug (S3). L represented the ladder.

References:

Allen, A. E., Moustafa, A., Montsant, A., Montsant, A., Eckert, A., Kroth, P. G., Bowler, C. (2011). Evolution and functional diversification of fructose bisphosphate aldolase genes in photosynthetic marine diatoms. *Mol. Biol. Evol.* 29, 367-379.

Anbar, A.D. & Knoll, A. H. (2002). Proterozoic ocean chemistry and evolution: a bioinorganic bridge? *Science* 297, 542-556.

Anbar, A. D., Duan, Y., Lyons, T. W., Arnold, G. L., Kendall, B., Creaser, R. A., Kaufman, A. J., Gordon, G. W., Scott, C., Garvin, J. Buick, R. (2007). A whiff of oxygen before the Great Oxidation Event? *Science* 317, 1903-1906.

Anderson, L. D. & Delaney, M. L. (2005). Middle Eocene to early Oligocene paleoceanography from Agulhas Ridge, Southern Ocean (Ocean Drilling Program Leg 177, Site 1090). *Paleoceanography 20*, PA1013, doi:10.1029/2004PA001043.

Andersson, I., Knight, S., Schneider, G., Lindqvist, Y., Lundqvist, C. I., Branden, C. I., Lorimer, G. H. (1989). Crystal structure of the active site of ribulose-bisphosphate carboxylase. *Nature* 337, 229-234.

Andrews, T. J. & Lorimer, G.H. (1987) in The Biochemistry of Plants, eds. Hatch, M. D., & Boardman, N. K., Academic Press, New York, pp. 131-218

Armbrust, E.V., Berges, J., Bowler, C., Green, B., Martinez, D. (2004) The genome of the diatom *Thalassiosira pseudonana*: ecology, evolution, and metabolism. *Science* 306, 79-86.

Arnon, D. I. (1971) The light reactions of photosynthesis. *Proc. Nat. Acad. Sci.* 68, 2883-2892.

Bach, L. T., Mackinder, L. C. M., Schulz, K. G., Wheeler, G., Schroeder, D. C., Brownlee, C., Riebesell, U. (2013). Dissecting the impact of CO_2 and pH on the mechanisms of photosynthesis and calcification in the coccolithophore *Emiliania huxleyi*. *New Phytol.* 199, 121-134.

Badger, M. R. & Andrews, T. J. (1987). Co-evolution of Rubisco and CO_2 concentrating mechanisms. *Prog. Photosyn. Res.* 10, 335-346.

Badger, M. R. & Price, G. D. (1994). The role of carbonic anhydrase in photosynthesis. *Ann. Rev. Plant Physiology Plant Mol. Biol.* 45, 369-392.

Badger, M. R., Andrews, J., Whitney, S. M., Ludwig, M., Yellowlees, D. C., Leggat, W., Price, G. D. (1998). The diversity and coevolution of Rubisco, plastids, pyrenoids, and chloroplast-based CO_2-concentrating mechanisms in algae. *Can. J. Bot.* 76, 1052-1071.

Badger, M. R., Hanson, D., Price, G. (2002). Evolution and diversity of CO_2 concentrating mechanisms in cyanobacteria. *Funct. Plant Biol.* 29, 161-173.

Badger, M. R. & Price, G. (2003). CO_2 concentrating mechanisms in cyanobacteria: molecular components, their diversity and evolution. *J. Exp. Bot.* 54, 609-622.

Bainbridge, G., Madgwick, P., Parmar, S., Mitchell, R., Paul, M., Pitts, J., Keys, A. J., Parry, M. A. J. (1995). Engineering Rubisco to change its catalytic properties. *J. Exp. Bot.* 46, 1269-1276.

Baird, M. E., Emsley, S. M., Mcglade, J. M. (2001). Using phytoplankton growth model to predict fractionation of stable carbon isotopes. *J. Plankton Res.* 23, 391-398.

Baker, T. S., Eisenberg, D., Eiserling, F. A., Weissman, L. (1975). Structure of form in crystals of D-ribulose-1,5-disphosphate carboxylase. *J. Mol. Biol.* 91, 391.

Baldauf, S. L. (2003). The deep roots of eukaryotes. *Science* 300, 1703-1706.

Barker, S., Higgins, J. A., Elderfield, H. (2003). The future of the carbon cycle: review, calcification response, ballast and feedback on atmospheric CO_2. *Phil. Trans. Roy. Soc. Lon. Series A: Math., Phys. Engin. Sci.* 361, 1977-1999.

Bedoshvili, Y., Popkova, T., Likhoshway, T. (2009). Chloroplast structure of diatoms of different classes. *Cell Tiss. Biol.* 3, 297-310.

Beaufort, L., Probert, I., de Garidel-Thoron, T., Bendif, E. M., Ruiz-Pino, D., Metzl, N., Goyet, C., Buchet, N., Coupel, P., Grelaud, M., Rost, B., Rickaby, R. E. M., de Vargas, C. (2011) Sensitivity of coccolithophores to carbonate chemistry and ocean acidification. *Nature* 476, 80-83.

Beardall, J. (1989) Photosynthesis and photorespiration in marine phytoplankton. *Aquat. Bot.* 43, 104-130.

Beardall, J. & Giordano, M. (2002). Ecological implications of microalgal and cyanobacterial CO_2 concentrating mechanisms and their regulation. *Funct. Plant Biol.* 29, 421-434.

Beardall, J., Mukerji, D., Glover, H. E., Morris, I. (1976) The path of carbon in photosynthesis by marine phytoplankton. *J. Phycol.* 12, 406-417.

Beardall, J., Johnston, A., Raven, J. (1998). Environmental regulation of CO_2-concentrating mechanisms in microalgae. *Can. J. Bot.* 76, 1010-1017.

Beardall, J., & Raven, J.A. (2004). The potential effects of global climate change on microalgal photosynthesis, growth and ecology. *Phycologia.* 43, 26-40.

Bendif, E. M., Probert, I., Herve, A., Billard, C., Goux, D., Lelong, C., Cadoret, J., Veron, B. (2011). Integrative taxonomy of the Pavlovophyceae (Haptophyta): A reassessment. *Protist 162, 783-761.*

Berg, S., Leng, M. J., Kendrick, C. P., Cremer, H., Wagner, B. (2012). Bulk sediment and diatom silica carbon isotope composition from coastal marine dediments off East Antarctica. *Silicon 5*, 19–34.

Berner, R. A. (2009). Phanerozoic atmospheric oxygen: New results using the GEOCARBSULF model. *Am. J. Sci.* 309, 603-606.

Berner, R. A. (2006). GEOCARBSULF: A combined model for Phanerozoic atmospheric O_2 and CO_2. *Geochemica Cosmochim. Acta.* 70, 5653-5664.

Bidigare, R. R., Fluegge, A., Freeman, K. H., Hanson, K. L., Hayes, J. M., Hollander, D., Jasper, J. P., King, L. L., Laws, E. A., Milder, J., Millero, F. J., Pancost, R., Popp, B. N., Steinberg, P. A., Wakeham, S. G. (1997). Consistent fractionation of ^{13}C in nature and in the laboratory: Growth-rate effects in some haptophyte algae. *Glob. Biogeochem. Cy.*, *11*, 279–292.

Bijl, P. K., Houben, A. J. P., Schouten, S., Bohaty, S. M., Sluijs, A., Reichart, G., Sinninghe Damste, J. S., Brinkhuis, H. (2010). Transient middle Eocene atmospheric CO_2 and temperature variations. *Science* 330, 819-821.

Billard, C. & Inouye, I. (2004). "What is new in coccolithophore biology?" in coccolithophores, From Molecular Processes to Global Impact, eds. H.R. Thierstein & J. R. Young, Springer, Germany. 1-31.

Bird, K. T., Habig, C., DeBusk, T. (1982). Nitrogen allocation and storage patterns in *Gracilaria tikvahiae. J. Phycol.* 18, 344-348.

Bohaty, S. M., Zachos, J. C., Delaney, M. L. (2012). Foraminiferal Mg/Ca evidence for Southern Ocean cooling across the Eocene–Oligocene transition. *Earth Planet. Sci. Lett. 317-318*, 251–261.

Boller, A. J., Thomas, P. J., Cavanaugh, C. M., Scott, K. M. (2011). Low stable isotope fractionation by coccolithophore Rubisco. *Geochim. Cosmochim. Acta* 65, 7500-7207.

Boller, A. J., Thomas, P. J., Cavanaugh, C. M., Scott, K. M. (2015). Isotopic discrimination and kinetic parameters of RubisCO from the marine bloom-forming diatom, *Skeletonema costatum*. *Geobiol.* 13, 33-34.

Borkhsenious, O. N., Mason, C. B., Moroney, J. V. (1998). The intracellular localizaiton of ribulose-1,5-bisosphate carboxylase/oxygenase in *Chlamydomonas reinhardtii*. *Plant Physiol.* 116, 1585-1591.

Bown, P. R. (1987). Taxonomoy, biostratigaphy, and evolution of late Triassic-early Jurassic calcareous nannofossils. *Special papers in Palaeontology* 38, 1-118.

Bown, P. R., Lees, J. A., Young, J. R. (2004). "Calcareous nannoplankton evolution and diversity through time" in Coccolihtophores, From Molecular Processes to Global Impact, eds. H.R. Thierstein & J. R. Young, Springer, Germany. 481-505.

Bradford, M. M. (1976). Rapid and sensitive method for the quantitation of microgram quantities of protein utilizing the priciple of protein-dye binding. *Anal. Biochem.* 72, 248-254.

Bridoux, M. C. & Ingalls, A. E. (2010). Structural identification of long-chain polyamines associated with diatom biosilica in a Southern Ocena sediment core. *Geochim. Cosmochim. Acta* 74, 4044-4057.

Bridoux, M. C., Annenkov, V., Menzel, H., Keil, R., Ingalls, A. E. (2011) A new liquid chromatography/electrospray ionization mass spectrometry method for the analysis of underivatized aliphatic long-chain polyamines: application to diatom-rich sediments. *Rapid Comm. Mass Spec.* 25, 877-888.

Bridoux, M. C. & Ingalls, A. E. (2013). Diatom microfossils from Cretaceous and Eocene sediments contain native silica precipitating long-chain polyamines. *Geobiol.* 11, 215-223.

Brocks, J. J., Love, G. D., Summons, R. E., Knoll, A. H., Logan, G. A., Bowden, S. A. (2005). Biomarker evidence for green and purple sulphur bacteria in a stratified Palaeoproterozoic sea. *Nature* 437, 866-870.

Brown, S. R. (1967). The pyrenoid: Its structure, distribution and function. *J. Phycol.* 3, 5-7.

Brown, D. H., Ascaso, C., Rapsch, S. (1987). Ultrastructural changes in the pyrenoid of the Lichen *Parmelia sulcata* stored under controlled conditions. *Protoplasma* 136, 136-144.

Brownlee, C. & Taylor, A. R. (2002). Algal calcification and silification. *eLS* http://onlinelibrary.wiley.com/doi/10.1038/npg.els.0000313/abstract

Brunelle, B. G., Sigman, D. M., Cook, M. S., Keigwin, L. D., Haug, G. H., Plessen, B., Schettler, G., Jaccard, S. L. (2007). Evidence from diatom-bound nitrogen isotopes for subarctic Pacific stratification during the last ice age and a link to North Pacific denitrification changes. *Paleoceanography 22* doi: 10.1029/2005PA001205

Burkhardt, S., Amoroso, G., Riebesell, U., Su, D. (2001). CO_2 and HCO_3^- uptake in marine diatoms acclimated to different CO_2 concentrations. *Limnol. Oceanogr. 46*, 1378–1391.

Burkhardt, S., Riebesell, U., Zondervan, I. (1999). Effects of growth rate, CO_2 concentration, and cell size on the stable carbon isotope fractionation in marine phytoplankton. *Geochim. Cosmochim. Acta 63*, 3729–3741.

Burns, B. D. & Beardall, J. (1987). Utilization of inorganic carbon by marine microalgae. *J. Exp. Mar. Biol. Ecol.* 107, 75-86.

Campbell, D. A., Cockshutt, A. M., Porankiewicz-Asplund, J. (2003). Analysing photosynthetic complexes in uncharacterized species of mixed microalgal communities using global antibodies. *Physiologia Plantarum* 119, 322-327.

Cande, S. C. & Kent, D. V. (1995). Revised calibration of the geomagnetic polarity timescale for the Late Cretaceous and Cenozoic. *J. Geophys. Res.* 100, 6094-6095.

Canfield, D. E. (2005). The early history of atmospheric oxygen: Homage to Robert M. Garrels. *Ann. Rev. Earth Planet. Sci.* 33, 1-36.

Capone, D. G. & Hutchins, D. A. (2013). Microbial biogeochemistry of coastal upwelling regimes in a changing ocean. *Nature Geosci.* 6, 711-717.

Cavalier-Smith, T. (1999). Principles of protein and lipid targeting in secondary symbiogenesis: Euglenoid, dinoflagellate, and sporozoan plastid origins and the eukaryote family tree. *J. Eukaryotic Microbiol.* 46, 347-366.

Cavalier-Smith, T. (1981). Eukaryote kingdoms: Seven or nine? *Biosystems* 14, 461-481.

Channell, J. E. T., Galeotti, S., Martin, E. E., Billups, K., Scher, H. D., Stoner, J. S. (2003). Eocene to Miocene magnetostratigraphy, biostratigraphy, and chemostratigraphy at ODP Site 1090 (sub-Antarctic South Atlantic). *Geol. Soc. of Am. Bull. 115*, 607–623.

Chen, Y. R. & Harman, F. C. (1995). A signature of the oxygenase intermediate in catalysis by ribulose-bisphosphate carboxylase/oxygenase as provided by a site-directed mutant. *J. Biol. Chem.* 270, 11741-44.

Clegg, M. T. (1993). Chloroplast gene sequences and the study of plant evolution. *Proc. Natl. Acad. Sci.* 90, 363-67.

Clegg, M. T., Cummings, M. P., Durbin, M. L. (1997). The evolution of plant nuclear genes. *Proc. Natl. Acad. Sci.* 94, 7791-98.

Cleland, W. W., Andrews, T. J., Gutteridge, S., Hartman F. C., and Lorimer, G. H., (1998). *Chem. Rev.* 98, 549-561.

Colman, B. & Rotatore, C. (1995). Photosynthetic inorganic carbon uptake and accumulation in two marine diatoms. *Plant Cell Environ. 1*8, 919-924.

Conte, M. H., Volkman, J. K. Eglinton, G. (1994). "Lipid biomarkers of the Prymnesiophyceae" in The Haptophyte Algae, eds. J. C. Green & B. S. C. Leadbetter, Clarendon Press, Oxford. 351-377.

Conway, H. L., Holmes, R. W., Davis, C. O. (1977). Marine diatoms grown in chemostats under silicate or ammonium limitation. III. Cellular chemical composition and morphology of *Chaetoceros debilis*, *Skeletonema costatum*, and *Thalassiosira gravida*. *Mar. Biol. 31*, 19–31.

Cox, P. M., Betts, R. A., Jones, C. D., Small, S. A., Totterdell, I. J. (2000). Acceleration of global warming due to carbon-cycle feedbacks in a coupled climate model. *Nature* 408, 184-187.

Coxall, H. K., Wilson, P. A., Palike, H., Lear, C. H., Backman, J. (2005). Rapid stepwise onset of Antarctic glaciation and deeper calcite compensation in the Pacific Ocean. *Nature 433*, 53–57.

Cramer, B. S., Toggweiler, J. R., Wright, J. D., Katz, M. E., Miller, K. G., (2009). Ocean overturning since the late cretaceous: inferences from a new benthic foraminiferal isotope complilation. *Paleoceanography* 24, PA4216.

Crosta, X. & Shemesh, A. (2002). Reconciling down core anticorrelation of diatom carbon and nitrogen isotopic ratios from the Southern Ocean. *Paleoceanography 17*, 10-1 - 10-8.

Davis, C. O. (1976). Continuous culture of marine diatoms under silicate limitation. II. Effect of light intensity on growth and nutriet uptake of *Skeletonema costatum*. *J. Phycol. 12*, 291–300.

DeConto, R. M., Pollard, D. (2003). Rapid Cenozoic glaciation of Antarctica induced by declining atmospheric CO_2. *Nature 421*, 245–249.

DeConto, R. M., Pollard, D., Wilson, P. a, Pälike, H., Lear, C. H., Pagani, M. (2008). Thresholds for Cenozoic bipolar glaciation. *Nature 455*, 652–656.

DeVargas, C., Aubry, M., Probert, I., Young, J. (2007). "Origin and evolution of coccolithophores: from coastal hunters to oceanic farmers." in Evolution of Primary Producers in the Sea eds. Falkowski, P. & Knoll, A. H. Elsevier. 252-286.

Diester-Haass, L. & Zahn, R. (1996). Eocene-Oligocene transition in the Southern Ocean : History of water mass circulation and biological productivity. *Geology 24*, 163–166.

Dionisio-Sese, M. L., Fukuzawa, H., Miyachi, S. (1990). Light-inducted carbonic anhyrase expression in *Chlamydomonas reinhardtii. Plant Physiol.* 94, 1103-1110.

Edwards, E. J., Osborne, C. P., Strömberg, C. A. E., Smith, S. A., the C_4 Grasses Consortium (2010). The origins of C_4 grasslands: integrating evolutionary and ecosystem science. *Science* 328, 587-591.

Eckhardt, N. A., Snyder, G. W., Portis, A. R. Jr., Ogren, W. L. (1997). Growth and photosynthesis under high and low irradiance of *Arabidopsis thaliana* antisense mutants with reduced ribulose-1,5-bisphosphate carboxylase/oxygenase activase content. *Plant Physiol.* 113, 575-86.

Egan, K. E., Rickaby, R. E. M., Leng, M. J., Hendry, K. R., Hermoso, M., Sloane, H. J., Bostock, H., Halliday, A. N. (2012). Diatom silicon isotopes as a proxy for silicic acid utilisation: A Southern Ocean core top calibration. *Geochim. Cosmochim. Acta* 96, 174-192.

Egan, K. E., Rickaby, R. E. M., Hendry, K. R., Halliday, A. N. (2013). Opening the gateways for diatoms primes Earth for Antarctic glaciation. *Earth and Planet. Sci. Lett. 375*, 34–43.

Ehleringer, J. R. & Monson, R. K. (1993). Evolutionary and ecological aspects of photosynthetic pathway variation. *Annu. Rev. Ecol. Syst.* 24, 411-439

Ehrmann, W. U., Mackensen, A. (1992). Sedimentological evidence for the formation of an East Antarctic ice sheet in Eocene/Oligocene time. *Palaeogeogr. Palaeoclimatol. Palaeoecol. 93*, 85–112.

Engel, B. D., Schaffer, M., Cuellar, L. K., Villa, E., Plitzko, J. M., Baumeister, W. (2015). Native architecture of the *Chlamydomonas* chloroplast revealed by in situ cryo-electron tomography. eLIFE. elifesciences.org.

Eppley, R. W. (1972). Temperature and phytoplankton growth in the sea. *Fishery Bull.* 70, 1063-1085.

Falkowski, P. G. & Raven, J. A. (2007). Aquatic Photosynthesis, 2nd edn. Priceton University Press, Princeton, N.J.

Falkowski, P. G., Katz, M. E., Milligan, A. J., Fennel, K., Cramer, B. S., Aubry, M. P., Berner , R. A., Novacek, M. J., Zapol, W. M. (2005). The rise of oxygen over the past 205 million years and the evolution of large placental mammals. *Science* 309, 2202-2204.

Falkowski, P. G., Katz, M. E., Knoll, A. H., Quigg, A., Raven, J. A. (2004). The evolution of modern eukaryotic phytoplankton. *Science* 305, 354-360.

Farquhar, G. D., O'Leary, M. J., Berry, J. A. (1982). On the relationship between carbon isotope discrimination and the intercellular carbon dioxide concentration in leaves. *Aust. J. Plant. Physiol.* 9, 121-137.

Farrimond, P., Eglinton, G., Brassell, S. C. (1986). Alkenones in Cretaceous black shales, Blake-Bahama Basin, western North Atlantic. *Org. Geochem.* 10, 897-903.

Felsenstein, J. (1985). Confidence limits on phylogenies: an approach using the bootstrap. *Evolution* 39, 783-791.

Fennel, K., Follows, M., Falkowski, P. G. (2005). The co-evolution of the nitrogen, carbon and oxygen cycles in the Proterozoic ocean. *American Journal of Science* 305, 526-545.

Field, C. B., Behrenfeld, M. J., Randerson, J. T., Falkowski, P. (1998). Primary production of the biosphere: integrating terrestrial and oceanic components. *Science* 281, 237-240.

Fiorini, S., Middelburg, J.J., Gattuso, J.P. (2011a) Testing the effects of elevated pCO_2 on coccolithophores (Prymnesiophyceae): comparison between haploid and diploid life stages. *J. Phycol.* 47, 1281-1291.

Francois, R., Altabet, M., Goericke, R. (1993). Changes in the $d^{13}C$ of surface water particulate organic matter across the subtropical convergence in the SW Indian Ocean. *Glob. Biogeochem. Cycles 7*, 627–644.

Freeman, K. H., Hayes J.M. (1992). Fractionation of carbon isotopes by phytoplankton and estimates of ancient CO_2 levels. *Glob. Biogeochem. Cycles* 185-198.

Fresnel, J. & Billard, C. (1991). *Pleurochrysis placolithoides* sp. nov. (Prymnesiophiceae), a new marine coccolithophorid with remarks on the status of Cricolith-bearing species. *Brit. Phycol.* J. 26, 67-80.

Frigeri, L. G., Radabaugh, T. R., Haynes, P. A., Hildebrand, M. (2006). Identification of proteins from a cell wall fraction of the diatom *Thalassiosira pseudonana*: insights into silica structure formation. *Mol. & Cell. Proteomics 5*, 182–193.

Gerbaud, A. & Andre M. (1980). Effect of CO_2, O_2, and light on photosynthesis and photorespiration in wheat. *Plant Physiol.* 66, 1032-1036.

Gibbs, S. P. (1962). The ultrastructure of the pyrenoids of green algae. *J. Ultrastruc. Res.* 7, 262-272.

Gibbs, S. P. (1978). The chloroplasts of *Euglena* may have evolved from symbiotic green algae. *Can. J. Bot.* 56, 2883-2889.

Gilstad, M. & Sakshaug, E. (1990). Growth rates of ten diatom species from the Barents Sea at different irradiances and day lengths. *Mar. Ecol. Prog. Ser. 64*, 169–173.

Giordano, M., Beardall, J., Raven, J. A. (2005). CO_2 concentrating mechanisms in algae: mechanisms, environmental modulation, and evolution. *Ann. Rev. Plant Biol.* 56, 99-131.

Goering, J. J., Nelson, D. M., Carter, J. A. (1973). Silicic acid uptake by natural populations of marine phytoplankton. *Deep-Sea Res. 20*, 777–789.

Gould, S. J. & Lewontin, R. C. (1979). The spandrels of San Marco and the panglossian paradigm: a critique of the adaptationist programme. *Proc. Royal Soc. Lon.* 205, 581-598.

Gowik, U., Brautigam, A., Weber, K. L., Weber, A. P. M., Westhoff, P. (2011). Evolution of C_4 photosynthesis in the genus *Flaveria*: How many and which genes does it take to make C_4? *Plant Cell* 23, 2087-2105.

Graham, L. E. & Wilcox, L. W. (2000). Algae. Prentice Hall.

Griffiths, D. J. (1970) The pyrenoid. *Bot. Rev.* 36, 29-58.

Guillard, R. R. L. (1975). "Culture of phytoplankton for feeding marine invertebrates" in Culture of Marine Invertebrate Animals, eds. Smith, W. L. & Canley, M. R. Plenum Press, New York. 29-60.

Guillard, R. R. L. & Kilham, P. (1973). Kinetics of silicon-limited growth in the marine diatom *Thalassiosira pseudonana* hasle and heimdal. (=cyclotella nana hustedt). *J. Phycol. 9*, 233–237.

Halverson, G. P., Dudas, F., Maloof, A. C., Bowring, S. A. (2007). Evolution of the 87Sr/86Sr Composition of Neoproterozoic Seawater. *Palaeogeog. Palaeoclim. Palaeoecol.* 256, 103-129.

Hanson, T. E. & Tabita, F. R. (2001). A ribulose-1,5-bisphosphate carboxylase/oxygenase (RubisCO)-like protein from *Chlorobium tepidum* that is involved with sulfur metabolism and the response to oxidative stress. *Proc. Nat. Acad. Sci.* 98, 4397-4402.

Harada, H. & Matsuda, Y. (2005). Identification and characterization of a new carbonic anhydrase in the marine diatom *Phaeodactylum tricornutum*. *Can. J. Bot.* 83, 909-916.

Harada, H., Nakatsuma, D., Ishida, M., Matsuda, Y. (2005). Regulation of the expression of intracellular ß-carbonic anhydrase in response to CO_2 and light in the marine diatom *Phaeodactylum tricornutum*. *Plant Physiol.* 139, 1041-1050.

Harpel, M. R. & Hartman, F. C. (1996). Facilitation of the terminal proton transfer reaction of ribulose 1,5-bisphosphate carboxylase/oxygenase by active site Lys 166. *Biochemistry* 35, 13865-13870.

Harpel, M. R., Larimer, F. W., Hartman, F. C. (1998). Multiple catalytic roles of His 287 of *Phodospirillum rubrum* ribulose 1,5-bisphosphate carboxylase/oxygenase. *Protein Sci.* 7, 730-38.

Harper, J. T., Waanders, E., Keeling, P. J. (2005). On the monophyly of chromalveolates using a six-protein phylogeny of eukaryotes. *Int. J. Syst. Evol. Microbiol.* 55, 487-496.

Harrison, P. J., Boyd, P. W., Varela, D. E., Takeda, S., Shiomoto, A., Odate, T. (1999). Comparison of factors controlling phytoplankton productivity in the NE and NW Subarctic Pacific gyres. *Prog. Oceanogr.* 42, 205-234.

Hartman, F. C. & Harpel, M. R. (1994). Structure, function, regulation, and assembly of D-ribulose-1,5-bisphophate carboxylase/oxygenase. *Ann. Rev. Biochem.* 63, 197-234.

Hayes, J. M., Strauss, H., Kaufman, A. J. (1999). The abundance of ^{13}C in marine organic matter and isotopic fractionation in the global biogeochemical cycle of carbon during the past 800 Ma. *Chem. Geol. 161*, 103–125.

Hendry, K. R. & Rickaby, R. E. M. (2008). Opal (Zn/Si) ratios as a nearshore geochemical proxy in coastal Antarctica. *Paleoceanography 23*. doi: 10.1029/2007PA001576

Hiller, W. & Babcock, G. T. (2001). Photosynthetic reaction centers. *Plant Physiol.* 125, 33-37.

Hofle, M. G. (1984). Degradation of putrescine and cadaverine in seawater cultures by marine bacteria. *Appl. Env. Microbiol*. 47, 843-849.

Holdsworth, R. H. (1968). The presence of a crystalline matrix in pyrenoids of the diatom, Achnanthes brevipes. *J. Cell Biol.* 37, 831-837.

Holland, H. D. (2006). The oxygenation of the atmosphere and oceans. *Phil. Trans.* of the *R. Soc. B: Biol. Sci.* 361, 903-915.

Hopkinson, B. M., Dupont, C. L., Allen, A. E., Morel, F. M. M. (2011). Efficiency of the CO_2-concentrating mechanism of diatoms. *Proc.* of the *Natl. Acad.* of *Sci. 108*, 1-8.

Hopkinson, B. M., Xu, Y., Shi, D., McGinn, P. J., Morel, F. M. M. (2010). The effect of CO_2 on the photosynthetic physiology of phytoplankton in the Gulf of Alaska. *Limnol. Oceanogr.* 55, 2011-2024.

Iancu, C. V., Ding, H. J., Morris, D. M., Dias, D. P., Gozales, A. D., Martino, A., Jensen, G. J. (2007). The structure of isolated *Synechococcus* strain WH8102 carboxysomes as reavealed by electron cryotomography. *J. Mol. Biol.* 372, 764-773.

Iglesias-Rodriguez, M. D., Brown, C. W., Doney, S. C., Kleypas, J., Kolber, D., Kolber, Z., Hayes, P. K., Falkowski, P. G. (2002). Representing key phytoplankton functional groups in ocean carbon cycle models: Coccolithophorids. *Glob. Biogeochem. Cycles* 16, 1100.

Iglesias-Rodriguez, M. D., Halloran, P. R., Rickaby, R. E. M., Hall, I. R., Colmenero-Hidalgo, E., Gittins, J. R., Green, D. R. H., Tyrrell, T., Gibbs, S. J., von Dassow, P., Rehm, E., Armbrust, E. V., Boessenkool, K. P. (2008). Phytoplankton calcification in a high-CO_2 world. *Science* 320, 336-340.

Jeffrey, S. W. & LeRoi, J. M. (1997). "Simple procedures for growing SCOR reference microalgal cultures." in Phytoplankton pigments in oceanography; Monographs on oceanographic methology eds. Jeffrey, S.W., Mantoura, R. F. C., Wright, S. W. UNESCO, France. 181-205.

Jeffrey , A. W. A., Pflaum, R. C., Brooks, J. M., Sackett, W.M. (1983). Vertical trends in particulate organic carbon ^{13}C:^{12}C ratios in the upper water column. *Deep Sea Research Part A. Oceanographic Research Papers* 30, 971-983.

Jensen, R. G. & Bahr, J. T. (1977). Ribulose 1,5-bisphosphate carboxylase-oxygenase. *Plant Biol. Ann. Rev.* 28, 379-400.

Jin, P., Gao, K., Beardall, J. (2013). Evolutionary responses of a coccolithophorid *Gephyrocapsa oceanica* to ocean acidification. *Evolution* 67, 1869-1878.

Jordan, D. B. & Chollet, R. (1983). Inhibition of ribulose bisphosphate carboxylase by substrate ribulose 1,5-bisphosphate. *J. Biol. Chem.* 258,13752-58.

Jordan, D. B. & Ogren, W. L. (1981). Species variation in the specificity of ribulose bisphosphate carboxylase/oxygenase. *Nature* 291, 513-15.

Jordan, D. B. & Ogren, W. L. (1984). The CO_2/O_2 specificity of ribulose 1,5-bisphosphate carboxylase/oxygenase. *Planta* 161, 449-461.

Kane, H. J., Viil, J., Entsch, B., Paul, K., Morell, M. K., Andrews, T. J. (1994). An improved method for measuring CO_2/O_2 specificity of Ribulosebisphosphate carboxylase-oxygenase. *Aust. J. Plant Physiol.* 21, 449-461.

Karl, D. & Steinberg, D. (2001). Biological Pump Working Group Summary [Homepage of Ocean Carbon Transport, Exchanges and Trasformation], Online, http://www.msrc.sunysb.edu/octet/biological_pump.html [2011, 8/6].

Kasting, J. F. (1993). Earth's early atmosphere. *Science* 5097, 920-926.

Kasting, J. F. (2001). The rise of atmospheric oxygen. *Science* 293, 819-820.

Katz, M. E., Fennel, K., Falkowski, P. G. (2007). "Geochemical and biological consequences of phytoplankton evolution" in Evolution of Primary Producer in the Sea, eds. P. G. Falkowski & A. J. Knoll, Elsevier, China. 405-430.

Keeling, P. J. (2004). Diversity and evolutionary history of plastids and their hosts. *Am. J. Bot.* 91, 1481-1493.

Kennett, J. P. (1977). Cenozoic evolution of Antarctic glacation, the circum-Antarctic Ocean, and their impact on paleooceanography. *J. Geophys. Res. 82*, 3834-3860.

Knoll, A. H., Walter, M. R., Narbonne, G. M., Christie-Blick, N. (2006). The Ediacaran Period: a new addition to the geological time scale. *Lethaia* 39, 13-30.

Kooistra, W. H., Gersonde, R., Medlin, L., Mann, D. G. (2007). "The origin and evolution of the diatoms: Their adaptation to a planktonic existence" in Evoluiton of Primary Producers in the Sea, eds. P. G. Falkowski & A. H. Knoll, Elsevier, China. 207-249.

Kooistra, W. H. & Medlin, L. K. (1996). Evolution of the diatoms (Bacillariophyta). IV. A reconstruction of their age from small subunit rRNA coding regions and the fossil record. *Mol. Phylogenet. Evol.* 6, 391-407.

Kowallik, K. (1969). The crystal lattice of the pyrenoid matrix of *Prorocentrum micans*. *J. Cell Sci.* 5, 251-269.

Kröger, N., Lehmann, G., Rachel, R., Sumper, M. (1997). Characterization of a 200-kDa diatom protein that is specifically associated with a silica-based substructure of the cell wall. *Eur. J. Biochem. 250*, 99–105.

Kröger, N., Deutzmann R., Bergsdorf C., Sumper M. (2000). Species-specific polyamines from diatoms control silica morphology. *Proc. of the Nat. Acad. of Sciences* 97, 14133-14138.

Ku, M. S. B., Schmitt, M. R., Edwards, G. E. (1979). Quantitative determination of RuBP carboxylase-oxygenase protein in leaves of several C_3 and C_4 plants. *J. Exp. Bot.* 30, 89-98.

Laing, W. A., Ogren, W. L., Hageman, R. H. (1974). Regulation of soybean net photosynthetic CO_2 fixation by the interaction of CO_2, O_2 and ribulose 1,5-diphosphate carboxylase. *Plant Physiol.* 54, 678-85.

Lambert, F., Delmonte, B., Petit, J. R., Bigler, M., Kaufmann, P. R., Hutterli, M. A., Stocker, T. F., Ruth, U., Steffensen, J. P., Maggi, V. (2007). Dust-climate couplings over the past 800,000 years from the EPICA Dome C ice core. *Nature* 452, 616-619.

Lapointe, M., MacKenzie, T. D. B., Morse, D. (2008). An external δ-carbonic anhydrase in a free-living marine dinoflagellate may circumvent diffusion-limited carbon acquisition. *Plant Physiol.* 147, 1427-1436.

Lara, M. V. & Andreo, C. S. (2011). C_4 plants adaptation to high levels of CO_2 and to drought environments. *InTech.* 18, 415-428.

Laws, E. A., Popp, B. N., Bidigare, J. R. R., Kennicutt, M. C., Macko, S. A. (1995). Dependence of phytoplankton carbon isotopic composition on growth rate and $[CO_2]_{aq}$: Theoretical considerations and experimental results. *Geochem. Cosmochim. Acta 59*, 1131–1138.

Laws, E. A., Popp, B. N., Cassar, N., Tanimoto, J. (2002). ^{13}C discrimination patterns in oceanic phytoplankton: likely influence of CO_2 concentrating mechanisms, and implications for palaeoreconstructions. *Funct. Plant Biol. 29*, 323–333.

Lee, R. B. Y., Smith, J. A. C., Rickaby, R. E. M. (2013). Cloning, expression and characterization of the δ-carbonic anhydrase of *Thalassiosira weissflogii* (Bacillariophyceae). *J. Phycol.* 49, 170-177.

Levitan, O., Kranz, S.A., Spungin. D., Prasil, O., Rost, B., Berman-Frank, I. (2010). Combined effects of CO_2 and light on the N_2-fixing cyanoacterium *Trichodesmium* IMS101: a mechanistic view. *Plant Physiol.* 154, 346-356.

Li, H., Sawaya, M. R., Tabita, F. R. Eisenberg, D. (2005). Crystal structure of a Rubisco-like protein from the green sulfur bacterium *Chlorobium tepidum*. *Structure* 13, 779-789.

Lin, S. & Carpenter, E. J. (1997). Pyrenoid localization of Rubisco in relation to the cell cycle and growth phase of *Dunaliella tertiolecta* (Chlorophyceae). *Phycologia.* 36, 24-31.

Liu, H. (2010). Evolution, diversity, and biogeography in pelagic calcifying protists. PhD thesis. Rutgers University.

Liu, Z., Pagani, M., Zinniker, D., Deconto, R., Huber, M., Brinkhuis, H., Shah, S. R., Leckie, M., Pearson, A. (2009). Global Cooling During the Eocene-Oligocene Climate Transition. *Science 323*, 1187–1190.

Long, S. P. (1999). "Environmental responses" in C_4 plant biology, eds. Sage, R. F. & Monson, R. K. San Diego: Academic Press, 215-249.

Longhurst, A. R. & Harrison, W. G. (1989). The biological pump: Profiles of plankton production and consumption in the upper ocean. *Prog. Oceanog.* 22, 47-123.

Losh, J. L., Young, J. N., Morel, F. M. M. (2013). Rubisco is a small fraction of total protein in marine phytoplankton. *New Phytol.* 198, 52-58.

Lowenstein, T. K., Demicco, R. V. (2006). Elevated Eocene atmospheric CO_2 and its subsequent decline. *Science* 313, 1928.

Maeda N., Kitano K., Fukui T., Ezaki S., Atomi H. (1999). Ribulose bisphosphate carboxylase/oxygenase from the hyperthermophilic archaeon *Pyrococcus kodakaraensis* KOD1 is composed solely of large subunits and forms a pentagonal structure. *J. Mol. Biol.* 293, 57-66.

Marcus, Y., Harel, E., Kaplan, A. (1983). Adaptation of the cyanobacterium *Anabaena variabilis* to low CO_2 concentration in their environment. *Plant Physiol.* 71, 208-210.

Martin-Jézéquel, V., Hildebrand, M., Brzezinski, M. A. (2000). Silicon metabolism in diatoms: Implications for growth. *J. Phycol*. 36, 821-840.

Mate C. J., Hudson G. S. von Caemmerer S., Evans J. R., Andrews T. J. (1993). Reduction of ribulose bisphosphate carboxylase activase levels in tobacco (*Nicotiana tabacum*) by antisense RNA reduces ribulose bisphosphate carboxylase carbamylation and impairs photosynthesis. *Plant Physiol.* 102, 1119-28.

Matsuda, Y. & Colman, B. (1995a). Induction of CO_2 and bicarbonate transport in green alga *Chlorella ellipsoidea.* I Time course of induction of two systems. *Plant Physiol.* 108, 247-252.

Matsuda, Y. & Colman, B. (1995b). Induction of CO_2 and bicarbonate transport in green alga *Chlorella ellipsoidea.* II Evidence for induction in response to external CO_2 concentration. *Plant Physiol.* 108, 253-260.

Matsuda, Y., Nakajima, K., Tachibana, M. (2011). Recent progresses on the genetic basis of the regulation of CO_2 acquisition systems in response to CO_2 concentration. *Photosynth. Res.* 109, 191-203.

Mayo, W. P., Williams, T. G., Birch, D. G., Turpin, D. H. (1986). Photosynthetic adaptation by *Synechococcus leopoliensis* in reponse to exogenous dissolved inorganic carbon. *Plant Physiol.* 80, 1038-1040.

McCarthy, A., Rogers, S.P., Duffy, S.J., Campbell, D.A. (2012). Elevated carbon dioxide differentially alters the photophysiology of *Thalassiosira pseudonana* (Bacillariophyceae) and *Emiliania Huxleyi* (Haptophyta). *J. Phycol.* 48, 635-646.

McFadden, G. I. (2001). Primary and secondary endosymbiosis and the origin of plastids. *J. Phycol.* 37, 951-959.

Medlin, L. (1997). Evolution of the diatoms - a total approach using morphology, molecules and geology. Report on the Workshop June 1-2, 1997, *Diatom Res.* 371-363.

Medlin, L. K., Williams, D. M., Sims, P. A. (1993). The evolution of the diatoms (Bacillariophyta). I . Origin of the group and assessment of the monophyly of its major divisions. *Eur. J. Phycol.*, 28, 261–275.

Medlin, L. K., Gersonde, R., Kooistra, W. H. C. F., Wellbrock, U. (1996b). Evolution of the diatoms (Bacillariophyta): II. Nuclear-encoded small-subunit rRNA sequence comparions confirm a paraphyletic origin for the centric diatoms. *Molec. Biol. Evol.* 13, 65-75.

Medline, L. K., Kooistra, W. H. C. F., Potter, D., Saunders, G. W., Andersen, R. A. (1997). Phylogenetic relationships of the 'golden algae' (haptophytes, heterokont chromophytes) and their plastids. *Plant Syst. Evol.* 11, 187-219.

Miller, K. G., Fairbanks, R. G., Mountain, G. S. (1987). Tertiary oxygen isotope synthesis, sea level history, and continental margin erosion. *Paleoceanography 2*, 1–19.

Minoletti, F., Hermoso, M., Gressier, V. (2009). Separation of sedimentary micron-sized particles for palaeoceanography and calcareous nannoplankton biogeochemistry. *Nature Protoc. 4*, 14–24.

Montsant, A., Jabbari, K., Maheswari, U., Bowler C. (2005). Comparative genomics of the pennate diatom *Phaeodactylum tricornutum. Plant Physiol.* 137, 500-513.

Mook, W. G., Bommerson, J. C., Staverman, W. H. (1974). Carbon isotope fractionation between dissolved bicarbonate and gaseous carbon dioxide. *Earth and Planet. Sci. Lett. 22*, 169–176.

Morell, M. K., Kane, H. J., Hudson, G. S., Andrews, T. J. (1992). Effects of mutations at residue 309 of the large subunit of ribulosebisphosphate carboxylase from Synechococcus PCC 6301. *Arch. Biochem. Biophys.* 299, 295-301.

Morley, D. W., Leng, M. J., Mackay, A. W., Sloane, H. J., Rioual, P., Battarbee, R. W. (2004). Cleaning of lake sediment samples for diatom oxygen isotope analysis. *J. Paleolimnol. 31*, 391–401.

Moroney, J. V., Bartlett, S. G., Samuelsson G. (2001). Carbonic anhydrases in plants and algae. *Plant Cell Environ.* 24, 141-153.

Moroney, J. V., Ma, Y., Frey, W. D., Fusillier, K. A., Pham, T. T., Simms, T. A., DiMario R. J., Yang, J., Mukherjee, B. (2011). The carbonic anhyrase isoforms of *Chlamydomonas reinhardtii*: intracellular location, expression, and physiologicla roles. *Photosynth. Res.* 209, 133-149.

Moroney, J. V. & Somanchi, A. (1999). How do algae concentrate CO_2 to increase the efficiency of photosynthetic carbon fixation? *Plant Physiol.* 119, 9-16.

Morris, I. (1980). "Paths of carbon assimilation in marin phytoplankton." In *Primary Productivity in the Sea*, ed. Falkowski, P. G., New York: Plenum 139-159.

Morse, D., Salois, P., Markovic, P., Hastings, J. (1995). A nuclear-encoded form II Rubisco in dinoflagellates. *Science* 268, 1622-1624.

Muhaidat, R. (2007). Diversification of C_4 photosynthesis in the eudicots: anatomical, biochemical and physiological perspectives. PhD Thesis. Toronto, Canada: Univeristy of Toronto.

Müller, P. J., Čepek, M., Ruhland, G., Schneider, R. R. (1997). Alkenone and coccolithophorid species changes in late Quaternary sediments from the Walvis Ridge: Implications for the alkenone paleotemperature method. *Palaeogeogr. Palaeoclimatol. Palaeoecol. 135*, 71–96.

Newell, N. D. (1963). Crisis in the history of life. *Scientific American.* 208, 76-92.

Newell, N. D. (1973). The very last moment of the Paleozoic Era. *The Permian and Triassic systems and their mutual boundary* 2, 1-10.

Oaks, A. (1994). Efficiency of nitrogen utilization in C_3 and C_4 cereals. *Plant Physiol.* 106, 407-414.

Okazaki, K., Nishizawa, M., Furuno, N., Yasuda, H., Sagata, N. (1992). Differential occurrence of CSF-like activity and transforming activity of Mos during the cell cycle in fibroblasts. *EMBO J.* 11, 2447-2456.

Olsen, S. & Paasche, E. (1986). Variable kinetics of silicon-limited growth in *Thalassiosira pseudonana* (Bacillariophyceae) in response to changed chemical composition of the growth medium. *Br. Phycol. J. 21*, 183–190.

Paasche, E. (1975). Growth of the plankton diatom *Thlassiosira nordenskioeldii* Cleve at low silicate concentrations. *J. Exp. Mar. Biol. Ecol. 18*, 173–183.

Pagani, M., Zachos, J. C., Freeman, K. H., Tipple, B., Bohaty, S. (2005). Marked decline in atmospheric carbon dioxide concentrations during the Paleogene. *Science* 309, 600-603.

Pagani, M., Huber, M., Liu, Z., Bohaty, S. M., Henderiks, J., Sijp, W., Krishnan, S., DeConto, R. M. (2011). The role of carbon dioxide during the onset of Antarctic glaciation. *Science 334*, 1261–1264.

Pagani, M. (2014). "Biomarker-based inferences of past climate: the alkenone pCO_2 proxy." in Treatise of Geochemistry (Second Edition), eds. Heinrich, D. & Turekian, K., Elsevier, Oxford. 361-378.

Parry, M. A. J., Andralojc, P. J., Mitchell, R. A. C., Madgwick, P. J., Keys, A. J. (2003). Manipulaiton of Rubisco: the amount, activity, function and regulation. *J. Exp. Bot.* 54, 1321-1333.

Pearson, P. N., Foster, G. L., Wade, B. S. (2009). Atmospheric carbon dioxide through the Eocene–Oligocene climate transition. *Nature 461*, 1110–1113.

Peterson, K. J. & Butterfield, N. J. (2005). Origin of the Eumetazoa: testing ecological predictions of molecular clocks against the Proterozoic fossil record. *P. Nat. Acad. Sci.* 102, 9547-9552.

Petit, J. R., Jouzel, J., Raynaud, D., Barkov, N. I., Barnola, J. M., Basile, I., Bender, M., Chappelaz, J., Davis, M., Delaygue, G., Delmotte, M., Kotlyakov, V. M., Legrand, M., Lipenkov, V. Y., Lorius, C., Pepin, L., Ritz, C., Saltzman, E., Stievenard, M. (1999). Climate and atmospheric history of the past 420,000 years from the Vostok ice core, Antarctica. *Nature* 399, 429-436.

Pierce, J., Andrews, T. J., Lorimer, G. H. (1986). Reaction intermediate partitioning by ribulose-bisphosphate carboxylases with differing substrate specificities. *J. Biol. Chem.* 261, 10248-56.

Pinter, I. J. & Provasoli, L. (1968). Heterotrophy in subdued light of 3 *Chrysochromulina* species. *Bull. Misaki Mar. Biol. Inst. Kyoto* 12, 25-31.

Plancq, J., Grossi, V., Henderiks, J., Simon, L., Mattioli, E. (2012). Alkenone producers during late Oligocene-early Miocene revisited. *Paleoceanography 27 doi: 10.1029/2011PA002164*

Popp, B. N., Laws, E. A., Bidigare, R. R., Dore, J. E., Hanson, K. L., Wakeham, S. G. (1998). Effect of phytoplankton cell geometry on carbon isotopic fractionation. *Geochim. Cosmochim. Acta 62*, 69–77.

Portis, A. R. Jr (1995). The regulation of Rubisco by Rubisco activase. *J. Exp. Bot.* 46, 1285-91.

Poulsen, N. & Kröger, N. (2004). Silica morphogenesis by alternative processing of silaffins in the diatom Thalassiosira pseudonana. *J. Biol. Chem. 279*, 42993–42999.

Price, G. D. (2011). Inorganic carbon transporters of the cyanobacterial CO_2 concentrating mechanism. *Photosynth. Res.* 109, 47-57.

Price, G. D., Badger, M. R., Woodger, F. J., Long, B. M. (2008). Advances in understanding the cyanobacterial CO_2-concentrating mechanism (CCM): functional components, Ci transporters, diversity, genetic regulation and prospects for engineering into plants. *J. Exp. Bot.* 59, 1441-1461.

Pusz, A. E., Miller, K. G., Wright, J. D., Katz, M. E., Cramer, B. S., Kent, D. V. (2009). Stable isotopic response to late Eocene extraterrestrial impacts. *Geol. Soc. of Am. Spec. Pap. 452*, 1–13.

Pusz, A. E., Thunell, R. C., Miller, K. G. (2011). Deep water temperature, carbonate ion, and ice volume changes across the Eocene-Oligocene climate transition. *Paleoceanography 26* doi: 10.1022/2010PA001950

Rabosky, D. L., Sorhannus, U. (2009). Diversity dynamics of marine planktonic diatoms across the Cenozoic. *Nature* 457, 183-186.

Rae, B.D., Long B.M., Badger, M.R., Price, G.D. (2014). Functions, compositions, and evolution of the two types of carboxysomes: polyhedral microcompartments that facilitate CO_2 fixation in cyanobacteria and some proteobacteria. *Microbiol. Mol. Biol. Rev.* 77, 357-379.

Rau, G. H., Riebesell, U., Wolf-Gladrow, D. (1996). A model of photosynthetic ^{13}C fractionation by marine phytoplankton based on diffusive molecular CO_2 uptake. *Mar. Ecol. Prog. Ser.*, *133*, 275–285.

Raven, J. A. (2003). Inorganic carbon concentrating mechanisms in relations to the biology of algae. *Photosynth. Res.* 77, 155-171.

Raven, J. (2010). Inorganic carbon acquisition by eukaryotic algae: four current questions. *Photosynth. Res.* 106, 123-134.

Raven, J.A. (2011). Effects on marine algae of changed seawater chemistry with increasing atmospheric CO_2. *Biol. Environ.* 11, 1-17.

Raven, J. & Larkum, A. (2007). Are there ecological implications for the proposed energetic restrictions on photosynthetic oxygen evolution at high oxygen concentrations? *Photosynth. Res.* 94, 31-42.

Raven, J., Caldeira, J., Elderfield, H. (2005). Ocean acidification due to increasing atmospheric carbon dioxide, Royal Society policy document 12/05.

Raven, J., Giordano, M., Beardall, J., Maberly, S.C. (2011). Algal and aquatic plant carbon concentrating mechanisms in relation to environmental change. *Photosynth. Res.* 94, 31-42.

Raven, J. A., Cockell, C. S., De La Rocha, C. L. (2008). The evolution of inorganic carbon concentrating mechanism in photosynthesis. *Philos. T. Roy. Soc. B* 368, 2641-2650.

Raven, J. & Johnston, A. (1991). Mechanisms of inorganic-carbon acquisition in marine phytoplankton and their implications for the use of other resources. *Limnol. Oceanog.* 36, 1701-1714.

Raven, J.A., Giordano, M., Beardall, J., Maberly, S.C. (2012). Algal evolution in relation to atmospheric CO_2: carboxylases, carbon-concentrating mechanisms and carbon oxidation cycles. *Philos. T. Roy. Soc. B.* 367, 493-507.

Read, B. A., & Tabita, F. R. (1994). High substrate specificity factor ribulose bisphosphate carboxylase/oxygenase from eukaryotic marine algae and properties of recombinant cyanobacterial Rubisco containing "algal" residue modifications. *Arch. Biochem. Biophys.* 312, 210-218.

Read, B. A. & Tabita, F. R. (1992). Amino acid substitutions in the small subunit of ribulose-1,5-bisphosphate carboxylase/oxygenase that influence catalytic activity of the holoenzyme. *Biochemistry* 31, 519-525.

Rech, M., Morant-Manceau, A., Tremblin, G. (2008). Carbon fixation and carbonic anhydrase activity in *Heslea ostrearia* (Bacilarriophyceae) in relation to growth irradiance. *Photsynthetica* 46, 56-62.

Reinfelder, J. R., Kraepiel, A. M. L., Morel, F. M. M. (2000). Unicellular C_4 photosynthesis in a marine diatom. *Nature* 407, 996-999.

Reinfelder, J. R., Milligan, A. J., Morel, F. M. M. (2004) The role of the C_4 pathway in carbon accumulation and fixation in marine diatom. *Plant Physiol.* 135, 2106-21011.

Reinfelder, J. R. (2011). Carbon concentrating mechanisms in eukaryotic marine phytoplankton. *Annu. Rev. Mar. Sci. 3*, 291–315.

Reinhold, L., Kosloff. R., Kaplan, A. (1991). A model for inorganic carbon fluxes and photosynthesis in cyanobacterial carboxysomes. *Can. J. Bot.* 69, 984-988.

Reinhold, L., Zviman, M., Kaplan, A. (1987) "Inorganic carbon fluxes and photosynthesis in cyanobacteria--a quantitative model" in Proceedings of the VIIth International Congress on Photosynthesis ed. Biggins J. Provdience, Rhode Island, USA.

Rickaby, R. E. M., Henderiks, J., Young, J. (2010). Perturbing phytoplankton: A tale of isotopic fractionation in two coccolithophore species. *Clim. of the Past Discuss.*, 257-294.

Ridgwell, A. & Zeebe, R. E. (2005). The role of the global carbonate cycle in the regulation and evolution of the Earth System. *Earth Planetary Sc. Lett.* 234, 299-315.

Riebesell, U., Schulz, K. G. Bellerby, R. G. J., Botros, M., Fritsche, P., Meyerhofer, M., Neill, C., Nondal, G., Oschiles, A., Wohlers, J., Zollner, E. (2007). Enhanced biological carbon consumption in a high CO_2 ocean. *Nature* 450, 545-548.

Robinson, R. S. (2004). Revisiting nutrient utilization in the glacial Antarctic: Evidence from a new method for diatom-bound N isotopic analysis. *Paleoceanography 19*, 1-13.

Romanek, C. S., Grossman, E. L., Morse, J. W. (1992). Carbon isotopic fractionation in synthetic aragonite and calcite: Effects of temperature and precipitation rate. *Geochim. Cosmochim. Acta 56*, 419–430.

Rosenthal, Y., Dahan, M., Shemesh, A. (2000). Southern Ocean contributions to glacial-interglacial changes of atmospheric pCO_2: An assessment of carbon isotope records in diatoms. *Paleoceanography* 15, 65-75.

Rost, B., Riebesell, U., Burkhardt, S., Sültemeyer, D. (2003). Carbon acquisition of bloom-forming marine phytoplankton. *Limnol. Oceanogr.* 48, 55-67.

Royer, D. L., Berner, R. A., Park, J. (2007). Climate sensitivity constrained by CO_2 concentrations over the past 420 million years. *Nature* 446, 530-532.

Saez, A. G., Probert, I., Young, J. R., Edvardsen, B., Wenche, E., Medlin, L. K. (2004). "A review of the phylogeny of the Haptophyta." in Coccolithophores - from a molecular processes to global impact. eds. Thierstein, H. R. & Young, J. R. Springer, 251-270.

Sage, R. F. (2002). Variation in the k_{cat} of Rubisco in C_3 and C_4 plants and some implications for photosynthetic performance at high and low temperature. *J. Exp. Bot.* 53, 609-620.

Sage, R. F. (2004). The evolution of C_4 photosynthesis. *New Phytol.* 194, 787-795.

Sage, R. F. (2014). Photosynthetic efficiency and carbon concentration in terrestrial plants: the C_4 and CAM solutions. *J. Exp. Bot.* http://jxb.oxfordjournals.org/content/early/2014/06/23/jxb.eru262

Salamy, K. A. & Zachos, J. C. (1999). Latest Eocene–Early Oligocene climate change and Southern Ocean fertility: inferences from sediment accumulation and stable isotope data. *Palaeogeogr. Palaeoclimatol. Palaeoecol. 145*, 61–77.

Salvucci, M. E. & Ogren, W. L. (1996). The mechanism of Rubisco activase: insights from studies of the properties and structure of the enzyme. *Photosynth. Res.* 47, 1-11.

Satoh, D., Hiraoka, Y., Colman, B., Matsuda, Y. (2001). Physiological and molecular biological characterization of intracellular carbonic anhydrase from the marine diatom *Phaeodactylum tricornutum*. *Plant Physiol.* 126, 1459-1470.

Savir, Y., Noor, E., Milo, R., Tlusty, T. (2010). Cross-species analysis traces adaptation of Rubisco toward optimality in a low-dimensional landscape. *Proc. Nat. Acad. Sci.* 107, 3475-3480.

Scher, H. D., Martin, E. E. (2006). Timing and climatic consequences of the opening of Drake Passage. *Science* 312, 428-430.

Schidlowski, M. (1988). A 3,800-million-year isotopic record of life from carbon in sedimentary rocks. *Nature* 333, 313-318.

Schmitz, F. (1882). *Die Chromatophoren der Algen,* Verlag, von Max Cohen und Sohn, Bonn.

Schneider, C., Rasband, W. S., Eliceiri, K. W. (2012). NIH Image to ImageJ: 25 years of image analysis. *Nature* 9, 671-675.

Sharkey, T. D. (1988). Estimating the rate of photorespiration in leaves. *Physiologia Plantarum* 74, 147-152.

Sharkey, T. D. & Berry, J. A. (1985). "Carbon isotope fractionation in algae as influenced by inducible CO_2 concentrating mechanisms" in Inorganic Carbon Uptake by Aquatic Photosynthetic Organisms, eds. W. Lucas & J. A. Berry, Am. Soc. Plant Physiol., Rockville, Md. 389-401.

Sharwood, R., von Caemmerer, S., Maliga, P. (2008). The catalytic properties of hybrid Rubisco comprising tobacco small and sunflower large subunits mirror the kinetically equivalent source Rubiscos and can support tobacco growth 1[W][OA]. *Plant Physiol.* 146, 83-96.

Siegenthaler, U. & Sarmiento, J. L. (1993). Atmospheric carbon dioxide and the ocean. *Nature* 365, 119-125.

Sigman, D. M., Altabet, M. A., Francois, R., McCorkle, D. C., Gaillard, J. F. (1999). The isotopic composition of diatom-bound nitrogen in Southern Ocean sediments. *Paleoceanography 14*, 118–134.

Sims, P. A., Mann, D. G., Medlin, L. K. (2006). Evolution of the diatoms: insights from fossil, biological and molecular data. *Phycologia.* 45, 361-402.

Singer, A. J. & Shemesh, A. (1995). Climatically linked carbon isotope variation during the past 430,000 years. *Paleoceanography Currents 10*, 171–177.

Smetacek, V. (1999). Diatoms and the ocean carbon cycle. *Protist* 250, 25-32.

Sobrino, C., Segovia, M., Neale, P. J., Mercado, J. M., Garcia-Gomez, C., Kulk, G., Lorenzo, M. R., Camarena, T., van de Poll, W. H., Spilling, K., Ruan, Z. (2014). Effect of CO_2, nutrients and light on coastal plankton. IV. Physiological responses. *Aquat. Biol.* 22, 77-93.

Somerville, C. R. & Somerville, S. C. (1984). Cloning and expression of the *Rhodospirillum rubrum* ribulosebisphosphate carboxylase gene in *E. coli*. *Mol. Gen. Genet.* 193, 214-219.

Sorhannus, U. (2007). A nuclear-encoded small-subunit ribosomal RNA timescales for diatom evolution. *Mar. Micropaleontol.* 65, 1-12.

Soto, A. R., Zheng, H., Shoemaker, D., Rodriguez, J., Read, B. A., Wahlund, T. M. (2006). Identification and preliminary characterization of two cDNAs encoding unique carbonic anhydrases from the marine alga *Emiliania huxleyi. Appl. Environ. Microbiol.* 72, 5500-5511.

Spreitzer, R. J. (2003). Role of the small subunit in ribulose-1,5-bisphosphate carboxylase/oxygenase. *Arch. Biochem. Biophys.* 414, 141-149.

Spreitzer, R. J. & Salvucci, M. E. (2002). Rubisco: structure, regulatory interactions, and possibilities for a better enzyme. *Ann. Rev. Plant Biol.* 53, 449-475.

Stanley, S. M. & Yang, X. (1994). A double mass extinction at the end of the Paleozoic Era. *Science* 266, 340-344.

Sugawara, H., Yamamoto, H., Shibata, N., Inoue, T., Okada, S., Miyake, C., Yokota, A. Kai, Y. (1999). Crystal structure of carboxylase reaction-oriented ribulose-1,5-bisphosphate carboxylase/oxgenase from thermophilic red algae, *Galdieria partita*. *J. Biol. Chem.* 274, 15655-15661.

Suzuki, K. & Ikawa, T. (1993). Oxygen enhancement of photosynthetic $^{14}CO_2$ fixation in a freshwater diatom *Nitzschia ruttneri. Jpn. J. Phycol.* 41, 157-164.

Tabita, R. F. (1999). Microbial ribulose-1,5-bisphosphate carboxylase/oxygenase: a different perspective. *Photosynth. Res.* 60, 1-28

Tabita, R. F., Satagopan, S., Hanson, T. E., Kreel, N. E., Scott, S. S. (2008). Distinct form I, II, III, and IV Rubisco proteins from the three kingdoms of life provide clues about Rubisco evolution and structure/function relationships. *J. Exp. Bot.* 59, 1515-1524.

Tachibana, M., Allen, A., Kikutani, S., Endo, Y., Bowler, C., Matsuda, Y. (2011). Localization of putative carbonic anhyrases in two marine diatoms, *Phaeodactylum tricornutum* and *Thalassiosira pseudonana*. *Photosynth. Res.* 109, 205-221.

Takahashi, T., Sutherland, S. C., Wanninkhof, R., Sweeney, C., Feely, R. A., Chipman, D. W., Hales, B., Friederich, G., Chavez, F., Sabine, C., Watson, A., Bakker, D. C. E., Schuster, U., Metzl, N., Yoshikawa-Inoue, H., Ishii, M., Midorikawa, T., Nojiri, Y., Körtzinger, A., Steinhoff, T., Hoppema, M., Olafsson, J., Arnarson, T. S., Tilbrook, B., Johannessen, T., Olsen, A., Bellerby, R., Wong, C. S., Delille, B., Bates, N. R., de Baar, H. J. W. (2009). Climatological mean and decadal change in surface ocean pCO_2, and net sea–air CO_2 flux over the global oceans. *Deep Sea Research Part II: Topical Studies in Oceanography* 56, 554-577.

Tans, P. (2011). 02/2011-last update*, Trends in Carbon Dioxide* [Homepage of U.S. Department of Commerce, National Oceanic and Atmospheric Administration], [Online]. Available: www.esrl.noaa.gov/gmd/ccgg/trends/ [2011, 23/03/2011].

Tcherkez, G. G. B. (2013). Is the recovery of (photo) respiratory CO_2 and intermediates minimal? *New Phytol.* 198, 334-338.

Tcherkez, G. G. B., Farquhar, G. D., Andrews, J. T. (2006). Despite slow catalysis and confused substrate specificity, all ribulose bisphosphate carboxylases may be nearly perfectly optimized. *Proc. Natl. Acad. Sci.* 103, 7246-7251.

Thomas, W. H. & Dodson, A. N. (1975). On silicic acid limitation of diatoms in near-surface waters of the eastern tropical Pacific Ocean. *Deep-Sea Res.*, *22*, 671–677.

Torres, M. A., West, A. J., Li, G. (2014). Sulphide oxidation and carbonate dissolution as a source of CO_2 over geological timescales. *Nature 507*, 346–349.

Tortell, P. D. (2000). Evolutionary and ecological perspectives on carbon acquisition in phytoplankton. *Limnol. Oceanog.* 45, 744.

Trimborn, S., Langer, G., Rost, B. (2007). Effect of varying calcium concentrations and light intensities on calcification and photosynthesis in *Emiliania huxleyi*. *Limnol. Oceanog.* 52, 2285-2293.

Tsuji, Y., Suzuki, I., Shiraiwa, Y. (2009). Photosynthetic carbon assimilation in the coccolithophorid *Emiliania huxleyi* (Haptophyta): evidence for the predominant operation of the C_3 cycle and the contribution of β-carboxylases to the active anaplerotic reaction. *Plant Cell Physiol.* 50, 318-329.

Tsuji, Y., Suzuki, I., Shiraiwa, Y. (2012). Enzymological evidence for the function of a plastid-located pyruvate carboxylase in the Haptophyte alga *Emiliania huxleyi*: a novel pathway for the production of C_4 compounds. *Plant Cell Physiol.* 53, 1043-1052.

Tsuji, Y., Yamazaki, M., Suzuki, I., Shiraiwa, Y. (2015). Quantitative analysis of carbon flow into photosynthetic products functioning as carbon storage in the marine coccolithophore, *Emiliania huxleyi. Mar. Biotechnol.* doi:10.1007/s10126-015-9632-1.

Uemura, K., Anwaruzzaman, M., Miyachi, S., Yokota, A. (1997). Ribulose-1,5-bisphosphate carboxylase/oxygenase from thermophilic red algae with a strong specificity for CO_2 fixation. *Biochem. Biophys. Res. Commun.* 233, 568-71.

Vaucher. (1803). Historic des conterves. Génève.

Villarejo A., Martinez F., Plumed, M. D., Ramazanov, Z. (1996). The induction of the CO_2 concentrating mechanism in a starch-less mutant of *Chlamydomonas reinhardtii*. *Physiol. Plant* 98, 789-802.

von Caemmerer, S., Evans, J. R., Hudson, G. S., Andrews, T. J. (1994). The kinetics of ribulose-1,5-bisphosphate carboxylase/oxygenase in vivo inferred from measurements of photosynthesis in leaves of transgenic tabacco. *Planta* 185, 88-97.

Walker, L. J. Wilkinson, B. H., Ivany, L. C. (2002). Continental drift and Phanerozoic carbonate accumulation in shallow-shelf and deep-marine settings. *J. Geol.* 110, 75-87.

Walter, M. R., Veevers, J. J., Calver, C. R., Gorjan, P., Hill, A. C. (2000). Dating the 840-544 Ma Neoproterozoic interval by isotopes of strontium, carbon, and sulfur in seawater, and some interpretative models. *Precambrian Res.* 100, 371-433.

Wang, Z. Y. & Portis, A. R. Jr. (1992). Dissociation of ribulose-1,5-bisphosphate bound to ribulose-1,5-bisphosphate carboxylase/oxygenase and its enhancement by ribulose-1,5-bisphosphate carboxylase/oxygenase activase-mediated hydrolysis of ATP. *Plant Physiol.* 99, 1348-53.

Wang, D.S., Xu, D., Fan, X., Ye, N.H., Wang, W.Q., Zhang, X.W., Miao, Y., Guan, Z., Wang, S. (2015). Inter- and intra-specific responses of coccolithophores to CO_2-induced ocean acidification. *Biogeosci.* 12, 675-706.

Webster, R. J. (2009). The effects of light and CO_2 on photosynthesis in *Emiliania huxleyi*. Ph.D. Biological Science edn, University of Essex.

Weiss, R. F. (1974). Carbon dioxide in water and sea water: The soluability of a non-ideal gas. *Marine Chem.* 2, 203-215.

Whitney, S. M. & Andrews, T. J. (1998). The CO_2/O_2 specificity of single-subunit ribulose-bisphosphate carboxylase from the dinoflagellate, *Amphidinium carterae. Aust. J. Plant Physiol.* 25, 131-38.

Whitney, S. M., Houtz, R. L., Alonso, H. (2011). Advancing our understanding and capacity to engineer nature's CO_2-sequestering enzyme, Rubisco. *Plant Physiol.* 155, 27-35.

Whitney, S. M. & Sharwood, R. (2007). Linked Rubisco subunits can assemble into functional oligomers without impeding catalytic performance. *J. Biol. Chem.* 282, 3809-3818.

Yoon, H. S., Hackett, J. D., Ciniglia, C., Pinto, G., Bhattacharya D. (2004). A molecular timeline for the origin of photosynthetic eukaryotes. *Mol. Biol. Evol.* 21, 809-818.

Yoon, H. S., Hackett, J. D., Pinto, H. Bhattacharya D. (2002). The single, ancient origin of chromist plastids. *Proc. Nat. Acad. Sci.* 99, 15507-15512.

Young, J. N., Rickaby, R. E. M., Kapralov, M. V., Filatov, D. A. (2012). Adaptive signals in algal Rubisco reveal a hisotry of ancient atmospheric CO_2. *Philos. T. Roy. Soc. B.* 367, 483-492.

Zachos, J. C., Stott, D., Lohmann, K. C. (1994). Evolution of early Cenozoic marine temperatures. *Paleoceanography 9*, 353–387.

Zachos, J. C., Kump, L. (2005). Carbon cycle feedbacks and the initiation of Antarctic glaciation in the earliest Oligocene. *Glob. and Planet. Change 47*, 51–66.

Zeebe, R. E. & Wolf-Gladrow, D. A. (2001). *CO_2 in Seawater, Equilibrium, Kinetics, Isotopes,* Elsevier Science & Technology, Oxford/GB.

Zelitch, I. (1975) Improving the efficiency of photosynthesis. *Science* 188, 626-633.

Zhang, Y. G., Pagani, M., Liu, Z., Bohaty, S. M., Deconto, R. (2013). A 40-million-year history of atmospheric CO_2. *Philos. Trans. R. Soc.* 371. doi: 10.1098/rsta.2013.0096

Zhu, G. & Jensen, R. G. (1991). Xylulose bisphosphate synthesized by ribulose-1,5-bisphosphate carboxylase/oxygenase during catalysis binds to decarbamylated enzyme. *Plant Physiol.* 97, 1348-53.